ACTIVE REMOTE SETPOINT OPTIMIZATION UTILIZING BAS TREND DATA

A Dissertation

by

MITCHELL THOMAS PAULUS

Submitted to the Office of Graduate and Professional Studies of
Texas A&M University
in partial fulfillment of the requirements for the degree of

DOCTOR OF PHILOSOPHY

Chair of Committee,	David Claridge
Committee Members,	Charles Culp
	Bryan Rasmussen
	Juan-Carlos Baltazar
Head of Department,	Andreas Polycarpou

December 2017

Major Subject: Mechanical Engineering

ABSTRACT

In this work, a new concept was explored for the optimization of heating, ventilating, and air-conditioning (HVAC) systems in buildings. The methods assume that only commonly trended sensor data would be available and that no live connection to sensor values would exist. An actual implementation would only require a small script to be written at the target building to request information from a centralized server and update setpoint values.

A prioritization of sensors to trend at buildings is presented. Investigations into the feasibility were completed on a case study building on the Texas A&M Campus, the National Center for Therapeutic Medicine (NCTM) and the Preston Royal Library. The algorithms and models for the optimization are presented, along with uncertainty analysis into several key model parameters.

23-29% energy savings were found for AHU-2-3 at the NCTM building from June 1st, 2016 to January 1st, 2017. Missing fan power and air flow sensors reduced effectiveness, along with uncertainty in the plenum temperature for the series fan powered terminal units. Lack of readily available, accurate, manufacturers' specifications were also limitations.

A prototype of the system was developed on the web application *CC-Compass*, available at Texas A&M.

DEDICATION

To those relentlessly making this world a better place...

ACKNOWLEDGEMENTS

There are certainly too many people to thank for a single page.

I would like to first thank my advisor and chair Dr. Claridge for his support throughout the entire process, serving as both a mentor and role model. It has been an absolute pleasure being a graduate student under his direction, and I have learned so much.

I want to thank Dr. Culp for his leadership and support of the CC-Compass team. He has always made sure that we have the resources and backing to make it all go and he is always our biggest promoter. I'm so glad I got to be part of a project like CC-Compass.

I'd like to thank committee members Dr. Baltazar and Dr. Rasmussen for their comments and feedback, helping to vastly improve the quality of this document.

To the entire CC-Compass team, past and present, especially Kevin Christman and Sebastian Eluvathingal, it's been an amazing 5 years. I couldn't imagine a better or more enjoyable work environment, and it's hard to leave.

I would also like to thank all of those related to Texas A&M volleyball. I've gained so many incredible friends, and I'll never forget all the experiences playing, coaching, and having fun.

Special thanks to my family, Mom, Dad, Joe, and Val – I miss you all every day and more than you know.

And to Whitney, who has shown incredible patience with all of the inherent uncertainty in the pursuit of a Ph.D. and has provided all the personal support to make this a reality.

CONTRIBUTORS AND FUNDING SOURCES

Contributors

This work was supported by a dissertation committee consisting of Professors David Claridge, Charles Culp, and Bryan Rasmussen of the Department of Mechanical Engineering, and Professor Juan-Carlos Baltazar of the Department of Architecture.

The data analyzed for Section 6 was provided by Christopher Dieckert of Texas A&M Utilities and Energy Services. The data analyzed in Section 7 was provided through the Energy Systems Laboratory.

All other work conducted for the dissertation was completed by the student independently.

Funding Sources

Graduate study was supported by a fellowship from Texas A&M University.

NOMENCLATURE

AHU	Air Handling Unit
ANN	Artificial Neural Network
API	Application Program Interface
ARMA	Autoregressive-Moving Average
BAS	Building Automation System
CAV	Constant Air Volume
CCLT	Cooling Coil Leaving Temperature
CFM	Cubic Feet per Minute
CHW	Chilled Water
COP	Coefficient of Performance
CV	Coefficient of Variation
DAT	Discharge Air Temperature
DDC	Direct Digital Control
DX	Direct Expansion
EIB	European Installation Bus
FFLP	Fraction of Full Load Power
FPVAV	Fan Powered Variable Air Volume
FSM	Finite State Machine
HP	Horsepower
HTTP	Hypertext Transfer Protocol
HVAC	Heating, Ventilation, and Air-Conditioning
IAQ	Indoor Air Quality
JSON	JavaScript Object Notation

MPC	Model Predictive Control
NCTM	National Center for Therapeutics Manufacturing
NOAA	National Oceanic and Atmospheric Administration
OA	Outdoor Air
OAHU	Outdoor Air Handling Unit
PID	Proportional-Integral-Derivative
PLR	Part Load Ratio
RA	Return Air
RH	Relative Humidity
RMSE	Root Mean Squared Error
RT	Return Temperature
S/S	Start/Stop
SA	Supply Air (from AHU)
VAV	Variable Air Volume
XML	eXtensible Markup Language
δ	Uncertainty
ρ	Density
A	Constant for Fraction of Full Load Power
c_p	Specific Heat
$\dot{E}$	Power
h_v	Latent Heat of Vaporization
$\dot{Q}$	Heat Load
ΔP	Change in Pressure
t	Time
T	Temperature

$\dot{V}$	Volume Flow Rate
$\dot{W}$	Power
X	Fraction
C_{air}	Volumetric Heat Capacity [Energy per unit Volume per unit Temperature Difference]
H	Volumetric Heat of Vaporization [Energy per unit Volume]

Subscripts

a	air
db	dry-bulb
des	design
dis	discharge (from terminal unit to zone)
ma	mixed air
oa	outdoor air
plen	plenum
pri	primary
ra	return air
sa	supply air (from AHU)
tot	total
z	zone

TABLE OF CONTENTS

Page

LIST OF FIGURES

FIGURE Page

LIST OF TABLES

TABLE Page

1. INTRODUCTION

Adjusting the HVAC control sequences in existing building commissioning is a common method to reduce energy consumption. Many of the original control sequences for building equipment are never optimized or adjusted using detailed engineering, due not only to the amount of time and effort that such an analysis may take but also due to the lack of skill the on-site maintenance staff may have.

Sensor data from building automation systems are becoming more abundant as computing resources decrease in price and software improves in quality. Software applications can use this wealth of information in an automated process to actively optimize the air conditioning system, without detailed input from an engineer.

This work attempts to leverage commonly available trend data to optimize the setpoint values that air handling units of single duct variable air volume systems typically use. Ideally, to be considered optimal, the entire airside system needs to be considered as a whole, including fan energy, cooling energy, and reheat energy. While demand-based controls can often significantly reduce energy use for one component of the system, it does not necessarily optimize the whole.

It is desired to refrain from adjusting the existing control logic or low-level electronics to accomplish this outcome. This work attempts to acquire trend data, run the necessary methods to determine the optimal setpoints from a separate dedicated system, and then send the information back and *actively* change the air handling unit setpoints in the BAS. In this way, the methodology can scale quickly to many different air handlers and buildings, being indifferent to the vendor of the BAS.

2. LITERATURE REVIEW

A significant amount of research has been completed in the field of control optimization schemes. Several different approaches including direct search methods, non-linear programming, genetic algorithms, and artificial neural networks have been researched. Optimizations have been completed at all levels of the HVAC system: Zone, AHU, and Plant.

When discussing optimization, it is important to be clear on what is meant by *Controls Optimization*. When discussing the subject with a controls engineer, they will likely be analyzing parameters such as the settling time, overshoot, and rise time — dynamic parameters. In contrast, this research focused on the optimization of the *steady-state* behavior of the system.

2.1 Setpoint Optimization

Since the time constant of AHU dynamics is on the order of minutes and the time constant of the thermal loads on the building are on the order of minutes to hours, it is appropriate to focus on the steady state behavior of AHUs [1].

Ke and Mumma were among the first to attempt to balance the benefits of raising the supply air temperature with the penalties associated with increased fan energy and decreased dehumidification potential [2]. This paper was limited in the fact that it made no discussion on actual implementation. The simulated results showed that optimizing the balance between fan, cooling, and reheat energy resulted in approximately 6% energy savings annually versus a fixed supply air temperature setpoint. They showed that the benefit was most promising in the more temperate weather when the VAV system was running above the minimum primary airflow. Ideally, the fan static pressure pressure setpoint would be optimized in conjunction

with the supply air temperature as well.

Wang and Song also balanced supply air temperature with fan power and included economizer control [3]. They found energy savings reaching up to 90% under the specific outdoor air conditions and space loads in their simulation. The universal control sequence they proposed relied on an outside air temperature sensor, supply air temperature sensor, and supply air flow sensor. A hindering assumption was that the terminal units did not have reheat. It is well known that terminal unit reheat energy can be a significant contributor to the total energy consumption and the reduction of reheat is often a source of significant energy and money savings in existing building commissioning.

Qin completed a dissertation in 2014 entitled, "A Data-Driven Approach for System Approximation and Set Point Optimization, With a Focus in HVAC Systems" [4]. The focus of this work was related to the programming of thermostats in residential homes and did not cover any buildings in the commercial sector. The control responses for the rooms were being optimized and not the temperature setpoints of the rooms.

Huh and Brandemuehl optimized the setpoint for hot and humid climates [5]. The most significant limitation of this work was that it was heavily focused on a DX unit that would be common to a retail or supermarket and was also focused on only a hot and humid climate. Engdahl and Johansson also devoted investigation into the optimization of the supply air temperature setpoint in a VAV system [6], but only studied AHUs with 100% outside air.

While the focus of this research is on air handling units, the research regarding the optimization of central plants should not be ignored [7, 8]. At the plant level, Braun has completed a great deal of research [9, 10, 11, 12]. He has investigated optimizations of various systems, such as ones for night precooling with packaged

rooftop systems [13]. Crowther and Furlong showed that advanced optimization controls for chiller-tower condenser-pump systems could make a 5-8% improvement in annual energy use [14]. Henze has also been active in optimizing thermal storage systems [15] along with Kintner-Meyer and Emery [16]. Lu et al. also focused on the optimization of the entire HVAC system, plant, and building, in a series of papers [17, 18, 19, 20].

United States patents have even been written on the topic of HVAC optimization. Cascia has a patent on optimal control for a cooling and heating plant with DDC control [21] and Seem has a patent that describes the strategy to optimally control an air side economizer [22].

Numerous other researchers have thoroughly covered many aspects of an optimally operating HVAC system, which is not limited to [23, 24, 25, 26, 27, 28, 29, 30, 31, 32, 33, 34, 35, 36, 37]. Wang and Ma provided a comprehensive review of supervisory control research [38]. The literature is limited in regards to efficient methods of rapid implementation. This research also presents a different optimization methodology that focuses on the use BAS trend data paired with first-principle models.

2.2 Advanced Computation Techniques and Controls

The HVAC industry has slowly begun to employ the advances in computer science. Researchers from the University of Iowa (Kusiak, Li, Xu, Tang, Wei) have published a great deal of work on the optimization of all types of HVAC systems. They have applied data mining algorithms and computational intelligence algorithms to data-driven optimization for the cooling output of air handling units and plants [39, 40, 41, 42, 43, 44, 45, 46, 47, 48, 49]. They have used techniques like neural networks, evolutionary type programming, and multi-perceptron ensembles. They have also

applied particle-swarm optimization in several of their publications.

The use of genetic algorithms or general evolutionary programming techniques has been applied in several pieces of research. Genetic algorithms have been used to optimize chilled water supply temperature, supply air temperature, fan control, and outdoor air control, related to many different kinds of systems, including variable air volume and variable refrigerant volume [50, 51, 52, 53].

2.2.1 Model Predictive Control

Model predictive (or receding-horizon) control (MPC) has been a popular research field in control theory and has been successfully implemented in practice. Li et. al [54] recently showed the benefits of MPC in both simulation and in experimental work. They estimated electrical consumption savings to be 18% for a 75,150 ft^2 building in Philadelphia during a week in August, and found that in 75% of their 20 test days they had energy consumption savings of over 20%. They also used a centralized architecture where BAS data were passed through a middleware with a historical database to Matlab and an AMPL (A Mathematical Programming Language) optimization system, with results of that system dynamically changing the building HVAC system.

Afram et al. also studied the combination of ANNs and MPC [55]. As described in [55], the combination of these two techniques has been used for the following different control objectives:

1. Minimize energy consumption [56, 57, 49, 39, 45, 58, 59, 20, 31]
2. Maintain thermal comfort [56, 49, 39, 45, 58, 59]
3. Maintain indoor air quality (IAQ) at an acceptable level [43]
4. Minimize operating cost [58, 60, 57, 61, 62]

5. Maintain visual comfort at an acceptable level [59]

6. Minimize retrofit cost [63]

7. Minimize thermal discomfort hours [63]

This dissertation has a focus on steady state behavior, but the dynamic behavior of buildings and its controls are also important. Seem has published research comparing a finite state machine (FSM) sequencing to the more common split-range sequencing control logic [64]. Xu, Li, and Cai proposed a receding-horizon optimization control that uses a typical PID type controller [65]. This work had a focus on practicability in that it required no changes in the hardware or the definitions of the common control parameters related to a PID controller. Yuan and Perez used a model-predictive controller to control temperature and ventilation for multiple zones [66]. Freire, Oliveira, and Mendes also used predictive controllers for thermal comfort optimization [67]. Guo, Song, and Cai investigated neural networks in HVAC control [68].

2.3 BAS Communication

There are many different networking and communication levels and protocols related to buildings. Kastner, Neugschwandtner, and Soucek et al. provided a summary of the different systems that exist in buildings [69]. An understanding of the different levels (described as management, automation, and field by [69]) is important for developing any automated system. The most important open systems related to building automation include BACnet, LonWorks, EIB/KNX. Other important and relative standards, protocols, and technologies are shown in Table 2.2.

Project Haystack is an important open source initiative that is looking to bring specific naming conventions to building operational data (project-haystack.org). It

Table 2.1: Techniques applied in HVAC system optimization.

Techniques	Sources
Quadratic Least Square Regression	[7]
Gradient Based Optimization, Golden Complex Search	[5][32]
Genetic Algorithms	[17][19][20][25][27][34] [37][53][51][46]
Analytical Linear Optimization	[33]
Evolutionary Programming	[50][43]
Evolutionary Strategy	[47]
Model Predictive Control/Receding Horizon	[15][23][67][44][65][66]
Neural Networks	[31][47][68][42][49][39]
Particle Swarm Optimization	[40][44][48][42][49][45][46]
Harmony Search	[40]
Model Free Reinforcement Learning	[28][29]
ARMA	[51]
Data Mining Algorithms	[43][47][44][48]
Multiple-Linear Perceptron Ensemble	[39][48][45][41]
Interior Point Method	[39]
Adaptive Neuro-Fuzzy Inference Systems (ANFIS)	[20]
Genetic Fuzzy Optimization	[52]
Finite State Machine	[64]

accomplishes this at a more abstract level than BACnet, LonWorks, and EIB/KNX, using lexical rules. Before data from sensors in buildings can be used effectively, an "association" of the data to an HVAC object (say data being associated with an air temperature sensor located in a specific air handling unit) needs to occur. To create an environment where an intelligent building makes sense, raw numeric data needs to have extensive meta-data to give it context. This meta-data can be related to engineering units, what piece of equipment the data belongs to, the hierarchy of equipment and relationships to one another, and other modifiers.

Table 2.2: Important standards/technologies in building automation.

Network Communication Protocols
BACnet
LonWorks
EIB/KNX
IP
Object Access Protocols
Common Object Request Broker Architecture (CORBA)
Java Remote Method Invocation (RMI)
Microsoft Distributed Component Object Model (DCOM)
Simple Object Access Protocol (SOAP)
Architecture Style
Representational State Transfer (REST)
Local Area Network Type
Ethernet
ARCNET
Master-Slave/Token-Passing (MS/TP)
LonTalk
Point-to-Point (PTP)
Data Format
Javascript Object Notation (JSON)
Extensible Markup Language (XML)

2.4 Summary of Literature

Not surprisingly, the goal of any controlled system is to operate optimally. It is to be expected that there would be a wealth of literature on the optimization of all different components in a particular HVAC system.

Any optimization problem has objectives and constraints. Many different objective functions and constraints to optimization problems in HVAC have been proposed. Numerous different optimization techniques and methods have been implemented and analyzed by different researchers.

However, there are several limitations and deficiencies in the optimization literature. Not all authors have focused on the scalability of different optimization methodologies. Presently it is not feasible to implement complicated data-mining algorithms on every individual BAS or controller, partly due to installation time and partly due to the lack of facilities managers that have the necessary training to understand the algorithms and that can keep the system running properly. Facility managers already have difficulties in maintaining traditional and straightforward HVAC systems.

Many of the techniques proposed in the literature also are dependent on sensors or information that are currently unavailable in typical commercial HVAC systems. For large-scale implementation, a methodology must function with a minimal number of sensors and remain useful.

For an individual system, there are more than enough well-documented and effective optimization methods and algorithms. Few buildings in practice have these optimizations in place because other numerous challenges have not been fully solved. These challenges include complexity in implementing with different BAS vendors, training staff members to understand the logic behind the optimizations, and simply

the technician effort to install and setup implementations.

This research proposes an intuitive optimization method based on small first-principle models using historical data that is designed to efficiently scale. The research investigates how to use current communication protocols with BAS systems and implementable methodologies to apply a single set of optimization logic and code to many and varied air handling units.

2.5 Typical Trends Available from Commissioning Projects

Unfortunately, at the current time, it is uncommon to have all the sensor data trended for all portions of the HVAC system. It is rare to have the capability to submeter the energy use of all the individual components including the fans, cooling coils, and heating coils. This section investigates what sensors have been typically available from existing building commissioning and provides suggestions for which trends are most important for energy-use breakdowns.

2.5.1 Common Case

The following suggestions are based on the data for over 150,000 trends stored in Implementer along with personal experience. Implementer is a web application developed by the Energy Systems Laboratory that aids engineers in the collection and analysis of trend data from buildings. The statistical results presented use data until April 13, 2016. The total number of configured single duct AHUs at this time was 846. The number of trends that existed in these 846 AHUs was 11,806, or approximately 14 trends per AHU. Table 2.3 gives the percentage breakdown of the types of points that we have seen in current Implementer projects. Note that due to special Implementer considerations, the occurrence percentage should not be evaluated in absolute terms (due to some projects not being properly set up at all). The relative relationship between trend types is the more significant result.

Table 2.3: Breakdown of points typically available in single duct AHU systems currently in Implementer.

Point Type	Occurrence
65%+	
DAT/SAT	83%
CHW Valve	73%
Duct Static Pressure	67%
45% - 65%	
Outdoor Air Damper	65%
Return Air Temp	58%
DAT/SAT Setpoint	53%
Return RH	52%
Fan Status Points	50%
Mixed Air Temp	48%
Return Air CO_2	48%
25%-45%	
Filter ΔP	35%
Static Pressure Stpt.	35%
Outdoor Air Flow	28%
Return Air Damper	27%
Occupied Status	25%
5% - 25%	
Space Temp	21%
Supply Air Flow	15%
Fan Status	15%
Fan S/S	14%
Outdoor Air Temp	13%
Heating Coil Valve	21%
Modes	10%
Fan Power	9%
Preheat Temp	9%
CCLT	8%
Mixed Air Damper	7%
CHW Supply Temp	6%
Return Air Flow	6%
CHW RT	6%
Air Changes	5%
Fan Proofs	5%
Limits	5%
0% - 5%	
# Boxes In Reheat	4%
Misc. Alarms	4%
Supply Fan kW	4%
Economizer Status	3%
Space Humidity	3%
CCLT Setpoint	3%
% Load	2%
Cool/Heat Coil Flows	2%
Runtimes	2%
Water Pressure	1%
Fan Volts	1%
HW Supply Temp	<1%
HW Return Temp	<1%
Fan Current	<1%
Outdoor Air Flow Stpt	<1%

If the building in question consumes district chilled and hot water for thermal HVAC processes, the importance of additional trends is lessened since it is clear that the chilled water is used to meet the cooling load of the building and similarly for the hot water. The electricity use is then left to lights and equipment, along with the fan and pump energy.

However, if natural gas and electricity are the only energy supply types for the building, additional information coming from trend data becomes more important for disaggregating the energy end uses.

It can normally be assumed that monthly utility bills are available. Having a smaller time interval on the utility data can also aid significantly in calibration. Daily data can help aid in discriminating weekday/weekend profiles, while hourly data can aid in exposing the diurnal cycle of the building.

2.5.1.1 Fan Power

In all cases, having the fan power trended will aid in the energy use breakdown, as this immediately provides information regarding this portion of the electricity use. In many cases, it is acceptable to combine lighting energy and the non-HVAC related internal electricity use.

The fan power is trended directly on less than 10% of systems in Implementer. The next best option in 15% of the cases is using the supply flow along with manufacturers' specifications to estimate fan power. With the design flow values from mechanical drawings, fractional power curves based on part-load ratio can be used to estimate the fan energy use.

2.5.1.2 Cooling Energy

At the air handler level, the sensible cooling energy is related to the supply flow, and the difference between the mixed air temperature, and the supply air

temperature. The supply flows can vary significantly from one air handler to another, and also under different loadings.

The mixed air temperature is the lowest priority of the three air-side parameters for estimating the sensible cooling energy in the AHU. A reasonable estimate of the outdoor air temperature is available from local weather stations, in addition to commonly trended outdoor air temperatures at the site itself. The return air temperature in air handling units is normally near the space temperature setpoints. It is known that the mixed air temperature must be between the return and outdoor air temperature (if the air streams are indeed being mixed). Without any other information, the safest estimate for the mixed air temperature would be halfway between these two measurements.

As an argument for the claim that mixed air temperature is the lowest priority of the three parameters, the difference between T_{oa} and 72°F for the hourly outdoor air dry-bulb temperature weather data for College Station during the year of 2015 was calculated. 1/2 of this difference would be the worst case error estimation. The median of these half-differences was 4.9°F, and the mean was 6.4°F. These are robust estimates of the upper bounds on the error of the estimation of mixed air temperature with no guidance other than the assumption that the mixed air temperature is between the outdoor air temperature and return air temperature. With any additional information regarding the outdoor air fraction, the estimate would be even better.

Determining the latent load across the cooling coil is difficult using air-side parameters. Humidity sensors are traditionally unreliable, and two would be necessary to calculate an absolute humidity difference.

In this sense, metering the water-side parameters would be a more reliable estimator of the total cooling load, including the latent effect. However, trended water-side

sensors have not been seen in the five years of Implementer projects.

2.5.1.3 Reheat Energy

Unless the building has some other large hot water end uses, if the building consumes natural gas, much of this will be directly related to heating/reheat. Electricity use will then be distributed between lights and non-HVAC equipment, fans, along with chiller/HVAC equipment.

If the building is heated using natural gas, the natural gas consumption can be an adequate indicator of the level of reheat use in the building. At the current time, trended data from all terminal unit points is uncommon. The sensors are typically available, however, the number of terminal units and a large amount of data to be handled are issues that cause persons to decline to pursue the collection of the terminal unit data.

Having the supply air temperature and supply air flow is important because it not only helps fix the parameters for the cooling energy end use at the AHU but also the parameters for estimating reheat in the terminal units. If the terminal units are aggregated together, with the knowledge of the total flow and supply air temperature, along with potentially having measured natural gas use, the only parameter left to estimate reheat is the discharge temperature to the zones.

2.5.1.4 Prioritization

The following sensors, in no particular order, are the most useful with regards to energy modeling and determining the energy use breakdown.

- Supply air temperature – This parameter is crucial in estimating both the sensible cooling energy and the reheat energy of the system.
- Fan power – Directly returns the energy end use for fans.

- Supply air flow – A key parameter in estimating the flow both at the AHU and the total of which is going to the terminal units, affecting both the cooling and reheat energy end uses.
- Outdoor air flow – Important in fixing the ventilation load at the AHU.
- Terminal unit flows – Helps set the minimum primary air flow parameter, a sensitive parameter affecting the reheat.
- Terminal unit discharge temperatures – Aids the estimation of zone reheat.
- Space temperature – Defines the zone temperatures.
- Mixed air temperature – Aids in the determination of the sensible and latent cooling load and estimation of the outdoor air fraction.
- Return air temperature – Aids in the estimation of the outdoor air fraction or ventilation load.
- VSD speed, VFD frequency, etc. – Indicator of the part-load ratio for the equipment, which may be used in the estimation of fan energy.
- Preheat Temperature – Sets this parameter in the model, aiding in the estimation of the heating end uses.

Sensors that may be of medium usefulness:

- Fan Status or occupied/unoccupied status – Can indicate the run times and schedules of the building.
- Supply air static pressure – Unless the precise location of the sensor and the overall duct layout is known, it is of little use in calculating the fan power. It

does indicate whether the fan is on or off which is useful for determining AHU schedules.

- Various Setpoints – In a well-controlled building, ideally, the value of the controlled sensor will be equivalent to the setpoint. However, the setpoint trends may not represent reality, especially under conditions of control overrides or other faults.

- Return air relative humidity – May be an indicator of the level of latent load in the building. If the return air absolute humidity levels are relatively dry, the latent load may be zero or negligible.

- Outdoor air temperatures – In some circumstances, the temperature of the ventilation air may differ from the outdoor air temperature in the local community, in which the local measurement will be a better indicator of the temperature of the air that is entering the AHU from the outdoors. However, the local weather station measurements are typically much more reliable and trustworthy than the sensors maintained at the site, and this needs to be taken into consideration.

Sensors that are commonly trended and are not useful for estimating the energy use breakdown of a building:

- Return air CO_2 – Not directly related to estimating the energy use.

- Damper commands – Since duct layout and fluid flow models are not feasible, the damper commands do not provide information towards the calculation of the energy use.

- Chilled water valve/hot water valve – It is the actuator for controlling the supply air temperature, but does not provide information related to energy use.

3. OPTIMIZATION METHODOLOGY

The energy use from each of the components comprising the air-side equipment needs to be estimated to optimize the system. This includes fan energy, cooling energy, and reheat energy.

The optimization problem to be solved in standard form is

$$\begin{aligned} \underset{T_{sa}}{\text{minimize}} \quad & \dot{E}_{fan} + \dot{E}_{cooling} + \dot{E}_{reheat} \\ \text{subject to} \quad & T_{sa} \geq T_{sa,min} \\ & T_{sa} \leq \text{MIN}\left(T_{ma}, \text{MIN}\left(T_{dis,1}, T_{dis,2}, \ldots, T_{dis,n}\right)\right) \\ & \text{IF } \omega_{oa} > \omega_{max},\ T_{sa} \leq T_{sa,\omega} \end{aligned} \tag{3.1}$$

In other words, minimize the total power of the AHU and terminal unit system as a function of the supply air temperature, with the constraints that the supply air temperature is above a preset minimum, and less than both the mixed air temperature and the minimum of the discharge air temperatures from the terminal units. If the outdoor air humidity ratio is above a preset humidity ratio threshold, ω_{max}, then the supply air temperature must stay below a different minimum $T_{sa,\omega}$, likely near 55°F.

If energy prices are available, the objective function can be modified to be to total cost, rather than the total power.

3.1 Reheat in Terminal Units

Terminal units can be distributed into three classifications for this work. Terminal units with no fans, series flow, or parallel flow arrangements.

3.1.1 No Fan in Terminal Unit

If there is no fan and only a damper for air volume modulation, then the reheat power is

$$\dot{E}_{reheat} = \sum_i \dot{V}_i \rho_a c_{p,a} \ (T_{i,dis} - T_{i,sa}) \tag{3.2}$$

3.1.2 Series Flow Configuration

For a series flow terminal unit, the total flow is ideally constant. $\dot{V}_{tot}$ is known from the specification of the terminal unit, and $\dot{V}_{pri}$ is a measured variable. $\dot{V}_{plen}$ can be calculated from Equation (3.3).

$$\dot{V}_{plen} = \dot{V}_{tot} - \dot{V}_{pri} \tag{3.3}$$

T_{dis} will be sensed. The temperature of the air after mixing can be estimated from the flow information and an assumption or measurement of plenum air.

$$T_{mix} = \frac{\dot{V}_{pri}\,(T_{sa}) + \dot{V}_{plen}\,(T_{plen})}{\dot{V}_{tot}} \tag{3.4}$$

Another rearrangement of 3.4 that is important is solving for $\dot{V}_{pri}$. Under conditions when there is no reheat, and the primary flow is not at the minimum setting, the energy balance across the terminal unit is

$$\dot{V}_{pri} T_{sa} + \dot{V}_{plen} T_{plen} = \dot{V}_{tot} T_{dis} \tag{3.5}$$

Replacing $\dot{V}_{plen}$ with Equation 3.3 gives

$$\dot{V}_{pri} T_{sa} + \left(\dot{V}_{tot} - \dot{V}_{pri}\right) T_{plen} = \dot{V}_{tot} T_{dis} \tag{3.6}$$

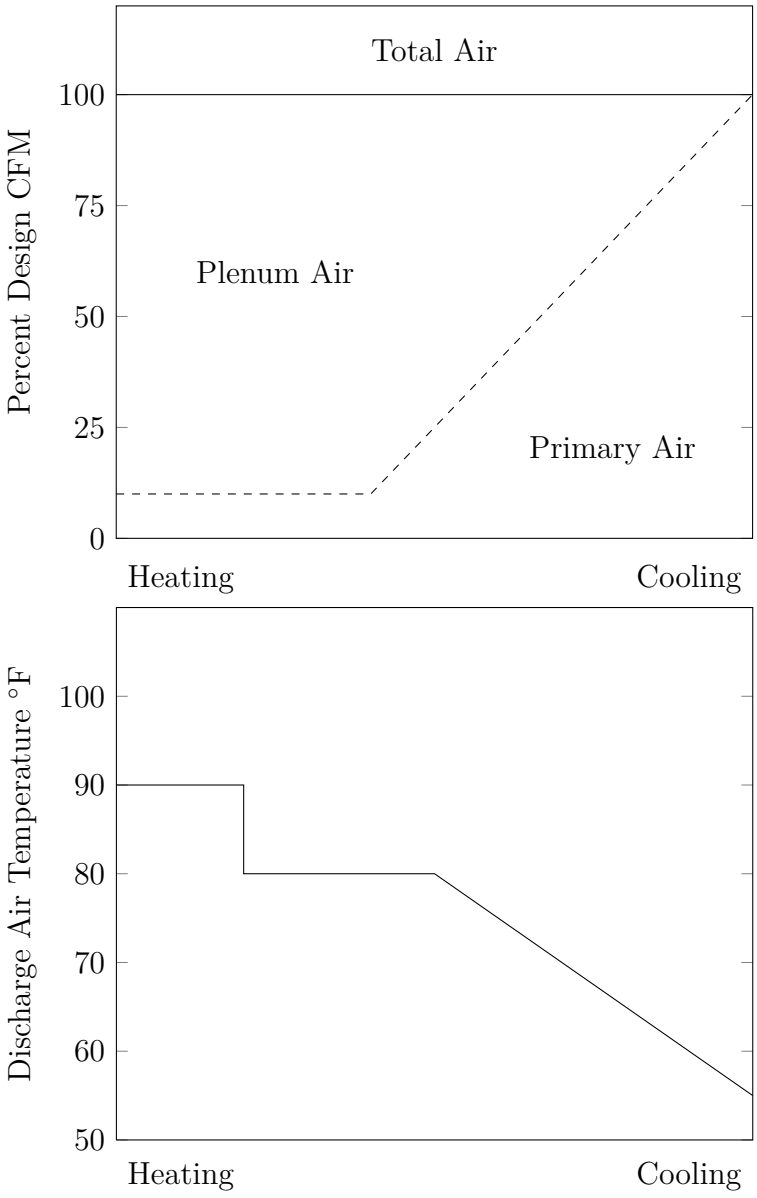

Figure 3.1: Example series terminal unit flow operation.

$$\dot{V}_{tot}T_{plen} - \dot{V}_{tot}T_{dis} = \dot{V}_{pri}T_{plen} - \dot{V}_{pri}T_{sa} \tag{3.7}$$

$$\dot{V}_{pri} = \dot{V}_{tot}\left(\frac{T_{plen} - T_{dis}}{T_{plen} - T_{sa}}\right) \tag{3.8}$$

The actual primary flow will be the maximum of Equation 3.8 and the minimum flow setting. When at minimum flow, there will be resulting reheat.

$$\dot{V}_{pri} = \text{MAX}\left(\frac{\dot{V}_{tot}\left(T_{dis} - T_{plen}\right)}{\left(T_{pri} - T_{plen}\right)}, \dot{V}_{pri,\text{min}}\right) \tag{3.9}$$

The increase in temperature is due to heat gain from the fan and any supplementary heating.

The temperature rise from the fan, ΔT_{fan}, can be estimated from historical data when the supplementary heating is off, either when the heating coil is completely closed, or all stages of electrical reheat are inactive. If there is no other heating, the temperature increase from the fan is

$$\Delta T_{fan} = T_{dis} - T_{mix}. \tag{3.10}$$

where T_{mix} is the temperature described by Equation 3.4. For other times, the temperature increase due to reheat will be

$$\Delta T_{reheat} = T_{dis} - \left(\Delta T_{fan} + T_{mix}\right), \tag{3.11}$$

and the reheat power will be

$$\dot{Q}_{reheat} = \dot{V}_{tot}\rho_a c_{p,a}\left(\Delta T_{reheat}\right). \tag{3.12}$$

3.1.3 Parallel Flow Configuration

During periods of cooling, the fan in a parallel arrangement is off and the total flow is equal to the primary flow.

The fan volume flow will be known from manufacturers' specifications, and the total flow can be calculated using Equation 3.3. The temperature from mixing the plenum air and primary can be estimated from Equation 3.4 or historical data when the primary flow is at the minimum, and there are no activated reheat components.

3.1.4 Other Terminal Unit Types

Terminal units come in even more configurations than the three specified in this document, induction units being one example. Models can be made using a combination of energy balances, historical data under particular conditions, and appropriate assumptions.

3.2 Predicting Zone Loads

The zone loads can be estimated from terminal unit data of airflow rate, terminal unit leaving temperature and zone temperature. Note that using

$$\dot{Q}_z = \dot{V}_z C_{air} \left(T_z - T_{dis}\right) \tag{3.13}$$

assumes that the zone is well-mixed and at steady-state. If the controls oscillate, then the zone load estimation will have some periodicity. In some sense, there is no "single" zone load coming from a point source, and as such we will have to rely on this estimation.

The independent variables available for prediction are the current time and outdoor air conditions. The current time can be separated into a time of day, the day of the week, weekdays/weekends and such. Outdoor air temperature correlates with

the external load. As a reminder, it is assumed that there is no access to live values of sensors and only historical data with the outdoor conditions and current time can be used.

The approach used to estimate parameters is a related to the concept of a *nearest neighbor*. The nearest neighbors are defined by any previous data that:

1. Was within n hours of the time of day, specified as plus or minus a certain number of integer time steps relating to the time interval between the data points.
2. Was the same day of the week.
3. Had the same T_{db} within a specified threshold (say 1°F of the current T_{db}).

The median value of the nearest neighbors can be used to estimate the particular zone load at any time and temperature. The median is a more robust statistic in comparison to the mean, having a breakdown point of 50%, meaning that up to 50% of the data can be contaminated before the median statistic will no longer be reliable. For the mean, one arbitrarily large data point can turn the mean statistic unreliable.

This work initially used the most recent 30 data points that met the nearest neighbor criterion in the median calculation. A threshold of 30 points was chosen since this is the threshold in which the sample median should approximate the actual median if the population is assumed to have a normal distribution.

It is advised that in this approach, that the initial historical data be sorted in order of temperature, followed by the date time. The lookup for the subsection of data to be used will then be $O(\log n)$ with a binary lookup.

The advantage of the nearest neighbor approach is that the resulting "function" is not limited to being linear, quadratic, or any particular form. It just simply matches the data as best it can during external conditions that are expected to be similar.

3.2.1 Zone Load Uncertainty

The Kline-McClintock form of uncertainty analysis can be applied to the zone loads.

If the sensible zone load is described as an open system with a constant specific heat, then

$$\dot{Q}_z = \frac{\dot{V}_{zone}}{\nu} c_a \left(T_z - T_{dis}\right) \tag{3.14}$$

The total uncertainty in the prediction will be

$$\delta\dot{Q}_z = c_a \left(\left(\frac{\left(T_z - T_{dis}\right)}{\nu} \delta\dot{V} \right)^2 + \left(\frac{-\left(T_z - T_{dis}\right)\dot{V}}{\nu^2} \delta\nu \right)^2 + \left(\frac{\dot{V}}{\nu} \delta T_z \right)^2 + \left(\frac{-\dot{V}}{\nu} \delta T_{dis} \right)^2 \right)^{\frac{1}{2}} \tag{3.15}$$

For the sake of analysis, the following reasonable parameters were assumed:

1. $T_z = 72°\text{F}$
2. $T_{dis} = 55°\text{F}$
3. $\nu = 13.5 \frac{\text{ft}^3}{\text{lb}_\text{m}}$
4. $\delta T_z = \delta T_{dis} = 1°\text{F}$
5. $\delta\nu = 1 \frac{\text{ft}^3}{\text{lb}_\text{m}}$

The resulting percent uncertainty in the zone load versus the uncertainty in the flow measurement is shown in Figure 3.2. Note that with no flow uncertainty, there is approximately 11% percent uncertainty contribution from the air density and temperatures. After about 20% uncertainty in the flow, it becomes the dominant source of uncertainty.

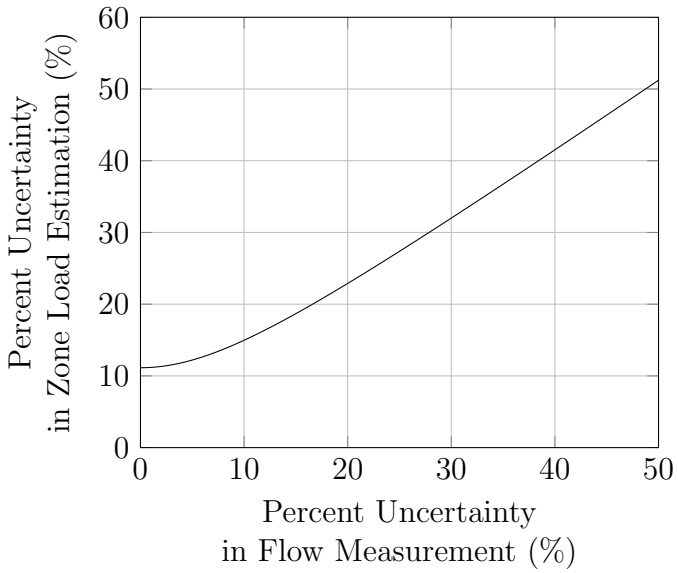

Figure 3.2: Zone load uncertainty versus flow uncertainty.

3.2.2 Analysis of Fraction of Full Load Power Uncertainty

In simplified air handling unit analysis, the fraction of full load power, F, can often be represented with the function shown in Figure 3.3

$$F = A + (1 - A)(\text{PLR})^n \tag{3.16}$$

where A is the fraction of power at zero load, n is an exponent typically ranging from 1 to 3, and PLR is the part load ratio defined to be

$$\text{PLR} = \frac{\dot{V}_{act}}{\dot{V}_{des}} \tag{3.17}$$

The actual fan power at any point is then

$$\dot{W}_{act} = F\dot{W}_{des} \tag{3.18}$$

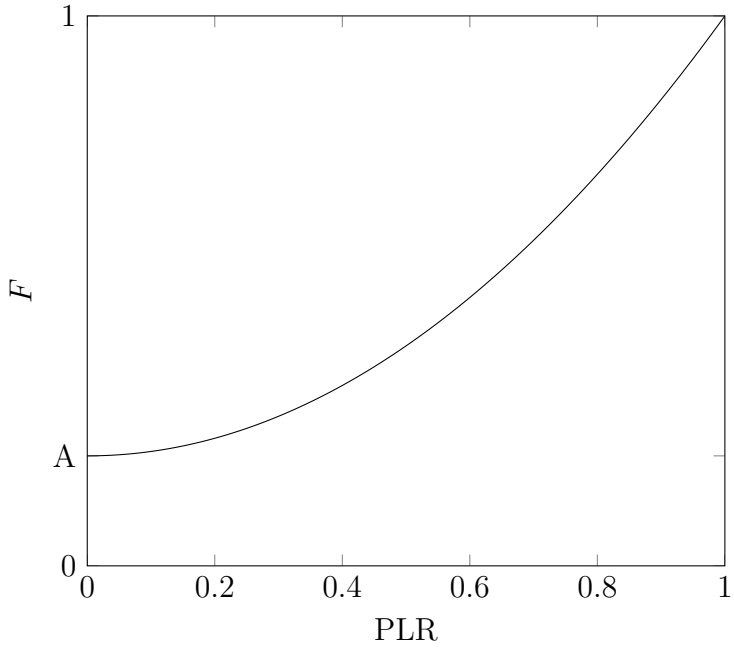

Figure 3.3: Fraction of full load power for a fan.

The uncertainty of F can be explored with the Kline-McClintock formulation.

The first uncertainty term, which is related to A is

$$A \text{ term} = \frac{\partial F}{\partial A}\delta A = (1 - \text{PLR}^n)\,\delta A \tag{3.19}$$

The uncertainty term related to n is

$$n \text{ term} = \frac{\partial F}{\partial n}\delta n = ((1 - A)\text{PLR}^n \ln(\text{PLR}))\,\delta n \tag{3.20}$$

and the uncertainty related to PLR is

$$\text{PLR term} = \frac{\partial F}{\partial \text{PLR}}\delta\text{PLR} = \left((1 - A)n\text{PLR}^{n-1}\right)\delta\text{PLR} \tag{3.21}$$

The total uncertainty in F is

$$\delta F = \sqrt{(A \text{ term})^2 + (n \text{ term})^2 + (\text{PLR term})^2} \tag{3.22}$$

The uncertainty is a function of 6 variables: A, n, PLR, δA, δn, and δPLR.

If the values of

1. $A = 0.2$
2. $n = 2$
3. $\delta A = 0.05$
4. $\delta PLR = 0.05$
5. $\delta n = 0.4$

are used, a plot can be created showing the relative importance in the uncertainty as a function of PLR. This plot is shown in Figure 3.4. The series are the squared values of the uncertainty terms, for example, the A series is

$$\left((1 - \text{PLR}^n)\,\delta A\right)^2 \tag{3.23}$$

Over the input range of PLR, there are three different regimes in which each input variable contributes the most to the uncertainty. The different regimes where specific terms are the largest are denoted in Figure 3.4 and 3.5. At high part load ratios, the uncertainty in the part load ratio itself is the most important factor. At part load ratios near 0.5, the exponent n, which determines the curvature is the most important. At low part load ratios, the uncertainty in the value of A, the limiting fraction of part load power at no load, is the most important.

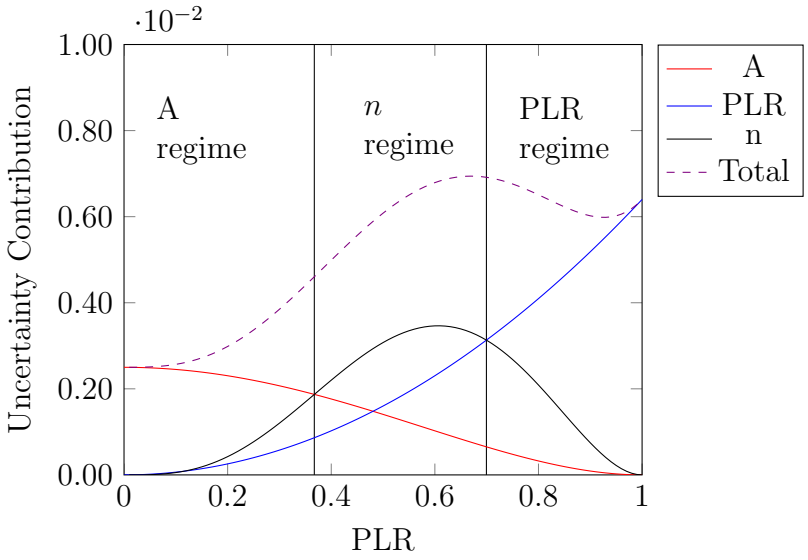

Figure 3.4: Relative uncertainty contributions for fraction of full load fan power when $n = 2$. ($A = 0.2$, $\delta A = 0.05$, $n = 2$, $\delta n = 0.04$, $\delta \text{PLR} = 0.05$)

At the extreme values of PLR, 0 and 1, the uncertainty from two the components is 0. At a PLR of 0, there is no uncertainty contribution from the exponent and PLR terms, and only uncertainty from the A term. At a PLR of 1, there is no uncertainty contribution from the exponent and the constant A terms, but only uncertainty in the PLR term.

So to reduce the total uncertainty across all ranges of part load ratios will require better knowledge of all the input variables.

If the value of n is increased to 2.4, the uncertainty values change, and the results are shown in Figure 3.5. The maximum contribution for the n term is decreased, and the PLR at which the maximum occurs shifts to the right. The contribution from the PLR term increases at the larger values of PLR, however.

Figure 3.6 shows the total uncertainty in F, given the assumed inputs listed. The total uncertainty using $n = 2$ and $n = 2.4$ are both plotted. At all levels of part load, the estimated uncertainty in the fraction of full load power is less than 0.1.

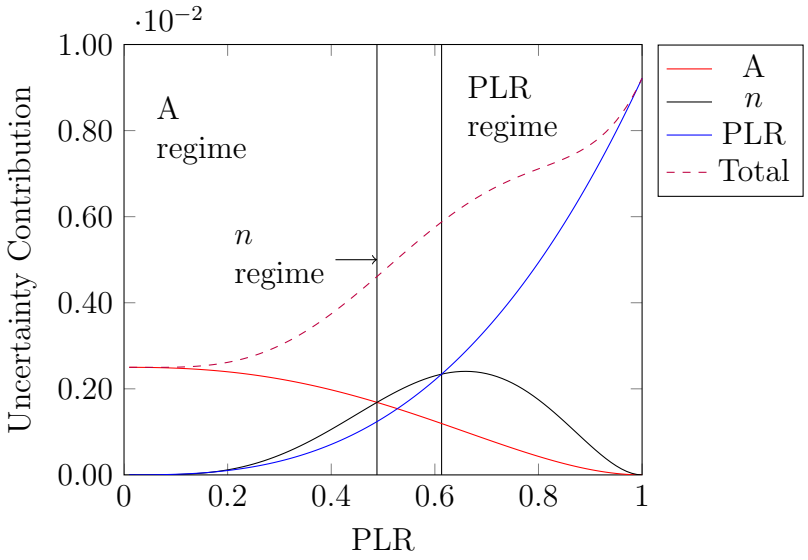

Figure 3.5: Relative uncertainty contributions for fraction of full load fan power when $n = 2.4$. ($A = 0.2$, $\delta A = 0.05$, $n = 2.4$, $\delta n = 0.04$, $\delta \text{PLR} = 0.05$)

If all the individual uncertainties are reduced by half, the total uncertainty will also be reduced by half. This would be feasible with trend data regarding the individual fan powers, flow, and pressures. This would put the maximum uncertainty in F to about 0.04.

3.3 Fan Modeling

Fan energy is a significant component of the air side energy use for air conditioning. Ideally, fan static pressure, flow, speed, and power would all be measured. The total primary air flow can either be measured directly (ideal) or estimated from the sum of the terminal unit flows. With this information, a complete set of fan curves can be created.

Without all these sensors it is difficult to create a first-principle based model of the air-side equipment. Statistical techniques would be necessary to relate the speed of the fan, $\dot{N}$, and the damper positions, $X_{i,damper}$.

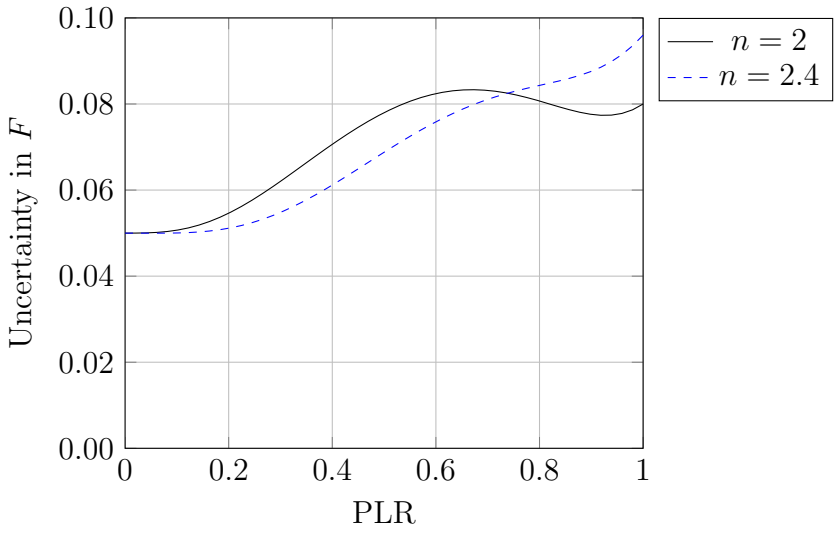

Figure 3.6: Total uncertainty in the fraction of full load fan power, F.

3.3.1 Air Distribution Modeling: First Method

This section is a bit of an aside and is presented to show the negative result given the following setup.

Estimating the system pressure loss for particular conditions is necessary for determining the potential fan energy at different speeds. The node layout of the terminal units will need to be created. If the air flow through each terminal unit is measured, the flow through each portion of the duct work can be estimated.

The first methodology developed attempted to break the air side pressure drops into parts for the major losses within the duct work and the minor losses due to the dampers at the terminal unit.

The following assumptions were made:

- Constant friction factors
- Reference pressure of 0 at each zone

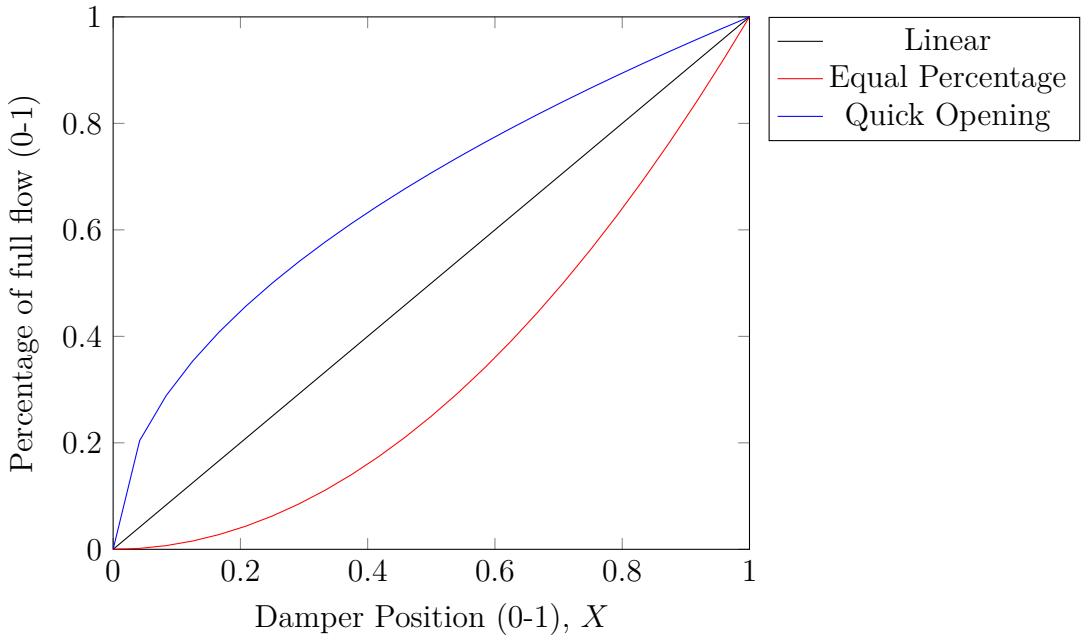

Figure 3.7: Terminal unit flow response as a function of damper position.

- Linear flow response from the damper position

With the assumption of the constant friction factor, the pressure drop in each duct section will be proportional to a constant and the flow through the section squared. Figure 3.7 shows the typical types of responses for a damper or valve.

Looking at the pressure drop through the dampers, at a given pressure drop, if the damper is fully open, "full flow" will result.

$$\Delta P_{\text{fan}} = C_{\text{full flow}} \left(\dot{V}_{\text{full flow}} \right)^2 \tag{3.24}$$

If $\dot{V}$ is reduced to some percentage of full flow, while keeping the same pressure drop then

$$\Delta P_{\text{fan}} = C_2 \left(\dot{V}_{\text{full flow}} \cdot \%_{\text{full flow}} \right)^2 \tag{3.25}$$

For a linear response

$$\%_{\text{full flow}} = X \tag{3.26}$$

If Equation 3.26 is substituted into Equation 3.25, and Equation 3.24 and 3.25 are set equal, then

$$C_{\text{full flow}} \left(\dot{V}_{\text{full flow}}\right)^2 = C_2 \left(\dot{V}_{\text{full flow}} \cdot X\right)^2 \tag{3.27}$$

The new loss coefficient is then

$$C_2 = \frac{C_{\text{full flow}}}{X^2} \tag{3.28}$$

and therefore has relationship to $1/X^2$. At $X = 0$, meaning the damper is closed, $C \to \infty$, as expected.

At any time, the pressure drop in all the flow loops must be equal. In a case where there are three terminal units, you would end up with relationships like the following

$$\Delta P_{fan} = C_1 \left(\dot{V}_1 + \dot{V}_2 + \dot{V}_3\right)^2 + \frac{C_2}{X_1^2}\dot{V}_1^2 \tag{3.29}$$

$$= C_1 \left(\dot{V}_1 + \dot{V}_2 + \dot{V}_3\right)^2 + C_3 \left(\dot{V}_2 + \dot{V}_3\right)^2 + \frac{C_4}{X_2^2}\dot{V}_2^2 \tag{3.30}$$

$$= C_1 \left(\dot{V}_1 + \dot{V}_2 + \dot{V}_3\right)^2 + C_3 \left(\dot{V}_2 + \dot{V}_3\right)^2 + C_5\dot{V}_3^2 + \frac{C_6}{X_3^2}\dot{V}_3^2 \tag{3.31}$$

With historical data, the terminal unit flows and the damper positions in the unit are known at each timestep. There are 3 equations with 6 unknowns (unknowns being C_1 through C_6), however, and the problem becomes underconstrained.

A calibration for the pressure drop coefficients is possible. If the sum of the standard deviations between the three equations is used to determine the goodness

of the calibration fit, then a trivial solution for a perfect fit arises. By setting all the coefficients besides the single shared major pressure loss coefficient C_1 to zero, the three equations will always be equal, and the total absolute pressure drop can be arbitrarily set with the single coefficient.

This method does have potential if the manufacturer's fan curves are available. While the loop pressure drop is normally not trended, the fan speed and flow is. Given the fan curves, the fan speed, and the total flow, the static pressure rise can be estimated, and used for all the ΔP_{fan} terms in Equation 3.29.

Without further information regarding the actual terminal unit pressure drop relationships, this method loses its potential usefulness. For this reason, a simple approach of using an exponential part load ratio (PLR) function was employed as shown in Equation 3.32. The value of n was varied from 2 to 3, and the sensitivity to this parameter was examined.

$$\dot{W}_{\text{fan}} = \dot{W}_{\text{des}} \left(\text{PLR}\right)^n \tag{3.32}$$

Later work also included a constant bias at zero load, having the form

$$\dot{W}_{\text{fan}} = \dot{W}_{\text{des}} \left(A + (1 - A) \, \text{PLR}^n\right) \tag{3.33}$$

3.4 Predicting the Mixed Air Temperature

The mixed air temperature is the third most common temperature sensor in air handling units based on the data available in Implementer (see Table 2.3). In most cases, the nearest neighbor approach can be applied directly to the mixed air temperature trend.

If a sensor is not available, it is possible to estimate the mixed air temperature

using an energy balance approach with the outdoor air temperature, return air temperature, and either measurements or estimation of the relative outdoor and return air flows.

3.5 Brute Force Approach

Since the system is not expected to determine semi-optimal control setpoints at small time intervals, say less than a second, it is plausible that a straightforward, brute-force approach would be appropriate to determine the optimal supply air temperature. The brute-force approach has several advantages including

1. Straightforward to program and debug

2. Robust to small changes in energy prediction algorithm

The uncertainty in the estimation of the zone loads, plenum temperatures, mixed air temperature, and the like, also tend to support the decision to use step sizes on the order of 0.1°F. The typical search range for the supply air temperature will be on the order of 20°F, making for a total number of calculations in the hundreds. This level of computation is feasible for modern computers to handle in the sub-second time range.

Some inputs for air handling units and terminal units need to be specified before determining the optimal supply air temperature. These inputs are listed in Table 3.1 and 3.2.

The algorithm described assumes series fan powered terminal units. For other types of terminal units, the method follows similarly.

1. Calculate discharge temperature for each terminal unit from

$$T_{dis} = T_z - \frac{\dot{Q}_z}{C_{air}\ \dot{V}_{z,tot}} \tag{3.34}$$

Table 3.1: Required inputs for air handling units.

Inputs for Air Handling Unit	Symbol	Coming From
Mixed Air Temperature	T_{ma}	Nearest Neighbor
Fan Exponent	n	Constant
Design Fan Power	$\dot{W}_{fan}$	Specifications
Design Fan Flow	$\dot{V}_{des}$	Specifications
Fan Curve Constant	A	Constant
Minimum Supply Air Temperature	$T_{sa,min}$	Constant

Table 3.2: Required inputs for terminal units.

Inputs for Terminal Units	Symbol	Coming From
Total Flow	$\dot{V}_{z,tot}$	Specifications
Minimum Flow	$\dot{V}_{pri,min}$	Constant
Zone Temperature	T_z	Nearest Neighbor
Plenum Temperature	T_{plen}	Constant
Zone Load	$\dot{Q}_z$	Nearest Neighbor

2. Calculate the maximum $T_{sa,max}$ for the search range as

$$T_{sa,max} = \text{MIN}\left(T_{ma}, \text{MIN}(T_{dis})\right) \tag{3.35}$$

The $T_{sa,max}$ cannot be greater than T_{ma} since it is assumed that only cooling is happening in the supply air duct after the mixing chamber. $T_{sa,max}$ cannot be greater than the minimum calculated discharge temperature because then that particular zone would not have sufficient cooling capacity.

3. For each T_{sa} ranging from $T_{sa,min}$ (which is chosen prior by the user) to the maximum $T_{sa,max}$ just calculated, using a reasonable step size (say 1/8°F), calculate the total power of the system using the following steps.

4. For each terminal unit, calculate the primary air flow required

$$\dot{V}_{pri,req} = \dot{V}_{z,tot} \left(\frac{T_{plen} - T_{dis}}{T_{plen} - T_{sa}} \right) \tag{3.36}$$

5. Calculate the actual primary airflow

$$\dot{V}_{pri} = \text{MAX} \left(\dot{V}_{pri,req}, \dot{V}_{pri,min} \right) \tag{3.37}$$

6. Calculate reheat power for each terminal unit using an energy balance

$$\dot{Q}_{reheat} = C_{air} \left(\dot{V}_{tot} T_{dis} - \dot{V}_{pri} T_{sa} - \dot{V}_{plen} T_{plen} \right) \tag{3.38}$$

7. Calculate cooling power using a cooling coil energy balance

$$\dot{Q}_{cooling} = \dot{V}_{supply}\, C_{air}\ (T_{ma} - T_{sa}) + h_v \rho_a \dot{V}_{supply}\ (\omega_{ma} - \omega_{sa}) \tag{3.39}$$

8. Calculate fan power using part load ratio curve

$$\dot{W}_{fan} = \left[A + (1 - A) \left(\frac{\dot{V}_{pri,tot}}{\dot{V}_{des}} \right)^n \right] \dot{W}_{fan,design} \tag{3.40}$$

9. Calculate total power

$$\dot{E}_{tot} = \dot{W}_{fan} + \dot{Q}_{cooling} + \dot{Q}_{reheat} \tag{3.41}$$

The brute-force approach was employed in the prototype code. In future implementations, improvements could be made to the optimization approach for improved performance.

Need the following information for the AHU
Data: T_{ma}, n, $\dot{W}_{fan,design}$, $\dot{V}_{des}$, A
For each terminal unit, will need the following information
Data: $\dot{V}_{z,tot}$, $\dot{V}_{pri,min}$, T_z, T_{plen}, $\dot{Q}_z$
Result: Optimal T_{sa}
for $T_{sa} \leftarrow T_{sa,min}$ **to** $T_{sa,max}$ **do**
    for $i \leftarrow 1$ **to** *number of terminal units* **do**
        Calculate $V_{pri,i}$ using Equation 3.37;
        Calculate $\dot{Q}_{reheat,i}$ using Equation 3.38;
    end
    Calculate total reheat power by summing all $\dot{Q}_{reheat,i}$;
    Calculate total primary flow, $\dot{V}_{supply}$ by summing all $\dot{V}_{pri,i}$;
    Calculate total cooling power from Equation 3.39;
    Calculate total fan power using Equation 3.40;
    Calculate total power using Equation 3.41;
end

Algorithm 1: Algorithm to determine optimal T_{sa}.

3.6 Determining the Supply Air Static Pressure Requirement

As shown in Section 3.3, building up a complete air flow model is challenging. A different approach is to reduce the number of parameters by focusing on the *critical zone*.

One method of determining the critical zone is to simply check the percentage of time that a particular damper is the most open. This check can occur over any period, for example, over the previous week, month, or 6 months.

At a particular static pressure, there should exist some relationship between the damper position and the flow through the terminal unit. For a conservative estimate of the maximum flow at a given static pressure, the measured values of flow at the 90% open damper position can be investigated.

In a live setting, if data does not exist for a particular static pressure setpoint, then the system can slowly begin to explore until the desired number of data points

Table 3.3: Necessary sensors.

Level	Sensor
Weather	Outdoor Air Temperature Outdoor Dew Point Temperature
AHU	Mixed Air Temperature
Terminal Units	Primary Air Flow Rate Discharge Air Temperature Zone Temperature

are available. For example, the system could reduce the static pressure setpoint in increments of 0.1" w.g.

3.7 Required Sensors

Table 3.3 lists the minimum set of sensors required. The discharge air temperature from terminal units is a required sensor that currently is the least likely to be available.

4. SIMPLIFIED EXAMPLE

This section serves to show a simplified example of the optimization of the supply air temperature under one given condition. The single example is studied in detail to elucidate the various competing components impacting the total power required to satisfy the building loads.

For simplicity, a single duct variable air volume system with two terminal units is assumed. Hot and dry outdoor air conditions are assumed such that both zones are under a cooling load and there are no latent load concerns.

Zone 1 is assumed to have a load of 20,000 $\frac{\text{BTU}}{\text{h}}$, while the load in Zone 2 is 7,344 $\frac{\text{BTU}}{\text{h}}$.

The minimum flow setting for the terminal units is 400 CFM. The room temperature is 72°F and the mixed air temperature is 80°F.

The fan is assumed to have the following part-load behavior described in Equation 4.1. The design flow is chosen so that at a supply temperature of 65°F the fan is at design flow.

The design power is chosen so that at the calculated design flow, the efficiency is 0.8 and the pressure rise is 4 in.w.g.. Under the chosen conditions, the design flow is 3,503 CFM, which is the resulting flow under the highest tested supply air temperature 65°F. The resulting design fan power is 2.75 hp.

$$\text{FFLP} = A + (1 - A)\,(\text{PLR})^n = 0.1 + (0.9)(\text{PLR})^{2.5} \tag{4.1}$$

The fan power is

$$\dot{W}_{fan} = \text{FFLP}\ \dot{W}_{des} = \text{FFLP}\,(2.75\,\text{hp}) \tag{4.2}$$

Table 4.1: Summary of parameters used for simplified example.

Parameter	Value
System Type	SDVAV
Mixed air temperature	80°F
Zone temperature	72°F
Zone 1 Cooling Load	20,000 $\frac{\text{BTU}}{\text{h}}$
Zone 2 Cooling Load	7,344 $\frac{\text{BTU}}{\text{h}}$
Design fan efficiency	0.80
Design fan pressure rise	4 in.w.g.
Design fan power	2.75 hp
Fan exponent, n	2.5

The required flow for each zone is calculated as

$$\dot{V}_z = \text{MAX}\left(\frac{\dot{Q}_z}{C_a\left(T_z - T_{sa}\right)}, \dot{V}_{min}\right) \tag{4.3}$$

The discharge temperature for each zone is

$$T_{dis} = T_z - \frac{\dot{Q}_z}{C_a\,\dot{V}_z} \tag{4.4}$$

The reheat power is

$$\dot{Q}_{reheat} = C_a \dot{V}_z \left(T_{dis} - T_{sa}\right) \tag{4.5}$$

and the sensible cooling power is

$$\dot{Q}_{cool} = C_a \dot{V}_{tot} \left(T_{ma} - T_{sa}\right) \tag{4.6}$$

where $\dot{V}_{tot}$ is the total flow for all the zones.

Increasing the supply air temperature has the effect of decreasing reheat and increasing fan power. Whether the cooling load increases or decreases depends on

several factors.

For example, during times when there is no reheat, the required flow for the terminal units is

$$\dot{V}_{req} = \frac{\dot{Q}_z}{C_a \left(T_z - T_{sa}\right)} \tag{4.7}$$

Substituting Equation 4.7 into Equation 4.6 results in

$$\dot{Q}_{cool} = C_a \frac{\dot{Q}_z}{C_a \left(T_z - T_{sa}\right)} \left(T_{ma} - T_{sa}\right) = \dot{Q}_z \frac{T_{ma} - T_{sa}}{T_z - T_{sa}} \tag{4.8}$$

Of interest is how the sensible cooling power is impacted when the supply air temperature is increased. To investigate, the derivative of the sensible cooling power equation is found.

$$\frac{\mathrm{d}\dot{Q}_{cool}}{\mathrm{d}T_{sa}} = \dot{Q}_z \frac{T_{ma} - T_z}{\left(T_z - T_{sa}\right)^2} \tag{4.9}$$

What Equation 4.9 shows is the non-intuitive result that during times of cooling (corresponding to a positive $\dot{Q}_z$) and when the mixed air temperature is greater than the zone temperature (corresponding to a positive value in the numerator of Equation 4.9), that the sensible cooling power *increases* with increasing supply air temperature. If a cooling load exists and the mixed air temperature is less than the zone temperature, then the opposite is true, increasing the supply air temperature will reduce the required sensible cooling power.

Figure 4.1 shows how the supply air flow changes with regards to the supply air temperature. The zone loads were chosen in such a way that Zone 1 operates above the minimum flow setpoint at all times, while Zone 2 is at the minimum flow setpoint at supply air temperatures less than 57°F. The system uses reheat at supply air temperatures less than 57°F.

With the selected system parameters, the total steady state power can be plotted with respect to the supply air temperature. The total power function ends up being convex with a minimum at 57°F.

What is important is the fact that the optimum supply air temperature is not simply the maximum supply air temperature in the search range. Under conditions such as the one in the first example, there is a competing balance between the cooling, reheat, and fan power. It is possible that the optimization will potentially suggest lowering the supply air temperature when the conditions are appropriate.

This conclusion is affirmed as well after investigating the impact of energy cost. The following analysis assumes the fan power uses electricity, the cooling is from district chilled water, and the reheat is from district hot water, and the prices are those from the posted Texas A&M Utilities and Energy Services rates for FY2016[1]. The rates are

- Electricity – \$0.082/kWh ≈ \$24/MMBTU
- Chilled Water – \$15.25/MMBTU
- Hot Water – \$15.03/MMBTU

When the cost of electricity is taken into account, the importance of the relationship between fan power and the supply air temperature is increased. Chilled water is usually produced with a chiller having a COP greater than 3 while the electricity is consumed directly for the fan. When the impact of cost is added, the cost penalty for fan power can grow significantly at higher supply air temperatures, which can be seen in Figure 4.3.

[1]https://utilities.tamu.edu/2015/08/31/cost-and-fees-for-utility-services-fy2016/

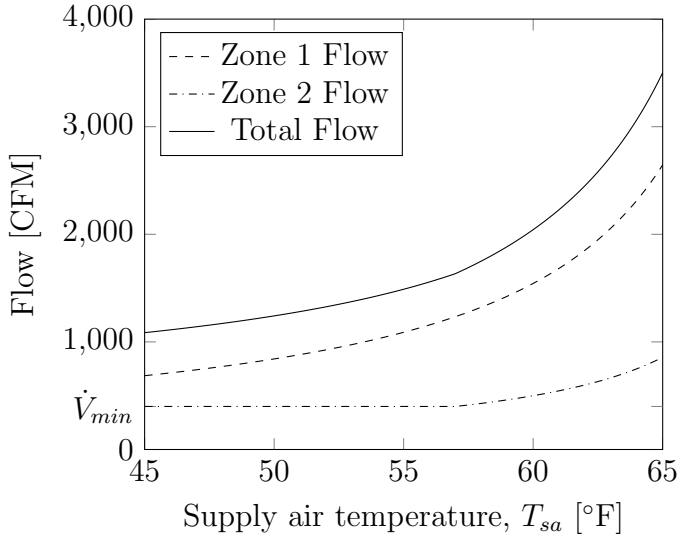

Figure 4.1: Variation of required air flow with respect to different supply air temperatures.

With cost as the optimization function, the optimal supply air temperature is reduced from 57°F to 56.7°F because of the higher price of electricity as compared to the district chilled water and hot water price.

If the mixed air temperature is reduced from 80°F to 65°F, the resulting total power function changes drastically. The required flow rates for each of the zones remains the same, along with the fan power and the reheat power. Since the mixed air temperature is less than the zone temperature, the slope of the sensible cooling power function is always negative, since the numerator in Equation 4.9 is negative. The result of this is that the minimum total power occurs at the maximum of the supply air temperature search range.

4.1 Function Analysis

While attempting to optimize an AHU system, it is helpful to understand how the supply temperature affects all portions of the total power. The analysis in this

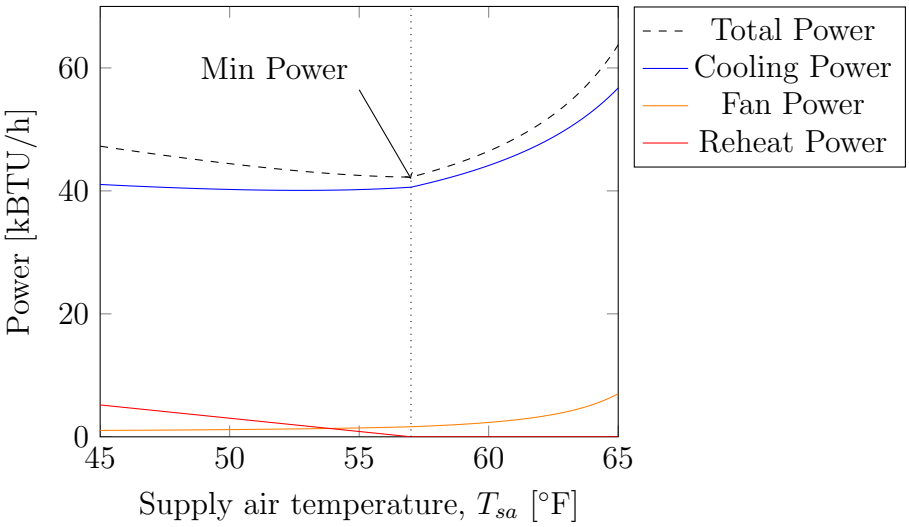

Figure 4.2: Variation of total power with respect to different supply air temperatures, using 80°F as the mixed air temperature.

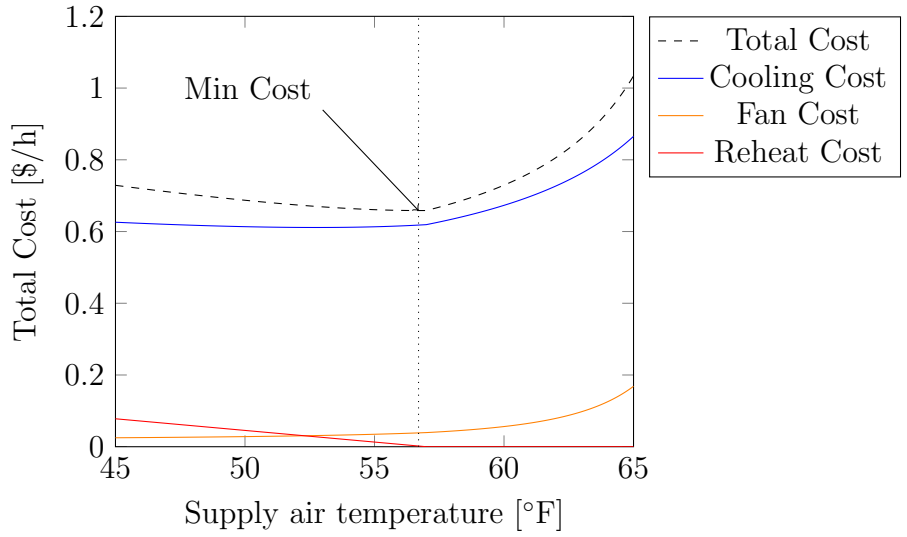

Figure 4.3: Variation of total cost with respect to different supply air temperatures, using 80°F as the mixed air temperature.

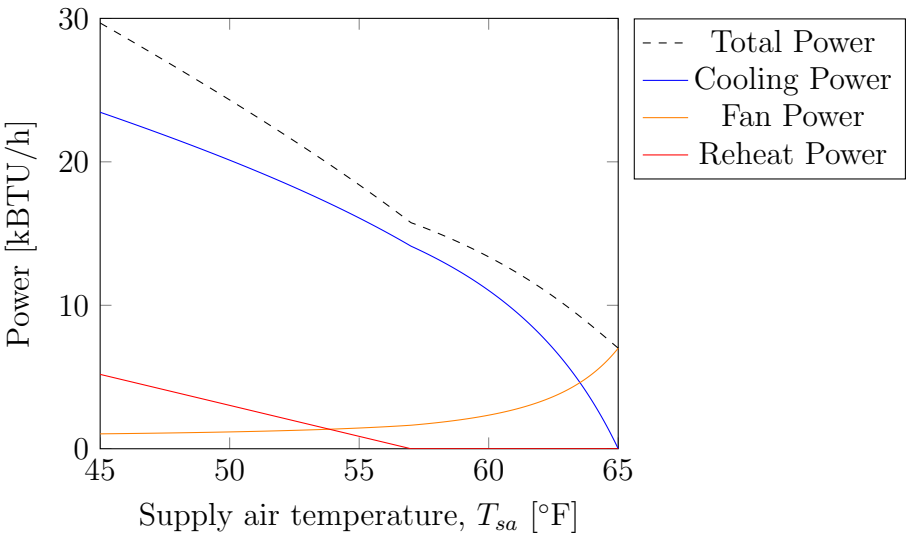

Figure 4.4: Variation of total power with respect to different supply air temperatures, with a mixed air temperature of 65°F instead of the original 80°F.

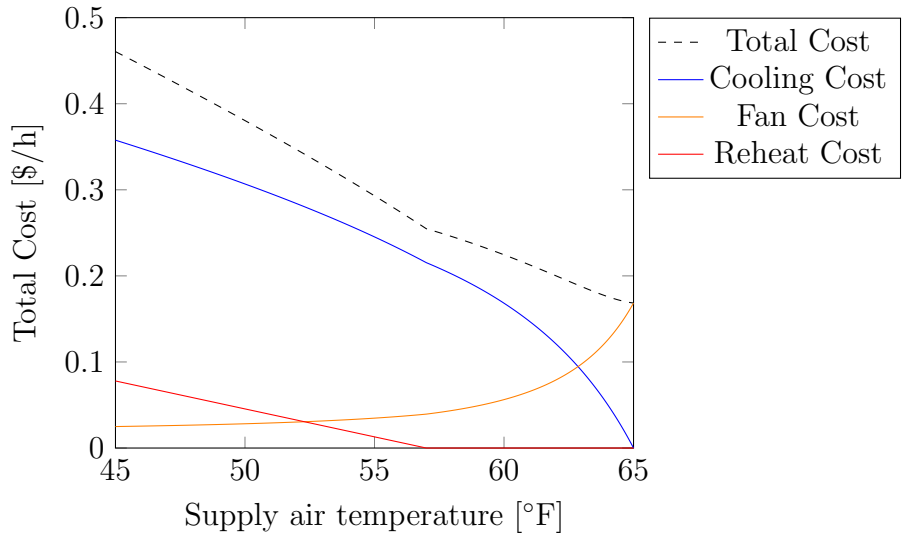

Figure 4.5: Variation of total cost with respect to different supply air temperatures, with a mixed air temperature of 65°F instead of the original 80°F.

section relates to a simplified single duct variable air volume system, with terminal units having a traditional control sequence, initiating reheat at a constant minimum flow.

The investigation is going to assume that at a given supply air temperature, a certain amount of terminal units are going to be in reheat mode, operating at minimum flow, while the others are operating in cooling mode. The total flow for the system is then

$$\dot{V}_{tot} = \dot{V}_{min,1} + \dot{V}_{min,2} + \ldots + \frac{\dot{Q}_{z,3}}{C_a \left(T_{z,3} - T_{sa}\right)} + \frac{\dot{Q}_{z,4}}{C_a \left(T_{z,4} - T_{sa}\right)} + \ldots \tag{4.10}$$

If the zone temperatures, T_z are all the same, then the terms related to zones in cooling can be combined. All the flows related to the zones operating at minimum flow can also be combined.

$$\dot{V}_{tot} = \sum \dot{V}_{mins} + \frac{\sum \dot{Q}_{z,tot}}{C_a \left(T_z - T_{sa}\right)} \tag{4.11}$$

For clarity, for the rest of the derivations, the sum will be assumed, and the system can just be imagined as a combined, two terminal unit system, in which one of the units is operating at minimum flow and the other terminal unit is in cooling mode.

4.1.1 Sensible Cooling Power

The total sensible cooling power, $\dot{Q}_{c,s}$, is

$$\dot{Q}_{c,s} = C_a \dot{V}_{tot} \left(T_{ma} - T_{sa}\right) \tag{4.12}$$

where $\dot{V}_{tot}$ is

$$\dot{V}_{tot} = \dot{V}_{min} + \frac{\dot{Q}_z}{C_a \left(T_z - T_{sa}\right)} \tag{4.13}$$

There are two different assumptions that can be made relating to the outside air flow. The first assumption is that the outside air flow is constant, while the second assumption is that the fraction of outside air is constant.

4.1.1.1 Constant Outside Air Flow

If the amount of outside air flow is constant at $\dot{V}_{oa}$, and the return air temperature is assumed to be equal to the zone temperature, then the mixed air temperature can be estimated as

$$T_{ma} = \frac{T_{oa}\dot{V}_{oa} + \left(\dot{V}_{tot} - \dot{V}_{oa}\right) T_z}{\dot{V}_{tot}} \tag{4.14}$$

Substituting Equation 4.14 into 4.12 results in

$$\dot{Q}_{c,s} = C_a \dot{V}_{tot} \left[\frac{T_{oa}\dot{V}_{oa} + \left(\dot{V}_{tot} - \dot{V}_{oa}\right) T_z}{\dot{V}_{tot}} - T_{sa} \right] \tag{4.15}$$

Rearranging results in

$$\dot{Q}_{c,s} = C_a \left[\dot{V}_{oa} \left(T_{oa} - T_z\right) + \dot{V}_{tot} \left(T_z - T_{sa}\right) \right] \tag{4.16}$$

When $\dot{V}_{tot}$ is replaced with Equation 4.13, the $(T_z - T_{sa})$ term cancels out, and the final form for $\dot{Q}_{c,s}$ is

$$\dot{Q}_{c,s} = \dot{Q}_z + C_a \dot{V}_{oa} \left(T_{oa} - T_z\right) + C_a \dot{V}_{min} \left(T_z - T_{sa}\right) \tag{4.17}$$

The portion of Equation 4.17 that depends on the supply air temperature is related to the minimum flow, or the zones that are in reheat. If no zones were in reheat, then the sensible cooling power would not depend on the supply air temperature.

The derivative of Equation 4.17 is

$$\frac{\mathrm{d}\dot{Q}_{c,s}}{\mathrm{d}T_{sa}} = -C_a\dot{V}_{min} \tag{4.18}$$

which means that the sensible cooling power decreases as the supply air temperature is raised at a constant slope.

4.1.1.2 Constant Outside Air Fraction

If the percentage of outside air is held constant instead of the flow, the analysis of the sensible cooling load changes. If the outside air fraction, X_{oa} is constant, and the return air temperature is assumed to be equal to the zone temperature, an estimation of the mixed air temperature is

$$T_{ma} = T_z + X_{oa}\left(T_{oa} - T_z\right) \tag{4.19}$$

Substituting Equation 4.19 into 4.12 and expanding $\dot{V}_{tot}$ results in

$$\dot{Q}_{c,s} = C_a\left[\dot{V}_{min} + \frac{\dot{Q}_z}{C_a\left(T_z - T_{sa}\right)}\right]\left[T_z + X_{oa}\left(T_{oa} - T_z\right) - T_{sa}\right] \tag{4.20}$$

Taking the derivative of Equation 4.20 with respect to T_{sa} results in

$$\frac{\mathrm{d}\dot{Q}_{c,s}}{\mathrm{d}T_{sa}} = \frac{\dot{Q}_z(T_{oa} - T_z)X_{oa}}{(T_{sa} - T_z)^2} - C_a\dot{V}_{min} \tag{4.21}$$

If the outdoor air temperature is less than the zone temperature, the numerator of the first term becomes negative and the second term is always negative, so $\frac{\mathrm{d}\dot{Q}_{c,s}}{\mathrm{d}T_{sa}}$ will be negative. $\dot{Q}_z$ is assumed to be a cooling load and therefore is always a positive value.

A negative slope for $\frac{\mathrm{d}\dot{Q}_{c,s}}{\mathrm{d}T_{sa}}$ implies that the total sensible cooling power decreases

as the supply air temperature is raised. However, if the outdoor air temperature is greater than the zone temperature, and the magnitude of the first term is greater than the contribution from the second term relating to the terminal units that are in reheat, this slope can become positive, implying the opposite case. This is similar to the case described at the beginning of this section.

The second derivative of the function is taken to determine the curvature of the function. Taking the derivative of Equation 4.21 results in

$$\frac{\mathrm{d}^2\dot{Q}_{c,s}}{\mathrm{d}{T_{sa}}^2} = \frac{2\dot{Q}_z\left(T_{oa} - T_z\right)X_{oa}}{\left(T_z - T_{sa}\right)^3} \tag{4.22}$$

The sign of $\frac{\mathrm{d}^2\dot{Q}_{c,s}}{\mathrm{d}{T_{sa}}^2}$ is solely determined by the sign of $(T_{oa} - T_{sa})$ since $\dot{Q}_z$ is positive and $T_z > T_{sa}$. This means that if the outdoor air temperature is greater than the zone temperature, there can be a power penalty for raising the supply air temperature, and this penalty gets worse as the supply air temperature is increased.

4.1.2 Latent Cooling Power

The total latent cooling power, $\dot{Q}_{c,l}$, is

$$\dot{Q}_{c,l} = H\left(\dot{V}_{min} + \frac{\dot{Q}_z}{C_a\left(T_z - T_{sa}\right)}\right)\left(\omega_{ma} - \omega_{sa}\right) \tag{4.23}$$

where H is a volumetric heat of vaporization for water and ω_{sa} is the saturation humidity ratio at a given supply air temperature, which means that it is a function of the supply air temperature. For this analysis it is assumed that a latent load does exist and $\omega_{ma} > \omega_{sa}(T_{sa})$. If $\omega_{sat}(T_{sa}) > \omega_{ma}$, then the latent load is zero and all its derivatives are zero as well.

Taking the derivative of Equation 4.23 results in

$$\frac{\mathrm{d}\dot{Q}_{c,l}}{\mathrm{d}T_{sa}} = \frac{H\dot{Q}_z\left(\omega_{ma} - \omega_{sa}\right)}{C_a(T_z - T_{sa})^2} - H\frac{\mathrm{d}\omega_{sa}}{\mathrm{d}T_{sa}}\left(\frac{\dot{Q}_z}{C_a(T_z - T_{sa})} + \dot{V}_{min}\right) \tag{4.24}$$

At this point, it is helpful to examine the relationship between the saturated humidity ratio versus temperature.

As a useful approximation, the relationship between the saturation humidity ratio and temperature can be described by a third order polynomial in a restricted range. Over the range of 20°F to 110°F, the saturation humidity ratio at sea level pressure can be approximated by

$$\begin{aligned}\omega_{sa} = {} & \left(8.0635 \times 10^{-8}\right) T^3 \\ & - \left(7.2284 \times 10^{-6}\right) T^2 + \left(3.8451 \times 10^{-4}\right) T \\ & - 3.5876 \times 10^{-3}\end{aligned} \tag{4.25}$$

where T is in units of °F. The maximum absolute error in this range is approximately 0.00058787 and the median absolute deviation is 0.000164. A plot of the fit versus the more explicit computation is shown in Figure 4.6. The first and second derivative of ω_{sa} is shown in Figure 4.7 and Figure 4.8. It is clear that the first derivative is always positive and the second derivative is positive after 30°F.

With this information about the derivatives of the saturation humidity ratio, it's clear that the first term in Equation 4.24 is positive, while the second term is negative. Through experimentation with typical values for the parameters, this results in a negative slope.

The second derivative of the saturation humidity ratio with respect to supply air

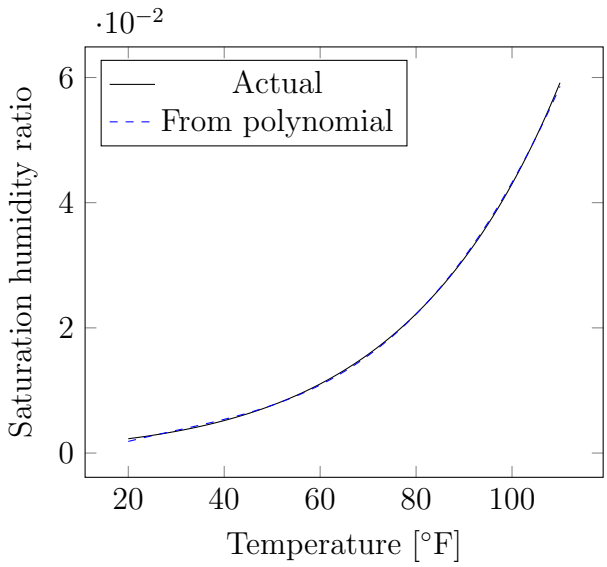

Figure 4.6: Saturation humidity ratio versus temperature.

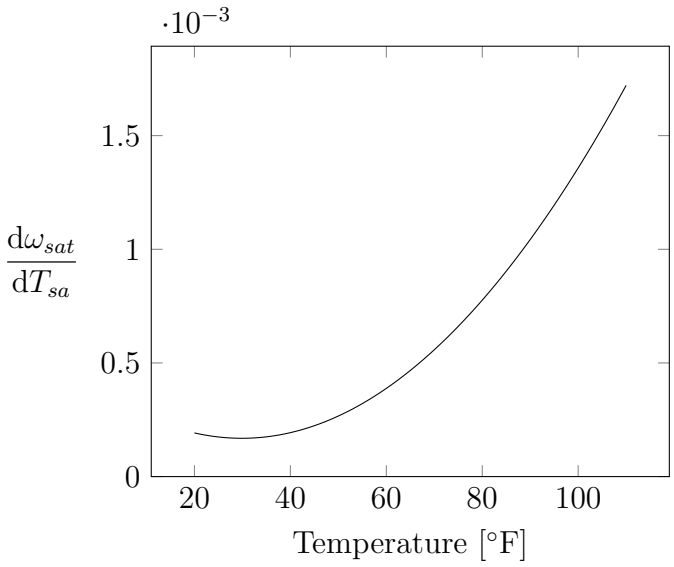

Figure 4.7: First derivative of the saturation humidity ratio versus temperature.

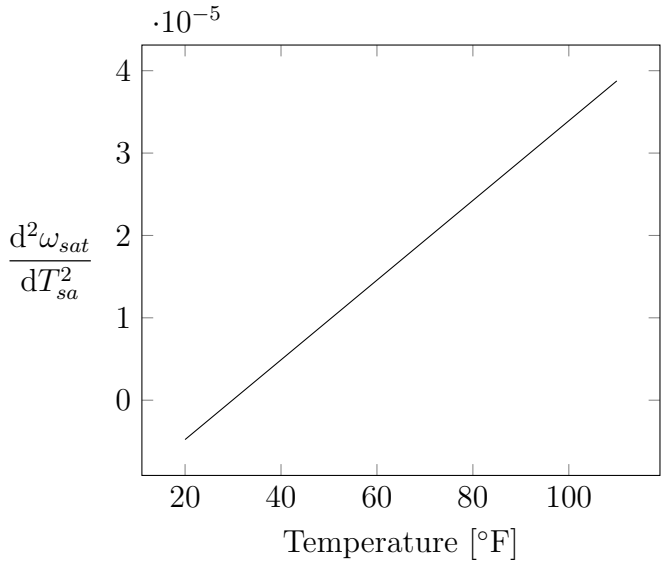

Figure 4.8: Second derivative of the saturation humidity ratio versus temperature.

temperature is

$$\frac{\mathrm{d}^2\dot{Q}_{c,l}}{\mathrm{d}{T_{sa}}^2} = -H\frac{\mathrm{d}^2\omega_{sa}}{\mathrm{d}{T_{sa}}^2}\left(\frac{\dot{Q}_z}{C_a(T_z - T_{sa})} + \dot{V}_{min}\right) + \frac{2H\dot{Q}_z(\omega_{ma} - \omega_{sa})}{C_a(T_z - T_{sa})^3} - \frac{2H\dot{Q}_z\frac{\mathrm{d}\omega_{sa}}{\mathrm{d}T_{sa}}}{C_a(T_z - T_{sa})^2} \tag{4.26}$$

From inspection, it is difficult to discern whether this second derivative is typically positive or negative. From experimentation it has been found that this value is typically negative, resulting in rapidly increasing savings with regards to the latent cooling power by increasing the supply air temperature.

4.1.3 Fan Power

The total fan power is

$$\dot{W}_{fan} = \left(A + (1 - A)\left(\frac{\dot{V}_{min} + \frac{\dot{Q}_z}{C_a(T_z - T_{sa})}}{\dot{V}_{des}}\right)^n\right)\dot{W}_{des} \tag{4.27}$$

The first derivative of the fan power with respect to supply air temperature is

$$\frac{\mathrm{d}\dot{W}_{fan}}{\mathrm{d}T_{sa}} = \frac{(1-A)n\dot{Q}_z\dot{W}_{des}\left(\frac{\frac{\dot{Q}_z}{C_a(T_z-T_{sa})}+\dot{V}_{min}}{\dot{V}_{des}}\right)^{n-1}}{C_a\dot{V}_{des}(T_z-T_{sa})^2} \tag{4.28}$$

or replacing with the definition of the part load ratio (PLR),

$$\frac{\mathrm{d}\dot{W}_{fan}}{\mathrm{d}T_{sa}} = \frac{(1-A)n\dot{Q}_z\dot{W}_{des}\,(\mathrm{PLR})^{n-1}}{C_a\dot{V}_{des}(T_z-T_{sa})^2} \tag{4.29}$$

The first derivative is always positive, as expected. As the supply air temperature is increased, it will require an increase in fan power.

The second derivative of fan power with respect to supply air temperature is

$$\frac{(1-A)\,n\dot{Q}_z\dot{W}_{des}\left(2C_a\dot{V}_{min}(T_z-T_{sa})+(n+1)\dot{Q}_z\right)\left(\frac{\frac{\dot{Q}_z}{C_a(T_z-T_{sa})}+\dot{V}_{min}}{\dot{V}_{des}}\right)^{n}}{(T_z-T_{sa})^2\left(C_a\dot{V}_{min}\,(T_z-T_{sa})+\dot{Q}_z\right)^2} \tag{4.30}$$

While Equation 4.30 is complicated and has many terms, it is strictly positive, which means that the fan power penalty from raising the supply air temperature increases with increasing supply air temperature, an expected result.

4.1.4 Reheat Power

Of the four major components (sensible cooling, latent cooling, fan, and reheat), reheat power is the most straightforward to analyze. The total reheat power has contributions from only the zones that are at minimum flow and is equal to

$$\dot{Q}_r = C_a\dot{V}_{min}\,(T_{dis}-T_{sa}) \tag{4.31}$$

The required discharge temperature is

$$T_{dis} = T_z - \frac{\dot{Q}_z}{C_a \dot{V}_{min}} \tag{4.32}$$

Substituting the equation for T_{dis} into the total reheat power equation results in

$$\dot{Q}_r = C_a \dot{V}_{min} \left(T_z - \frac{\dot{Q}_z}{C_a \dot{V}_{min}} - T_{sa} \right) \tag{4.33}$$

The derivative of the reheat power with respect to the supply air temperature is just

$$\frac{\mathrm{d}\dot{Q}_r}{\mathrm{d}T_{sa}} = -C_a \dot{V}_{min} \tag{4.34}$$

and the second derivative is 0.

As expected, when the supply air temperature is raised, the reheat power decreases, and this decrease is linear, different from the other components which have had a non-zero second derivative, implying curvature.

4.1.5 Summary

The following derivations were for a simplified model of a single duct variable air volume system. The zone temperatures from each zone were assumed to be equal which allowed for the zones in reheat and the zones not in reheat to be combined. The traditional control sequence analyzed here is also falling out of favor, with dual-maximum logic becoming more popular. The analysis is also only valid as long as a box does not transition from cooling to reheat in the span of supply air temperatures analyzed.

Even with these simplifications, it is clear that analytically solving for the optimal supply air temperature using traditional calculus techniques would be a difficult

endeavor. Even in the simplified model, there are many interactions between the four major contributors to energy use. The exercise showed that fan, reheat, and latent portions have a straightforward dependence on the supply air temperature. However, it was shown that the sensible cooling power can have its relationship flipped depending on the relationship between the mixed air temperature and the zone temperatures.

5. TECHNOLOGY SETUP

A major driving principle of the presented work is that the methodology needs to be scalable. One reason for difficulties in implementing fault detection and diagnostic algorithms and other optimization methods is that there is a significant amount of initial investment necessary, in time, risk, and money.

In more complex schemes, it may be necessary to install additional sensors that are typically not available in commercial HVAC systems. Along with the sensor cost, there is the cost to configure the sensors into the BAS. The updated logic will likely be coded by a controls contractor, adding more cost. On a large campus, this reprogramming can also take a significant amount of time to complete.

Another issue is that of risk. There is the risk that if the controls do not function properly and are too complex for the current building operator, the controls cannot be easily removed and set back to the previous state.

5.1 Proposed Setup

In the proposed setup, the change to the existing BAS is minimal. The control logic remains the same. A small executable script can be installed on the BAS computer that can host code that will send an HTTP request to a remote server holding the historical data and the optimization methods.

Figure 5.1 shows potential information flow. Over any period, historical trend data coming from the building or buildings are stored in a server. This data sync may only happen once, weekly, daily or even sub-daily. Once enough data has been stored on the server, a client BAS computer (potentially one of many) can make an HTTP request that will essentially carry information related to the current time and what equipment the request corresponds to. Each AHU will have a unique identifier

that the main web server understands.

The web server will implement the methods described in this document and will send a response back to the client with the *setpoint values* for the system that will be near-optimal in a steady-state sense, given the expected conditions at the building and individual zones.

5.1.1 Standards for Transmission

Standards for the format of information transfer are critical for rapid adoption. An Application Program Interface (API) is the public interface of methods and routines that allow third-party programmers to develop programs from the base building blocks.

Another important point of consideration is the format of the data being transferred. In the software industry, there are several types of data exchange formats, two popular ones being JavaScript Object Notation (JSON) and Extensible Markup Language (XML). The advantage of JSON over XML is that JSON requires fewer characters to describe simple objects, though, it does not support explicit schema definition.

5.1.2 Advantages to Proposed System

There are several key advantages to a system similar to the proposed:

1. No real-time data transmission. Managing the networking of large BAS systems is difficult enough as is. It is not feasible for a single server to handle live streams of BAS point information from thousands of buildings.

2. The system can be added or removed quickly and without side-effects. Because the logic lives at an abstraction level above the BAS code, no changes to the system need to be made locally.

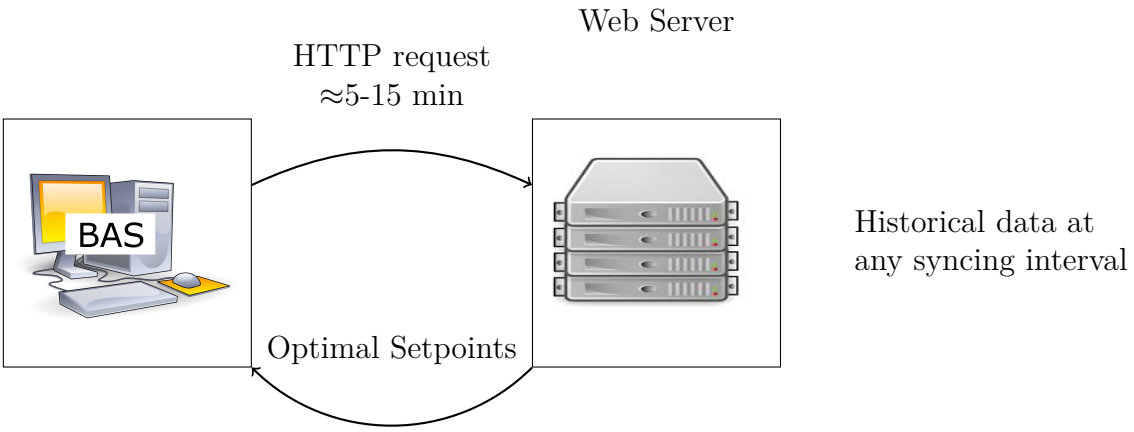

Figure 5.1: Diagram of networking flow.

3. Routines only have to be added once for different equipment and setup types, allowing the same methods to expand to many different buildings.

5.2 Prototype Information

The proposed system was implemented in the software tool *Implementer*, a web application developed at the Energy Systems Laboratory at Texas A&M University. Implementer can analyze trend data from any system that has an ability to store timestamp-value pairs and allow access to them. Various terms specifically related to Implementer are described in Table 5.1.

The current systems supported by Implementer include:

- Alerton
- Andover Continuum
- Automated Logic
- Delta Controls Historian
- Emerson Ovation

Table 5.1: Terms specific to Implementer.

Term	Description
Project	Information typically related to a collection of buildings
Label	A known sensor type that can be associated with a trend, also called a tag by other software
Container	An item that has a collection of trends associated, usually corresponding to a piece of equipment. Containers are set up into a tree structure with parent-child relationships, for example, a container representing an AHU would be a *parent* container to a terminal unit.

- Honeywell Hoboware
- Johnson Controls Metasys
- Reliable Controls
- Siemens APOGEE
- TAC I/NET Seven
- TAC I/A Series
- Trane Tracer
- Tridium Niagara

Before this process can begin, the sensors need to be mapped in a way that the server can understand.

In Implementer, trends are given meaning through the use of *Labels*. Labels are similar to the concept of tagging that is used in other systems, such as a system that implements Project Haystack.

Implementer stores data in *projects*. A project typically is a collection of buildings from a campus, but could be a single building.

Trends can receive labels in several ways. For trends in air handling units, the label can automatically be derived from the type of sensor and location on a schematic. A screenshot of a sample schematic from the NCTM project is shown in Figure 5.2. The different types of equipment such as fans, coils, and temperature sensors are placed on the schematic and are associated with an actual sensor. For example, a temperature sensor that is at the outlet of the air handling unit, unaffected by any other temperature affecting device, is defined to have the *supply air temperature* label.

Labels can also be created manually. Figure 5.3 shows a screenshot of how all the real *AUX TEMP* trends from the different fan powered VAV (FPVAV) units at the case study NCTM building are labeled as *DischargeTemps*.

An entire site or building is organized into a hierarchy of components. Each component is related to a *container*, which trends can be associated with. A building container is a parent to air handling unit containers, and air handling unit containers are parents to terminal unit containers. Figure 5.4 shows a screenshot of a portion of the container hierarchy for the NCTM project. Each line in Figure 5.4 is a different container. The indentation indicates the relationships. By organizing trends into containers which have parent-child relationships, along with labeling, automated algorithms and analysis can easily be set up.

To execute the optimization, the inputs and functions for the various trends need to be set up. It is proposed that the use of a container hierarchy, labels or tags, and custom equations be used to develop the system.

Implementer uses something called container properties, and one of the properties can be set to a JSON object that contains all the necessary pointers to values or custom equations.

The necessary inputs for the AHU container would be

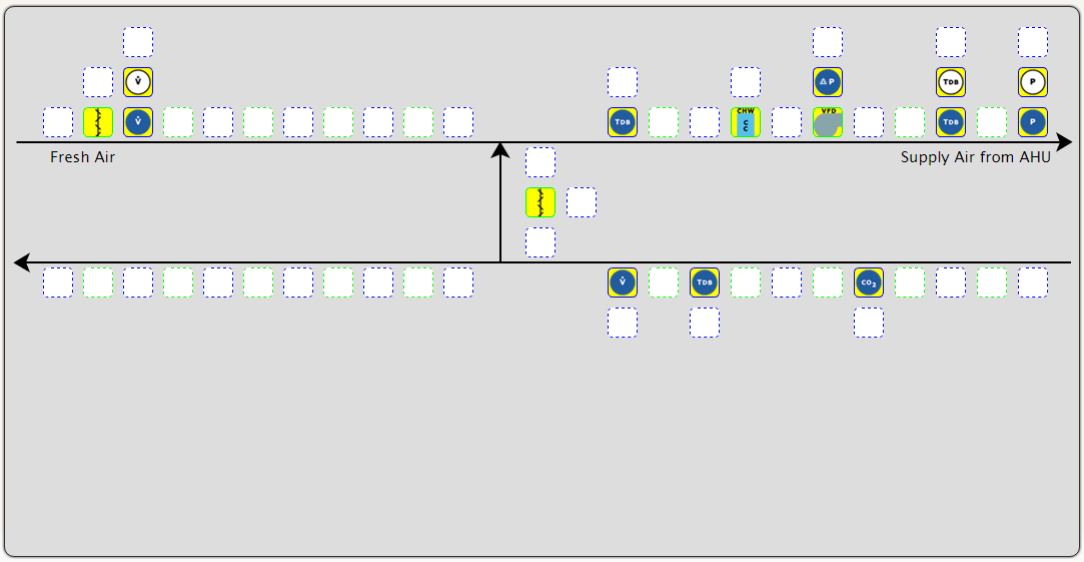

Figure 5.2: Screenshot of a sample AHU schematic for AHU-2-2 in the NCTM building in Implementer.

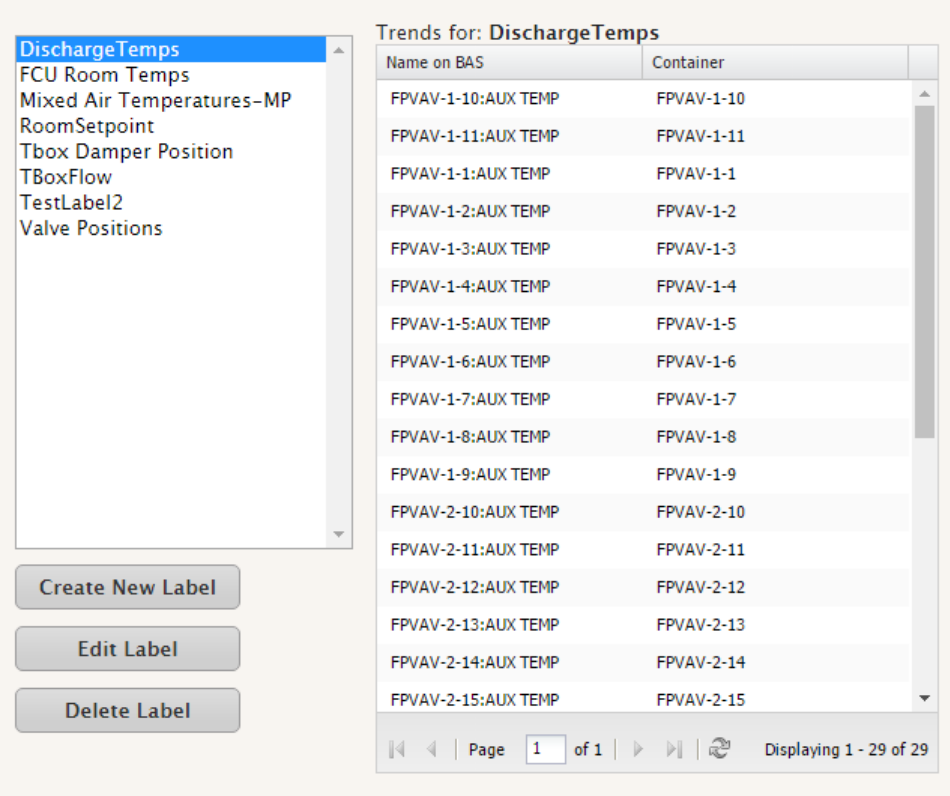

Figure 5.3: Screenshot of the custom labels setup in Implementer, showing how all *AUX TEMP* trends are associated to the label *DischargeTemps*.

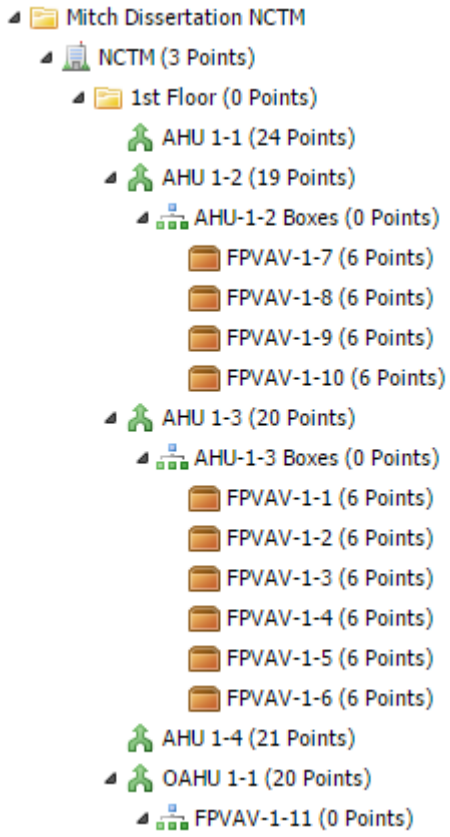

Figure 5.4: Screenshot of the container hierarchy for NCTM in Implementer.

1. Prediction function for T_{ma}
2. Design AHU flow
3. Exponent for the fan curve, n
4. Fan curve constant, A
5. Design fan power $\dot{W}_{des}$
6. Maximum supply humidity ratio
7. Minimum outdoor air flow percent

For the terminal units, if a series fan powered terminal unit is assumed, the necessary inputs will be

1. Design flow
2. Minimum flow percent
3. Prediction function for zone temperature setpoint.
4. Prediction function for zone load.
5. Prediction function for plenum temperature.

Parameters needed for the optimization are input for each container in the container details portion of Implementer. The settings are formatted in JSON, as shown in Figure 5.5. The properties include options such as pointers to how the mixed air temperature should be calculated, the maximum supply humidity ratio, and the assumed part load ratio fan exponent.

```
OptSATGenPoint =
{"MATPrediction":"MAT Prediction",
"VDesign":"VDesign",
"FanExponent":2,
"WDesign":"WDesign",
"MaxHumidityRatio":0.009,
"Name":"Optimal SAT–Ex−2",
"BoundTermUnitProp":"SeriesBoxOptions",
"SATEnergySelector":"SAT"};
```

Figure 5.5: JSON options for the second floor air handling units.

These pointers can be a static value, another property, an actual trend from the building automation system, or a custom equation built up using the powerful functions available in Implementer.

Any calculation from the optimization analysis can be output as a trend in Implementer and can be plotted and visualized using any of the tools available.

The equipment can be separated by project, which typically a building or collection of buildings, and a call such as `https://domain/GetEquipmentForProject?ProjectId={Project-Id}` could return all the possible set up equipment.

The interface for receiving the optimal setpoints could have a URL similar to `https://domain/setpoints?id={Equipment-Id}&{time=Datetime}`

6. NCTM CASE STUDY

The National Center for Therapeutics Manufacturing (NCTM) building was used as a test bed for the methodology. NCTM is a building located on the campus of Texas A&M University, in College Station, Texas. Figure 6.1 shows an image of the main entrance to the building.

The National Center for Therapeutics Manufacturing (NCTM) combines the educational and manufacturing focuses of the biopharmaceutical industry. The NCTM building is approximately 150,000 ft^2 with nearly 50,000 ft^2 of educational facilities that include wet labs, culture facilities, large lecture halls, and a mock current Good Manufacturing Practice (cGMP) training suite. Around 120,000 ft^2 are on the first level and 30,000 ft^2 are on the second level.

The cGMP Suite contains modern biopharmaceutical manufacturing equipment that students can use to learn industry practices. The wet labs are equipped with chemical fume hoods and the necessary electronic equipment for following standard operating procedures used in the biopharmaceutical industry. The two lecture halls seat up to 120 students and have large floor to ceiling windows. There is also an Apple Computer laboratory with 48 workstations on the second floor.

On the academic side, three dedicated outdoor air handling units (OAHU) serve seven air handling units. Two of the air handling units are constant speed, and the others are variable air volume. OAHU 1-1 serves its own wet lab and also feeds into AHU 1-1 and AHU 1-2. OAHU 1-2 serves AHU 1-3 and 1-4 on the first floor. OAHU 2-1 serves three air handlers on the second floor, AHU 2-1, 2-2, and 2-3.

Various specifications for the air handling units are shown in Tables 6.1 through 6.3.

Figure 6.1: Main entrance to the NCTM building at Texas A&M (`https://engineering.tamu.edu/media/15458/nctm-building.png`).

Table 6.1: Occupied/Unoccupied scheduling for the AHUs as described.

Level	OAHU	AHU #	AHU Schedule
Floor 1 Area B	OAHU 1-1	N/A	24/7
Floor 1 Area B	OAHU 1-1	AHU 1-1	24/7
Floor 1 Area B	OAHU 1-1	AHU 1-2	6am - 6pm, M-F
Floor 1 Area A	OAHU 1-2	AHU 1-3	6am - 8pm, M-F
Floor 1 Area A	OAHU 1-2	AHU 1-4	6am - 8pm, M-F
Floor 2	OAHU 2-1	AHU 2-1	6am - 10pm, M-F
Floor 2	OAHU 2-1	AHU 2-2	6am - 10pm, M-F
Floor 2	OAHU 2-1	AHU 2-3	6am - 10pm, M-F

This work focuses on the academic side of the building since Utilities and Energy Services with Texas A&M University are only allowed to make changes to the HVAC system and collect data on this side. In summary, the relevant facts concerning NCTM are that it houses several biopharmaceutical labs, it has an academic side that had available data, and relies on dedicated outdoor air handling units to pretreat outdoor air.

Figures 6.2 through 6.4 show the respective areas that the air handling units serve. Mechanical drawings for the floors are shown in Figures 6.5 through 6.7. Utilities and Energy Services provided access to these graphics and mechanical drawings.

Table 6.2: Fan schedule information for the dedicated outdoor air handlers.

OAHU	Design OA CFM	HP
OAHU 1-1	12,800	20
OAHU 1-2	4,500	5
OAHU 2-1	2,200	2
Total:	19,500	27

Table 6.3: Fan schedule information for the AHUs.

AHU	Type	Total Airflow (CFM)	HP	OA Served By
AHU 1-1	Constant	3,000	5	OAHU 1-1
AHU 1-2	VAV	4,800	5	OAHU 1-1
AHU 1-3	VAV	7,500	7.5	OAHU 1-2
AHU 1-4	Constant	5,000	7.5	OAHU 1-2
AHU 2-1	VAV	6,000	7.5	OAHU 2-1
AHU 2-2	VAV	8,500	10	OAHU 2-1
AHU 2-3	VAV	6,000	7.5	OAHU 2-1
	Total:	40,800	50	

6.1 Terminal Unit Information

On the academic side, there are a total of 10 series fan powered terminal units on the first floor and 18 on the second floor. Table 6.4 shows the design flowrates and type of space served for each of the terminal units.

It is critical to have an understanding of how the current controls are operating. It is better to rely on data, rather than relying on control code, although in practice, this will normally require that an engineer verifies both the control code along with the real measured performance.

Implementer can ease the difficulty in this analysis by producing certain plots en mass for terminal units. As an example of this, Figure 6.8 shows the results of tem-

Table 6.4: Terminal unit information.

AHU	Terminal Unit	Flow (CFM)	Space Served
AHU-1-2	FPVAV-1-7	1,400	Difficult to tell
(5 hp)	FPVAV-1-8	700	Vestibule/Men's & Women's bathroom
	FPVAV-1-9	1,200	Stairs/Front Corridor
	FPVAV-1-10	1,600	Hallway
AHU-1-3	FPVAV-1-1	1,480	Large Auditorium Lecture Hall
(7.5 hp)	FPVAV-1-2	1,160	Large Auditorium Lecture Hall
	FPVAV-1-3	1,300	Large Auditorium Lecture Hall
	FPVAV-1-4	1,400	Large Auditorium Lecture Hall
	FPVAV-1-5	1,040	Large Auditorium Lecture Hall
	FPVAV-1-6	1,120	Large Auditorium Lecture Hall
AHU-2-1	FPVAV-2-1	2,000	Large Study Area
(7.5 hp)	FPVAV-2-2	2,200	Large Study Area
	FPVAV-2-3	1,800	Open Corridor
AHU-2-2	FPVAV-2-9	2,400	Computer Lab
(10 hp)	FPVAV-2-12	500	Kitchen/Mail Room
	FPVAV-2-13	1,000	Open Corridor
	FPVAV-2-14	850	Men's/Women's Restroom Copy/Mail Waiting Area
	FPVAV-2-15	1,400	Reception/Seating/Admin Lobby
	FPVAV-2-16	500	Small Conference Room
	FPVAV-2-17	1,280	4 Small Offices
	FPVAV-2-18	600	Large Office
AHU-2-3	FPVAV-2-4	2,000	Open Corridor
(7.5 hp)	FPVAV-2-5	600	Open Seating
	FPVAV-2-6	400	Small Conference Room
	FPVAV-2-7	200	Office
	FPVAV-2-8	1,200	Visitor Conference
	FPVAV-2-10	540	3 Sponsor Offices
	FPVAV-2-11	560	3 Sponsor Offices

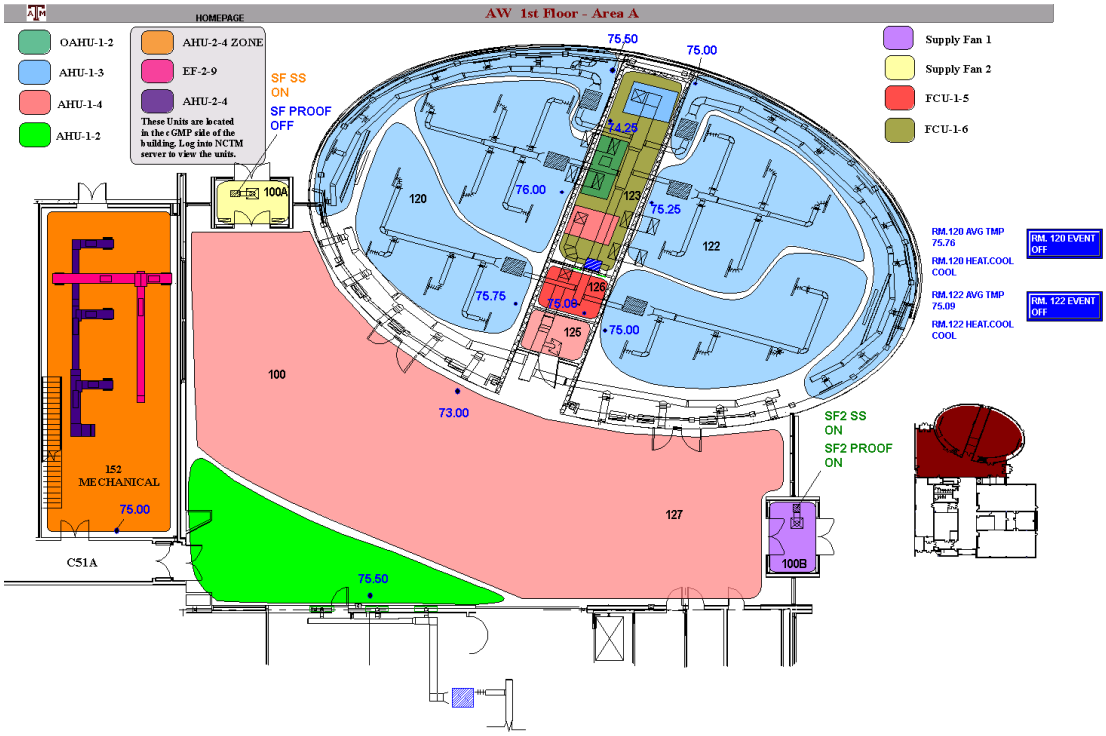

Figure 6.2: First floor plan for Area A.

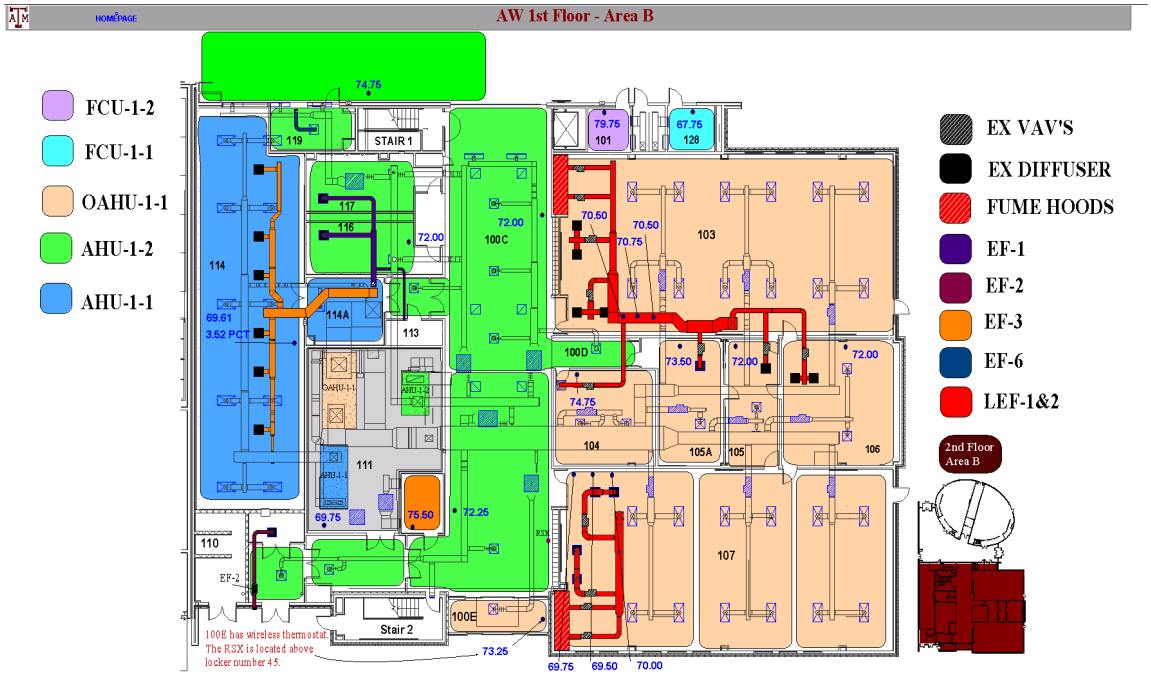

Figure 6.3: First floor plan for Area B.

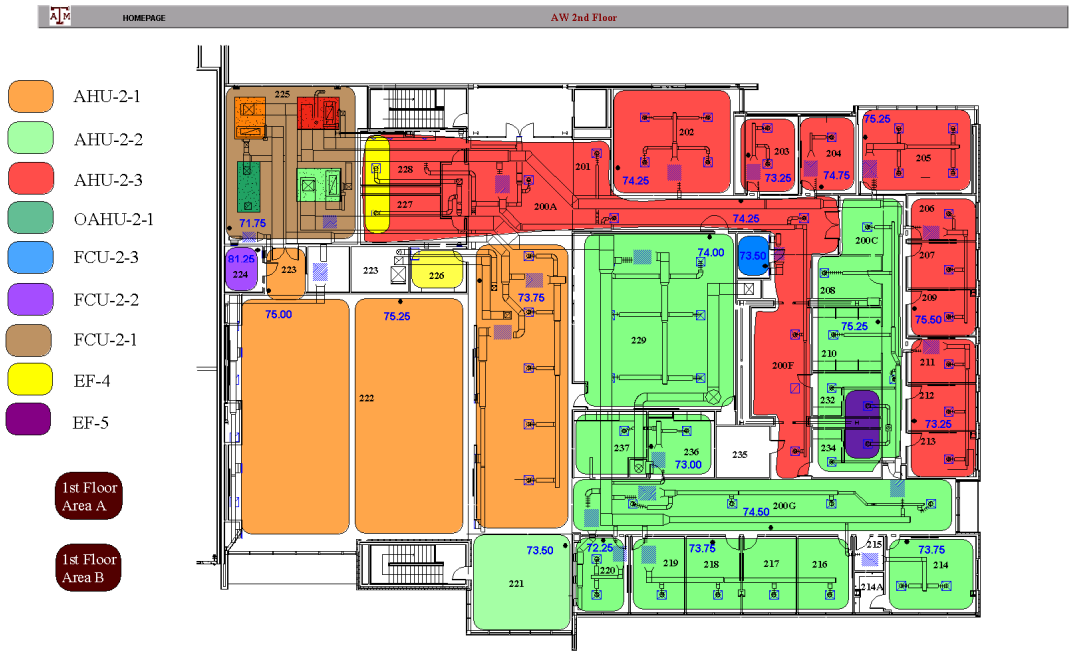

Figure 6.4: Second floor plan.

perature rise within the terminal unit, versus the part-load ratio of the terminal unit (assuming the design specifications for the design flow). Implementer can produce these plots for every terminal unit in a project at once. From these types of plots, the minimum primary air flow setpoint can quickly be visually determined.

From the data, it appears that the majority of the terminal units in NCTM are operating with 30% as the minimum flow rate. There are a few terminal units that have minimum flow rates less than this. Table 6.5 shows the estimated minimum percent flows based on data from February 1, 2016, through May 1, 2016.

Figure 6.9 shows the available points for the series fan powered terminal units at NCTM from a BAS graphic.

The points include

- Primary air flow

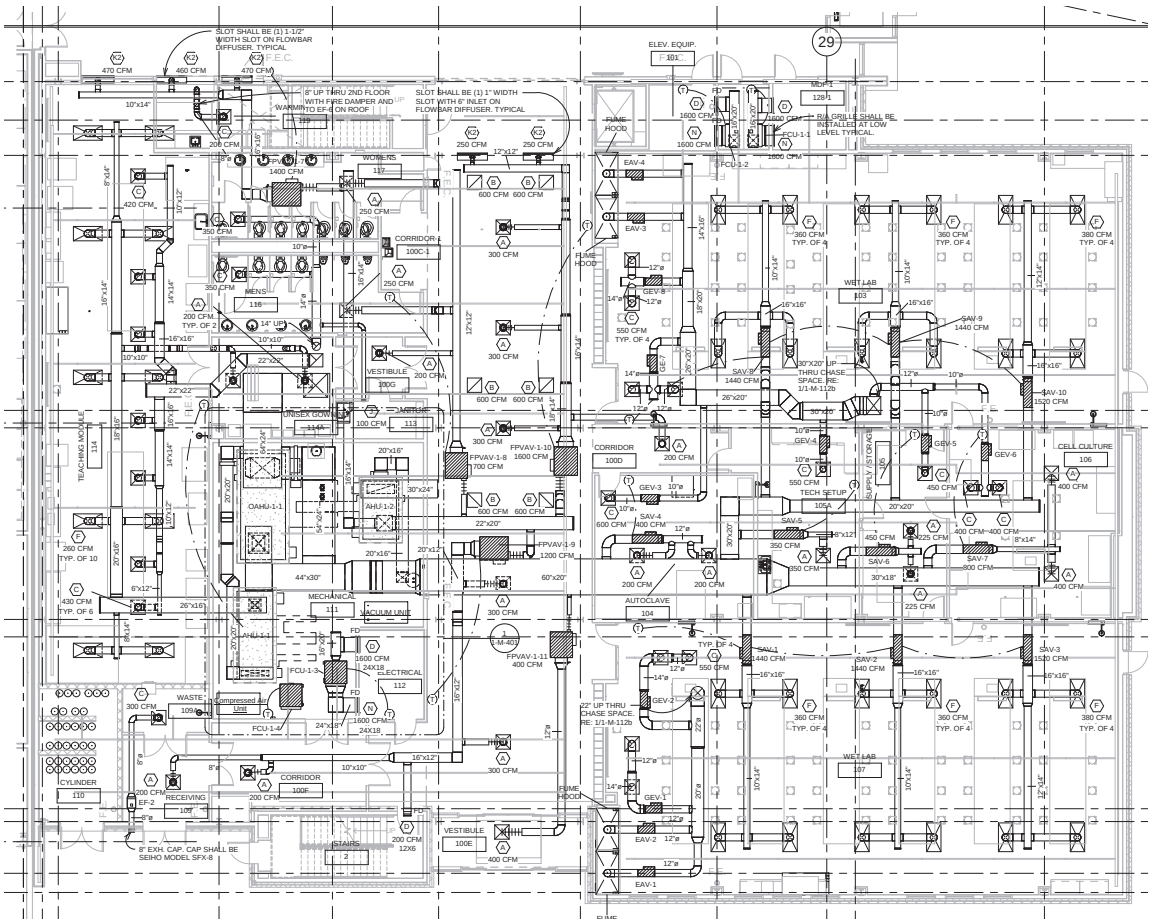

Figure 6.5: Floor plan for first floor Area A with terminal units.

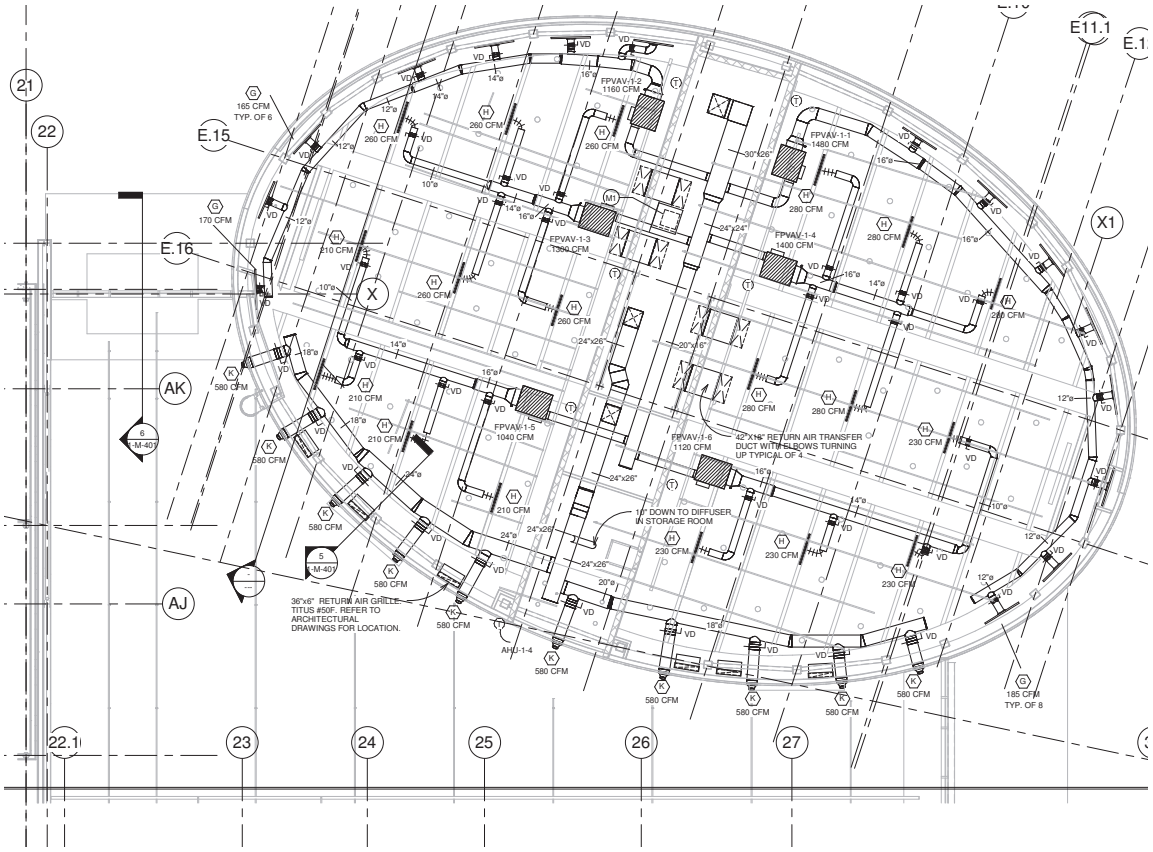

Figure 6.6: Floor plan for first floor Area B with terminal units.

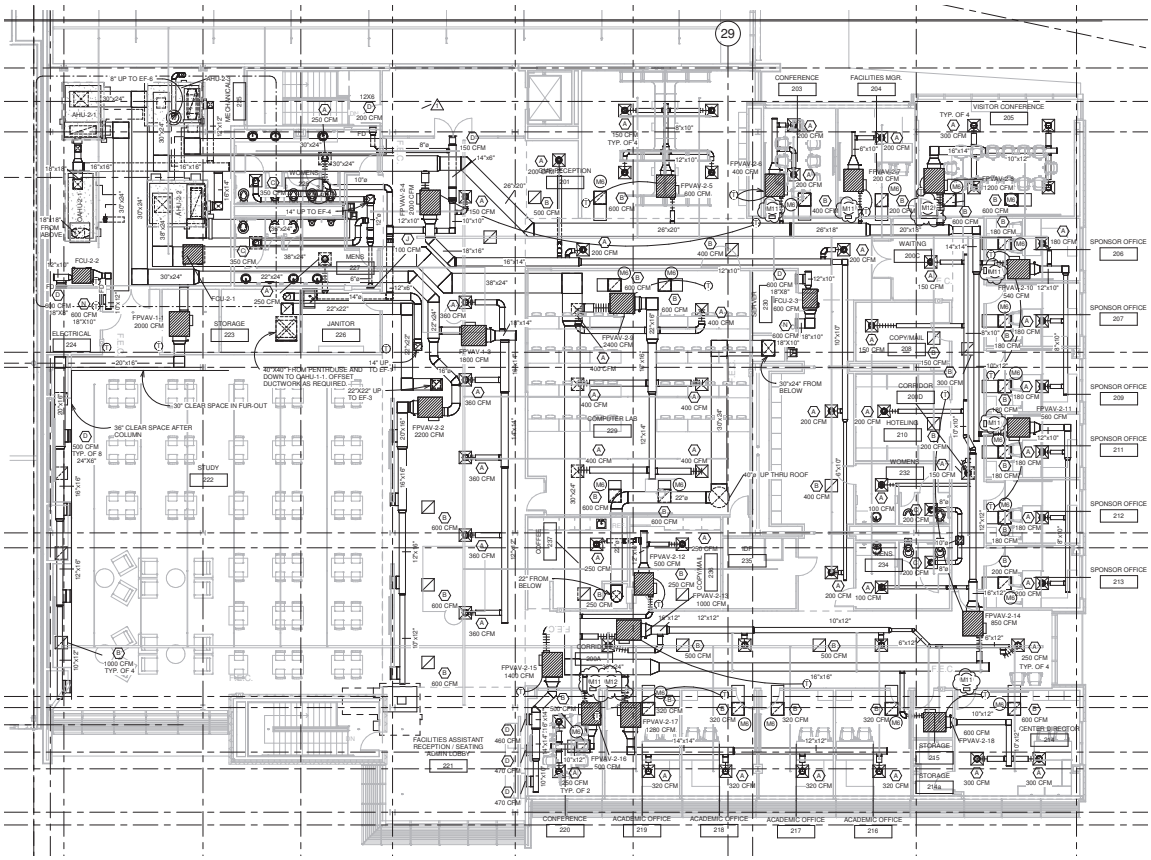

Figure 6.7: Floor plan for the second floor with terminal units.

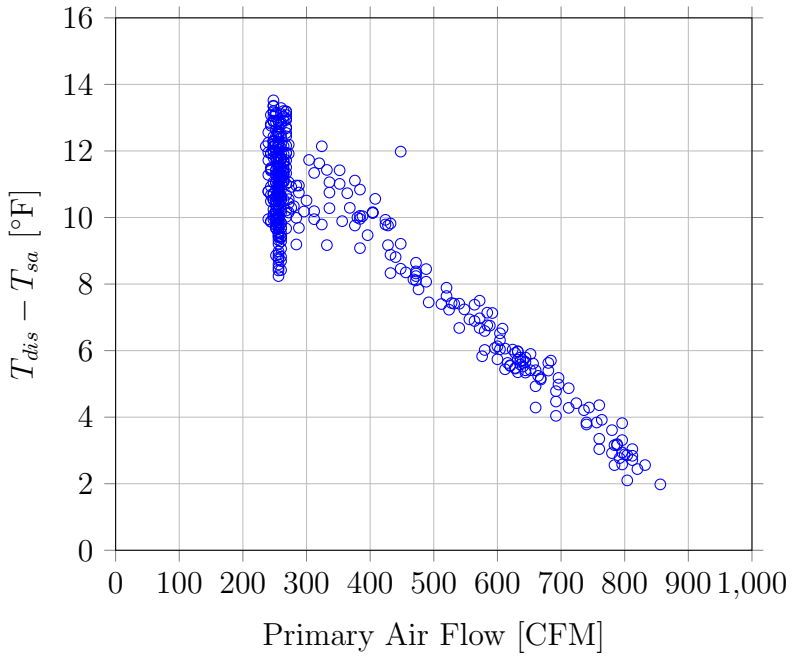

Figure 6.8: Temperature rise due to the mixing of plenum air at the terminal unit for FPVAV-2-14. Plots like this were used to estimate the current minimum flow rate settings.

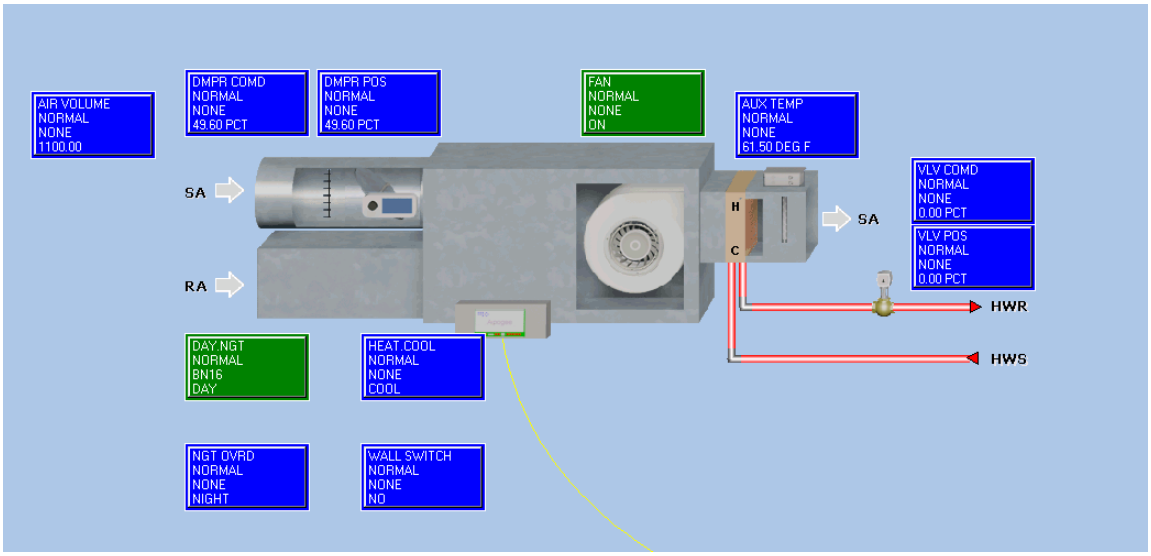

Figure 6.9: Typical graphic of the terminal units at NCTM.

- Damper command
- Discharge air temperature
- Heating coil valve command

6.2 Analysis of the Mixed Air Temperature at the AHU

This section investigates the feasibility of estimating the mixed air temperature based on historical data. The historical data of the mixed air temperature, T_{ma}, differs from one air handling unit to another. Figure 6.10 shows an example of an AHU in which T_{ma} does not change significantly throughout time, having a range of approximately 6°F, excluding a few outliers. In the case of Figure 6.11, T_{ma} is less constant but still appears to be a function of T_{oa} as a first order approximation. Figure 6.10 and 6.11 both show data spanning 90 days from March 14, 2016 to June 12, 2016.

The *nearest neighbor* approach was used to predict the mixed air temperatures. The algorithm looked back in history (at least a day before) under the following parameters:

- The same day of the week (Sun, Mon, etc.)
- Same hour of day ±1 hr.
- Same T_{oa} ±3°F
- Searching backward until 30 data points found

The median of the data points matching the criterion listed is the resulting predicted value. Figure 6.12 and 6.13 show the results versus outdoor air temperature. The following plots show the model fits for the different air handling units at NCTM.

Table 6.5: Terminal unit minimum air flow rate settings.

Terminal Unit	Min Percent Flow
FPVAV-2-1	20
FPVAV-2-2	30
FPVAV-2-3	20
FPVAV-2-12	30
FPVAV-2-13	30
FPVAV-2-14	30
FPVAV-2-15	30
FPVAV-2-16	30
FPVAV-2-17	30
FPVAV-2-18	30
FPVAV-2-9	5
FPVAV-2-10	30
FPVAV-2-11	30
FPVAV-2-4	30
FPVAV-2-5	30
FPVAV-2-6	30
FPVAV-2-7	30
FPVAV-2-8	30
FPVAV-1-10	30
FPVAV-1-7	30
FPVAV-1-8	N/A
FPVAV-1-9	N/A
FPVAV-1-1	30
FPVAV-1-2	30
FPVAV-1-3	25
FPVAV-1-4	25
FPVAV-1-5	N/A
FPVAV-1-6	30
FPVAV-1-11	30

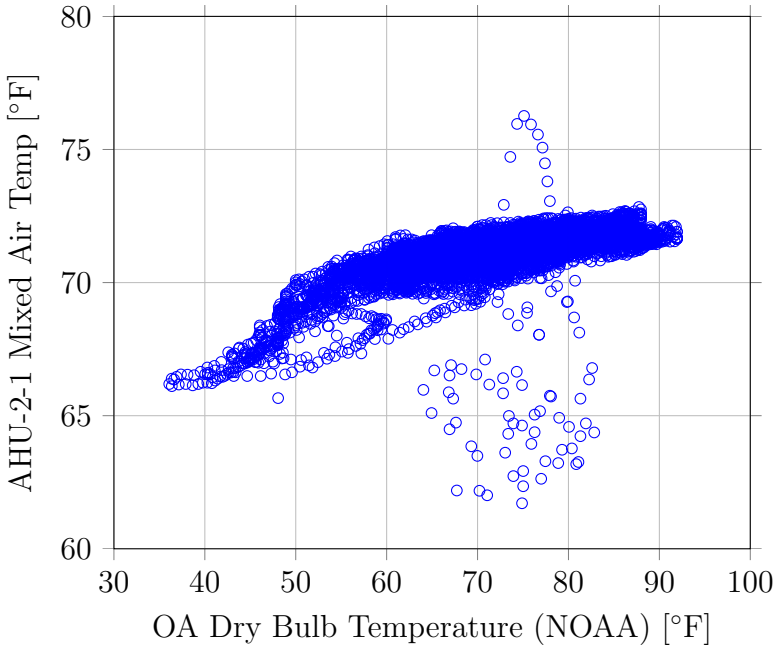

Figure 6.10: AHU-2-1 mixed air temperature vs. outdoor air temperature.

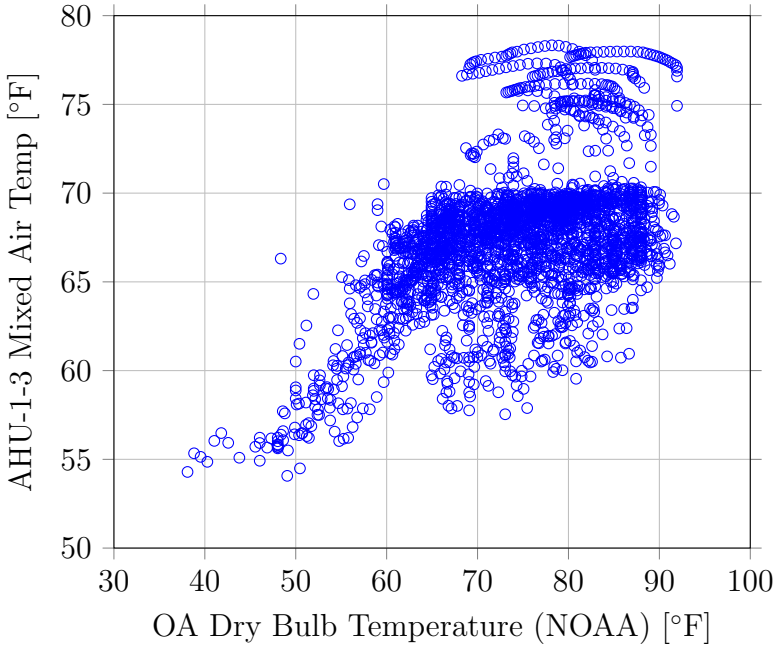

Figure 6.11: AHU-1-3 mixed air temperature vs. outdoor air temperature.

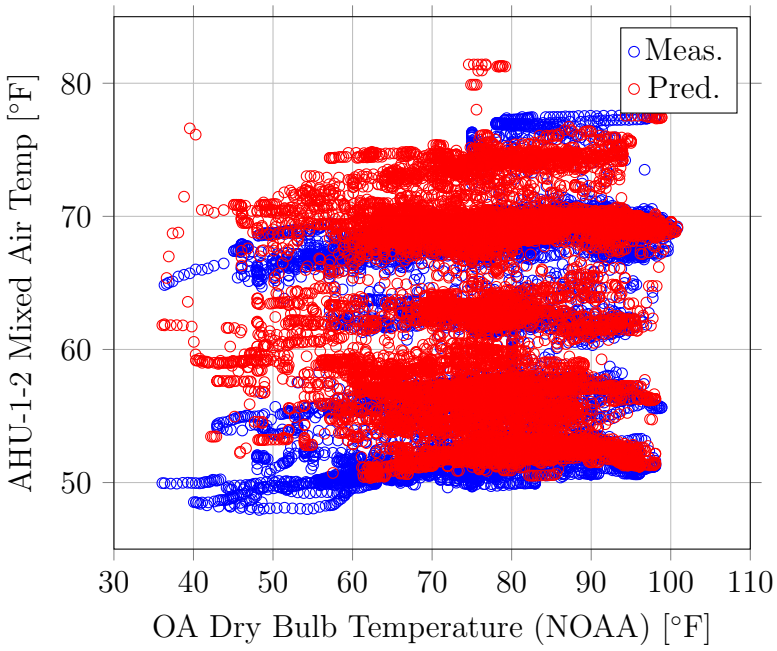

Figure 6.12: AHU-1-2 T_{ma} prediction for data from March 10, 2016 - September 5, 2016, not ignoring any data.

The data covers a period of 180 days. Figures 6.12 and 6.13 show that the prediction algorithm can adequately handle the differences from when the air handling unit is on as well as off. The significant amount of spread in the mixed air temperature is due to data in which the air handler turns off and is allowed to drift, typically to a higher temperature in the climate of College Station.

Figures 6.14 through 6.18 show the model fits ignoring times when the air handling units are off, weekends and holidays, and times between 6:00 PM and 8:00 AM.

The sensitivity of the prediction results to the selected nearest neighbor parameters was tested. The parameter values were varied as shown in Table 6.6.

With three parameters and three different variations for each, this resulted in 27 test cases. The results of this testing are shown in Table 6.7. TS stands for

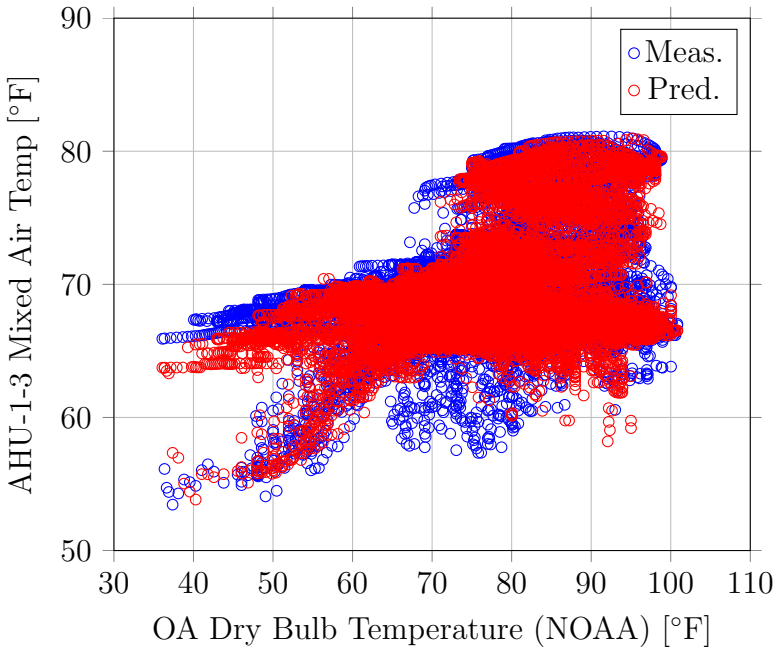

Figure 6.13: AHU-1-3 mixed air temperature prediction for data from March 10, 2016 - September 5, 2016, not ignoring any data.

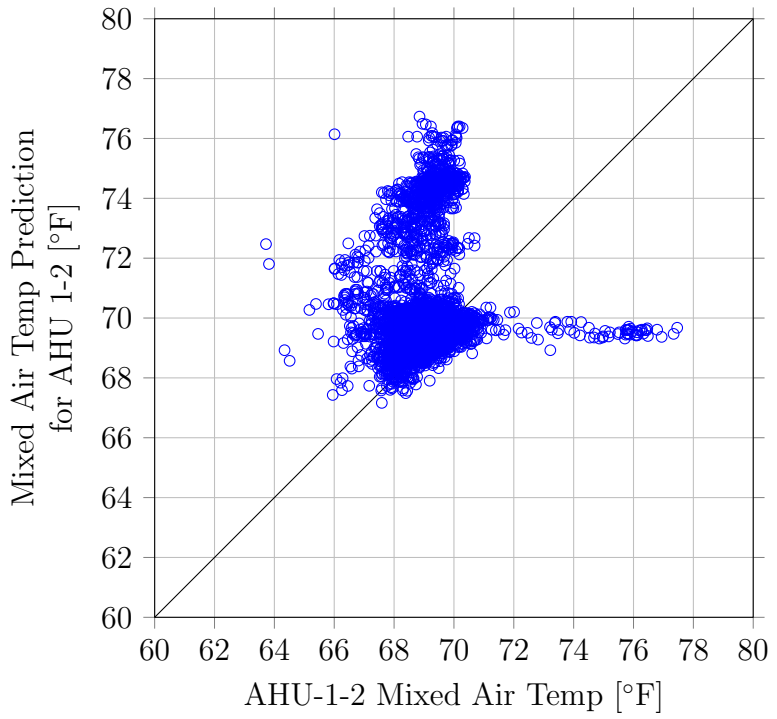

Figure 6.14: Mixed air temperature prediction results for AHU-1-2.

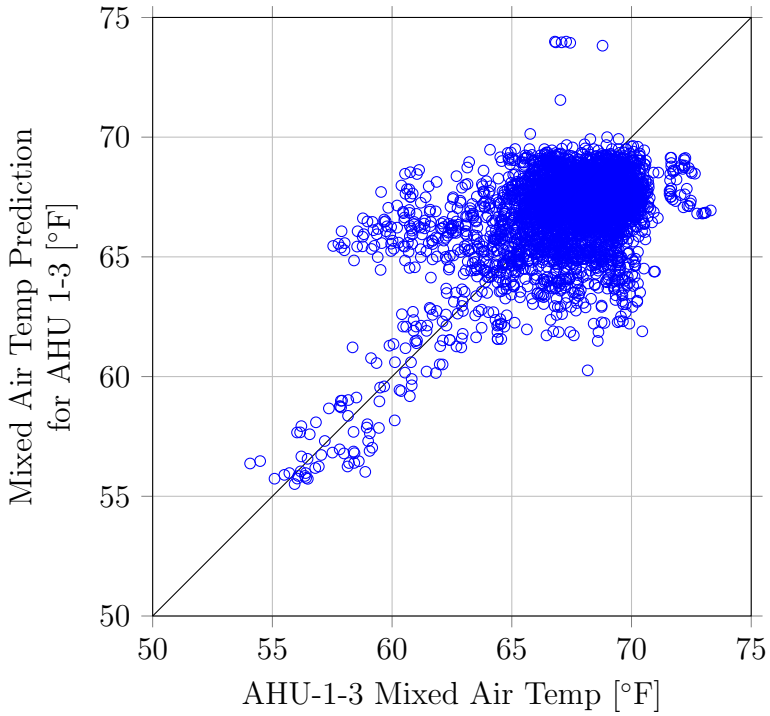

Figure 6.15: Mixed air temperature prediction results for AHU-1-3.

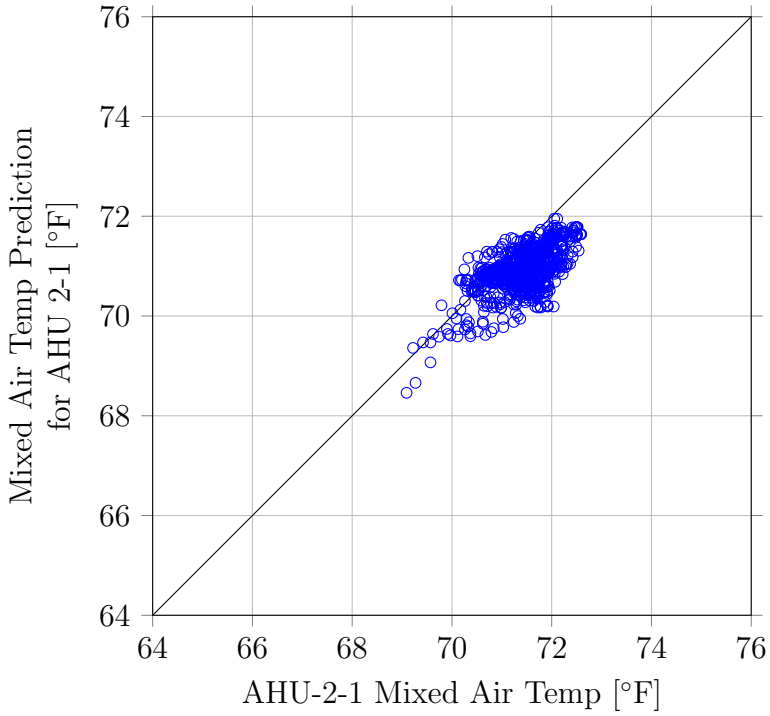

Figure 6.16: Mixed air temperature prediction results for AHU-2-1.

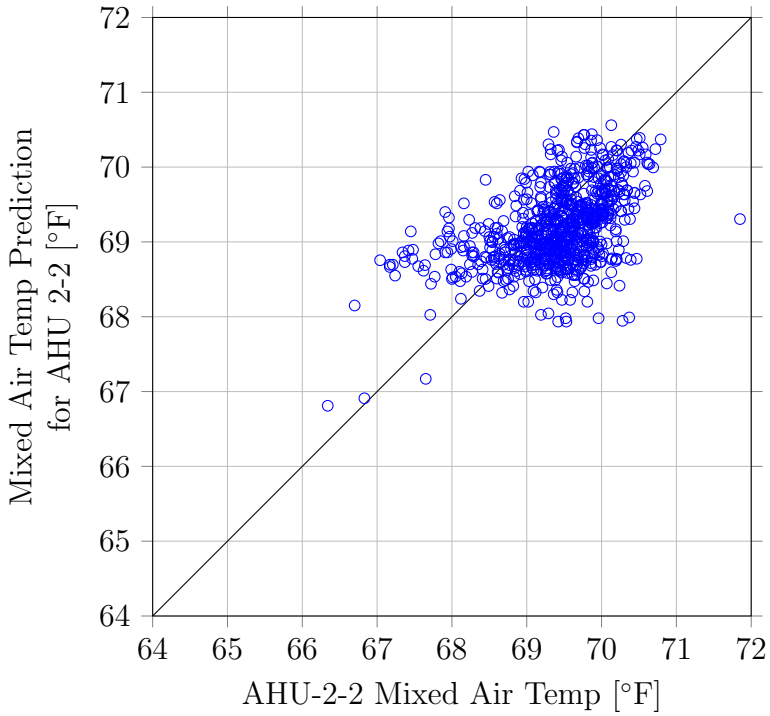

Figure 6.17: Mixed air temperature prediction results for AHU-2-2.

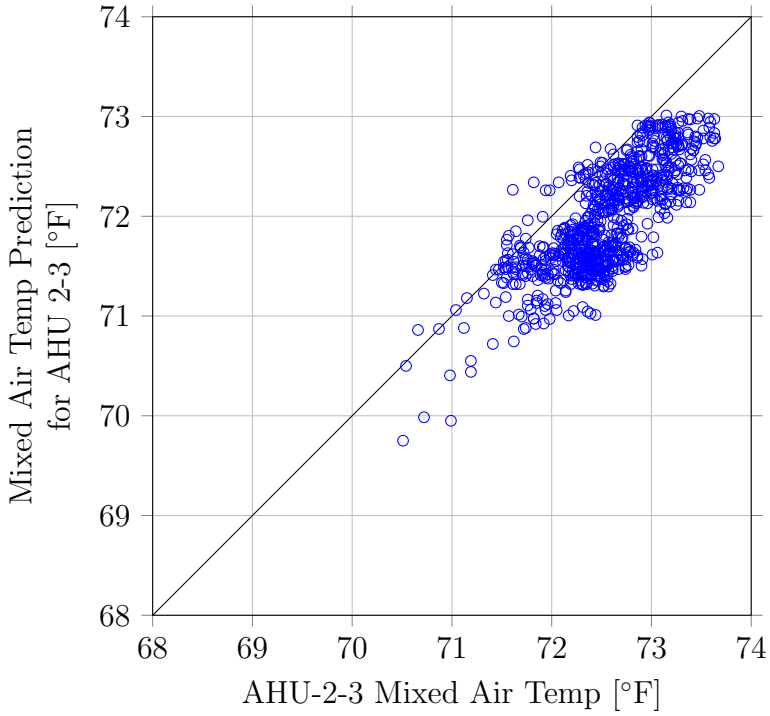

Figure 6.18: Mixed air temperature prediction results for AHU-2-3.

Table 6.6: Variations in the parameters for the nearest neighbor algorithm.

Threshold	Variations
Time stamp threshold	15, 30, and 60 minutes
T_{oa} threshold	1°F, 3°F, 5°F
Data points threshold	15, 30, and 45 data points.

timestamps and is related to the time of day threshold. Since the data was aligned to 15 minute intervals, a 1 timestamp threshold implies a threshold of ±15 minutes and a 4 timestamp threshold implies a threshold of ±60 minutes. The best model fit used a timestamp threshold of ±60 minutes, ±3°F for T_{oa}, and 15 data points. The worst case was using ±15 minutes, ±1°F, and 30 data points.

Because Fahrenheit is not on a ratio scale, that is, having a meaningful zero, the typical goodness-of-fit parameter, the coefficient of variation of the root mean squared error (RMSE), has less meaning. Therefore, instead of using the mean as the normalization parameter in the CV-RMSE metric, the range or the spread of the original data was used. It is denoted as CV-RMSE* for the remainder of this document.

$$\text{CV-RMSE*} = \frac{\text{RMSE}}{y_{max} - y_{min}} \tag{6.1}$$

The model was insensitive to the parameters. The average CV-RMSE* ranged from 8.97% to 10.75% across the 27 different test cases. The models with the lowest CVs had the largest range in the timestamp and T_{oa} threshold. This observation is an indication that using more recent data was more valuable than using data from conditions matching more closely, though the more important fact was that the overall difference from highest to lowest CV-RMSE* was only 1.78 percentage points.

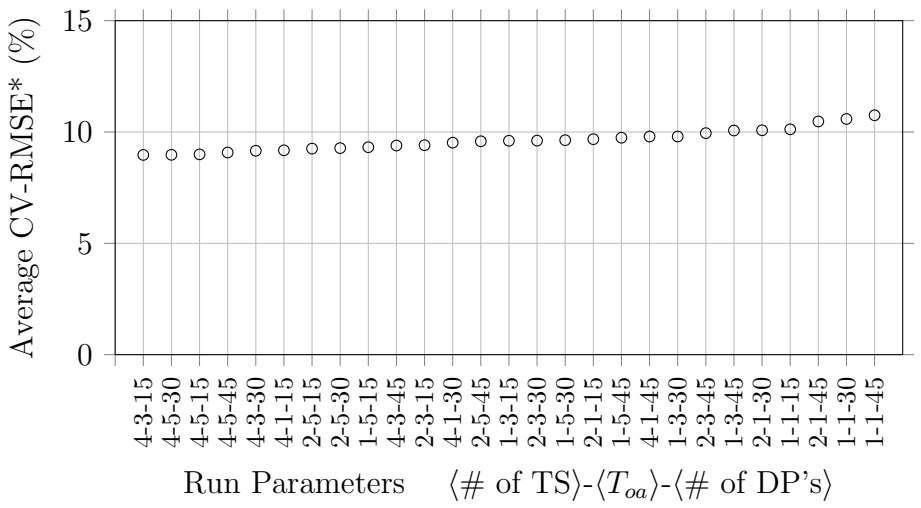

Figure 6.19: Results from testing different nearest neighbor model parameters used in predicting mixed air temperature.

A graphical view of the results in order of the best set parameters to the worst set of parameters is shown in Figure 6.19.

6.3 Analysis of the Plenum Air Temperature

Reheat is a major component of energy use, and for a series fan powered box, the plenum air temperature is required to calculate the reheat power. This section analyzes the estimation of the plenum air temperature and the corresponding uncertainty. If the terminal unit is modeled as a simple mixing problem, with negligible impact from the fan, the plenum air temperature will be

$$T_{plen} = \frac{\dot{V}_{tot} T_{dis} - \dot{V}_{pri} T_{sa}}{\dot{V}_{tot} - \dot{V}_{pri}} \tag{6.2}$$

Since T_{plen} is a function of 4 variables, each with their own uncertainties, it is important to consider the cumulative uncertainty in the estimation. Clearly, when $\dot{V}_{plen}$ (or $\dot{V}_{tot} - \dot{V}_{pri}$, the denominator of Equation 6.2) is low, the uncertainty in T_{plen}

Table 6.7: Results from testing different nearest neighbor model parameters for predicted T_{ma}.

Run	TS	T_{oa}	DP	Average CV-RMSE*
1	1	1	15	10.12
2	2	1	15	9.68
3	4	1	15	9.80
4	1	3	15	9.61
5	2	3	15	9.41
6	4	3	15	8.97
7	1	5	15	9.28
8	2	5	15	9.18
9	4	5	15	8.98
10	1	1	30	10.58
11	2	1	30	10.07
12	4	1	30	9.39
13	1	3	30	9.95
14	2	3	30	9.63
15	4	3	30	9.16
16	1	5	30	9.61
17	2	5	30	9.25
18	4	5	30	9.00
19	1	1	45	10.75
20	2	1	45	10.47
21	4	1	45	9.80
22	1	3	45	10.08
23	2	3	45	9.58
24	4	3	45	9.32
25	1	5	45	9.74
26	2	5	45	9.52
27	4	5	45	9.08

Table 6.8: T_{ma} prediction results using the parameters in Run 6.

AHU	RMSE (°F)
AHU 1-2	1.69
AHU 1-3	2.42
AHU 1-4	1.25
AHU 2-1	0.744
AHU 2-2	0.619
AHU 2-3	0.496

grows significantly, and when the flow is equal to zero, T_{plen} is undefined.

Using the Kline-McKlintock formulation of uncertainty, the uncertainty of T_{plen} is

$$\delta T_{plen} = \left[\left(\frac{\partial T_{plen}}{\partial \dot{V}_{pri}} \delta \dot{V}_{pri} \right)^2 + \left(\frac{\partial T_{plen}}{\partial \dot{V}_{tot}} \delta \dot{V}_{tot} \right)^2 + \left(\frac{\partial T_{plen}}{\partial T_{dis}} \delta T_{dis} \right)^2 + \left(\frac{\partial T_{plen}}{\partial T_{sa}} \delta T_{sa} \right)^2 \right]^{1/2} \quad (6.3)$$

$$\delta T_{plen} = \left[\left(\frac{\dot{V}_{tot} \left(T_{dis} - T_{sa} \right)}{\dot{V}_{plen}^2} \delta \dot{V}_{pri} \right)^2 + \left(\frac{\dot{V}_{pri} \left(T_{sa} - T_{dis} \right)}{\dot{V}_{plen}^2} \delta \dot{V}_{tot} \right)^2 + \left(\frac{\dot{V}_{tot}}{\dot{V}_{plen}} \delta T_{dis} \right)^2 + \left(\frac{\dot{V}_{pri}}{\dot{V}_{plen}} \delta T_{sa} \right)^2 \right]^{1/2} \quad (6.4)$$

As a concrete example, if the following arbitrary but reasonable parameters are used,

- $\dot{V}_{tot} = 2{,}200\,\text{CFM}$
- $\dot{V}_{pri} = 1{,}000\,\text{CFM}$
- $\dot{V}_{plen} = 2{,}200\,\text{CFM} - 1{,}000\,\text{CFM} = 1{,}200\,\text{CFM}$
- $T_{sa} = 55°\text{F}$
- $T_{dis} = 75°\text{F}$
- $\delta \dot{V}_{pri} = \delta \dot{V}_{plen} = \delta \dot{V}_{tot} = 100\ \text{CFM}$

- $\delta T_{sa} = \delta T_{dis} = 1°\text{F}$

Equation 6.4 becomes

$$\delta T_{plen} = \left[(3.06°\text{F})^2 + (-1.39°\text{F})^2 + (1.83°\text{F})^2 + (0.830°\text{F})^2\right]^{1/2} \tag{6.5}$$

which results in a final uncertainty of 3.91°F, which is nearly four times larger than the initially assumed uncertainties for the temperatures (1°F). When $\dot{V}_{plen}$ is reduced even further, this uncertainty grows substantially.

For a more detailed analysis, Equation 6.4 can be manipulated into a simpler form. The first substitution assumes the uncertainty for T_{dis} and T_{pri} are the same and constant at a value of δT. The uncertainty of the flows can be done on a percent basis ($\pm 10\%$ for example, and that percentage, a value from 0 to 1, can be denoted as $\delta \dot{V}_{perc}$). The difference between T_{dis} and T_{pri} can be replaced by ΔT. The final substitution is that the flows for $\dot{V}_{pri}$ and $\dot{V}_{plen}$ are replaced by the corresponding fraction of the total flow. F_{pri} is defined to be the fraction of the total flow that comes from the primary stream, a value between 0 and 1. Therefore,

$$\Delta T = T_{dis} - T_{pri} \tag{6.6}$$

and

$$\dot{V}_{pri} = F_{pri} \dot{V}_{tot} \tag{6.7}$$

and

$$\dot{V}_{plen} = (1 - F_{pri})\, \dot{V}_{tot}. \tag{6.8}$$

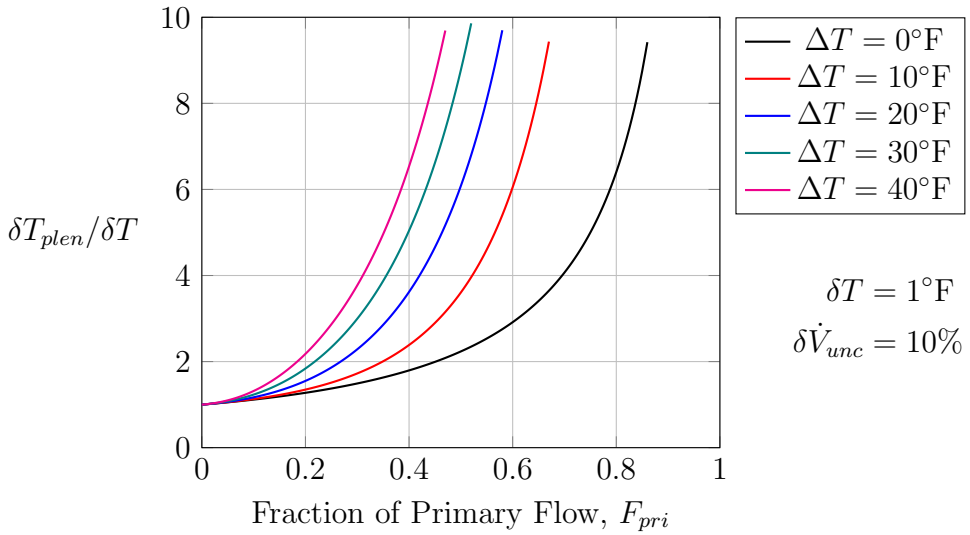

Figure 6.20: Uncertainty in T_{plen}, δT_{plen}, at different levels of $\Delta T = T_{dis} - T_{pri}$.

With these substitutions, the total uncertainty for T_{plen} is

$$\sqrt{\left(\frac{\delta T}{1 - F_{pri}}\right)^2 + \left(\frac{\delta T F_{pri}}{1 - F_{pri}}\right)^2 + 2\left(\frac{\Delta T\, F_{pri}\, \delta \dot{V}_{perc}}{(1 - F_{pri})^2}\right)^2} \tag{6.9}$$

Various combinations of values and the resulting uncertainty in T_{plen} are shown in Figure 6.20 through 6.22. The y-axis is normalized to the static uncertainty in the other temperatures, δT, which is the uncertainty for both T_{dis} and T_{pri}.

What the plots show is that the fraction of primary flow, F, has to be less than 40% in most cases to have an uncertainty in T_{plen} that is less than double the uncertainty in T_{dis} and T_{pri} (a value of 2 on the normalized y-axis).

As an example as to how unstable the calculation for the plenum temperature is, Figure 6.23 shows the calculated plenum temperature for FPVAV-1-9 over the period from February 1, 2016 - May 1, 2016. The calculated values are unrealistic ranging from -1,500°F to 1,500°F. The reason for this is made clear in a time series plot of

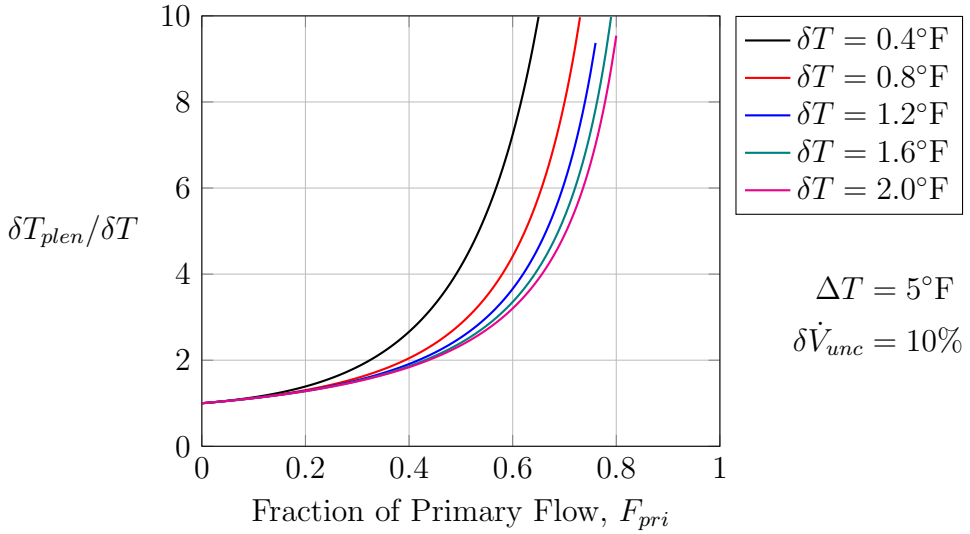

Figure 6.21: Uncertainty in T_{plen}, δT_{plen}, at different levels of δT.

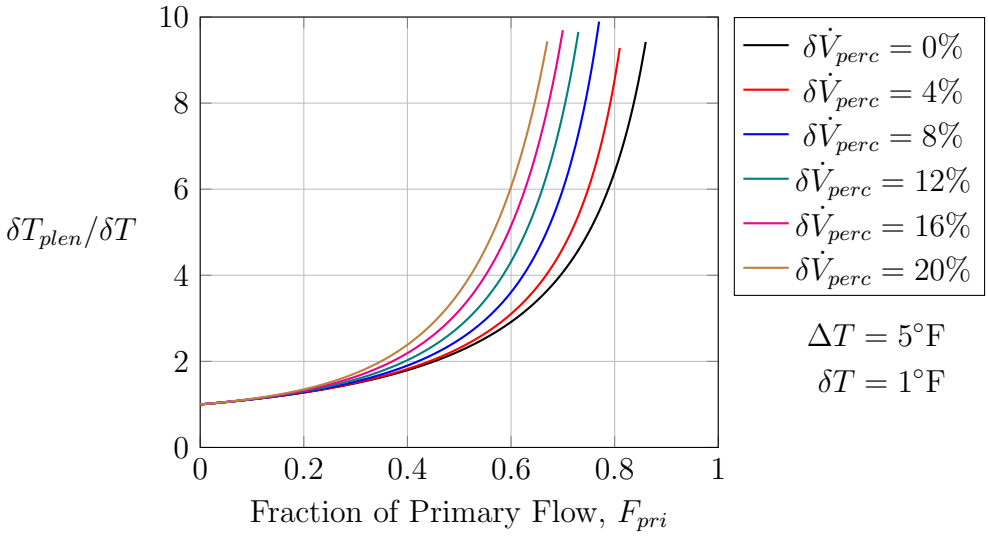

Figure 6.22: Uncertainty in T_{plen}, δT_{plen}, at different levels of $\delta \dot{V}_{unc}$.

the flows related to the terminal unit. As shown in Figure 6.24, for this particular terminal unit, the primary flow is either near zero or design. At times, the measured flow is also above the design specification, making the plenum flow calculation zero. When the plenum flow is calculated to be zero, the plenum temperature calculation becomes undefined.

Using the assumptions that the uncertainty in the flow was 100 CFM and the uncertainty in the temperature measurements was 1°F, the plenum temperature was calculated from October 6, 2015, to September 12, 2016, ignoring items that appear in Table 6.9. The distribution statistics for each terminal unit are found in Table 6.10. The table is listed in ascending order by the median of the plenum temperature calculated.

Note that the percentage of ignored points is below 96% for only 4 terminal units. The majority of the points are ignored because the uncertainty in the calculation was above the 2°F threshold that was arbitrarily chosen. In fact, at no point was the uncertainty below 2°F for FPVAV-2-7. The median plenum temperature ranges from 58.8°F for FPVAV-1-8 to 75.6°F for FPVAV-1-6.

Another interesting way to examine the difference between the plenum temperature and the zone temperature is to plot the estimated reheat in the terminal unit when the reheat valve is closed. Ideally, the amount of reheat would be at or near zero.

If the plenum temperature is assumed to be equal to the zone temperature, then an estimate of the mixed air temperature in the terminal unit would be

$$T_{ma} = \frac{\dot{V}_{pri} T_{sa} + T_z \left(\dot{V}_{tot} - \dot{V}_{pri} \right)}{\dot{V}_{tot}} \tag{6.10}$$

Table 6.9: Implementer settings for plenum temperature estimation for NCTM, used to calculate data in Table 6.10.

Project:	Mitch Dissertation NCTM—2016-09-19 10:34
Scope:	NCTM
Axis Parameters:	Plenum Temperature vs. OA Dry-bulb Temp (NOAA)
Date Period:	10/6/2015 - 9/12/2016 (342 days)
OAT range:	31 to 100°F
Ignoring:	When AHU is Off
	First 1.0 hours of operation
	Last 1.0 hours of operation
	Sundays
	Saturdays
	Federal Holidays
	Hours from 17:00 to 9:00
	When label Plenum Temp Uncertainty is greater than 2
	When label Valve Positions is greater than 1

and the reheat power could be estimated by

$$\dot{Q} = 1.08\,(CFM)\,(T_{ma} - T_{dis}) \tag{6.11}$$

Figures 6.25 through 6.27 show the reheat power as determined by Equation 6.11. They are from the period of February 1, 2016, through May 1, 2016. Timestamps during weekends, times between 5:00 PM and 9:00 AM, and when the corresponding reheat valve command is $< 1\%$ were ignored. Again, ideally, the estimated reheat power would be exactly zero.

Figure 6.25 shows an example of where the assumption appears to hold reasonably well. The median of the data set is near $500\,\frac{\text{BTU}}{\text{h}}$. Is should be noted that Equation 6.11 does not make a distinction between heating from the heating coils and heating from the fan. So the $500\,\frac{\text{BTU}}{\text{h}}$ could be due to the fan in the air stream.

Figure 6.26 shows a case in which there is either constant reheat or the actual

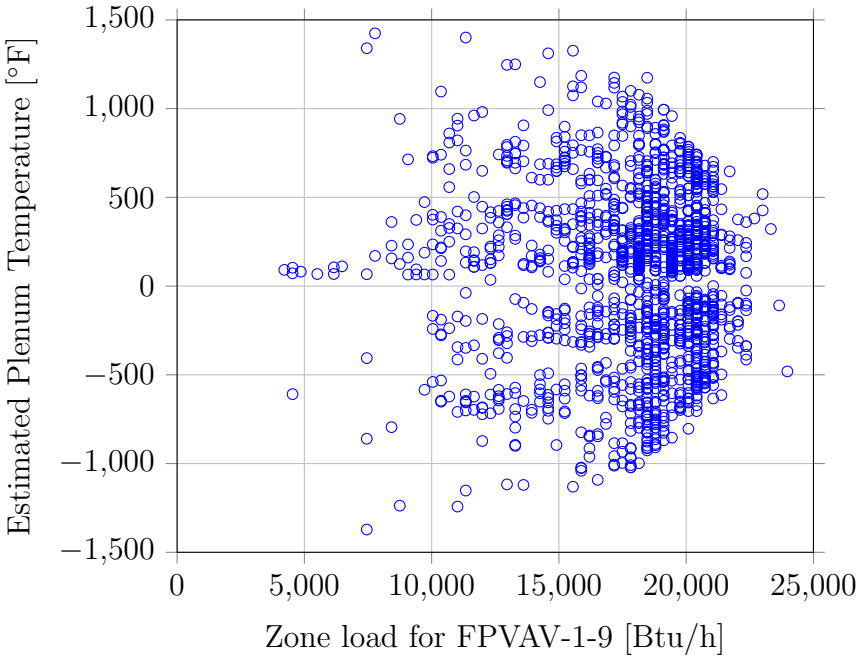

Figure 6.23: Calculated plenum temperature for FPVAV-1-9.

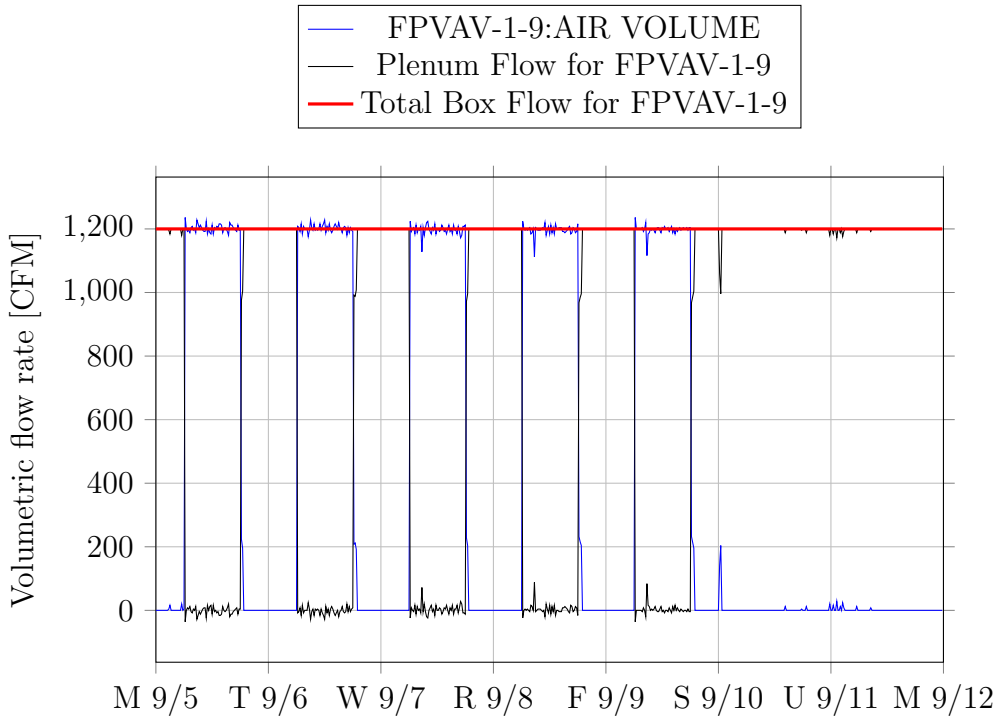

Figure 6.24: Flowrates for FPVAV-1-9.

Table 6.10: Calculated plenum temperature statistics for NCTM.

Unit	Min	5th Perc.	Mean	Med.	95th Perc.	Max	St. Dev.	Original Count	Final Count
1-8	56.5	56.5	60.6	58.8	71.8	71.8	4.25	29,199	26
2-12	52.8	55.7	60.8	61.8	62.5	75.0	2.23	29,319	3,500
2-15	52.1	57.4	61.3	61.8	62.6	78.5	1.84	29,324	6,262
1-9	57.0	57.0	63.6	65.0	73.5	73.8	5.34	27,961	17
2-6	65.0	65.0	65.0	65.0	65.0	65.0	0.00	29,311	1
2-18	61.5	62.7	69.6	67.0	80.2	80.5	5.60	29,312	45
2-16	67.0	67.0	67.3	67.5	67.5	67.5	0.29	29,325	3
2-10	66.5	66.5	67.8	67.8	69.0	69.0	1.44	29,236	4
2-14	60.0	61.0	68.8	68.5	79.0	79.8	6.28	29,318	41
2-11	66.5	66.5	68.0	68.5	69.5	69.5	1.01	28,557	12
2-5	68.5	68.5	69.1	69.0	70.0	70.0	0.65	29,309	5
2-8	68.2	69.1	70.0	70.0	70.7	72.5	0.55	29,304	410
2-13	68.0	68.5	70.0	70.0	71.5	72.6	1.34	29,312	33
1-5	55.0	63.8	71.1	70.1	78.0	79.0	4.62	30,170	166
2-17	61.5	68.5	70.3	70.4	71.5	72.5	1.23	29,287	256
2-2	52.5	67.3	70.7	70.8	73.6	75.6	2.69	29,363	386
1-7	60.0	64.5	71.8	71.8	75.1	75.7	3.11	29,955	233
2-3	64.5	71.0	73.0	72.8	75.3	76.2	1.49	29,367	1,060
1-2	67.0	70.8	73.9	72.9	77.8	78.5	2.60	30,166	124
2-1	67.5	70.8	73.6	73.8	75.5	81.7	1.44	29,366	1,170
1-3	71.4	72.6	74.2	74.4	75.4	76.9	0.94	30,145	542
2-9	69.0	70.7	73.9	74.5	76.5	78.4	1.88	29,272	6,921
1-1	57.0	71.8	74.6	74.8	79.0	82.5	2.64	30,152	708
1-10	58.5	62.0	73.8	74.9	76.0	78.2	3.61	29,941	297
1-4	54.0	72.4	74.9	75.1	77.2	81.7	2.51	30,086	455
2-4	69.5	73.7	75.3	75.2	76.7	77.6	0.96	29,304	3,834
1-6	56.5	66.2	74.1	75.6	81.3	81.6	5.43	30,170	79
2-7	N/A	N/A	N/A	N/A	N/A	N/A	N/A	28,906	0

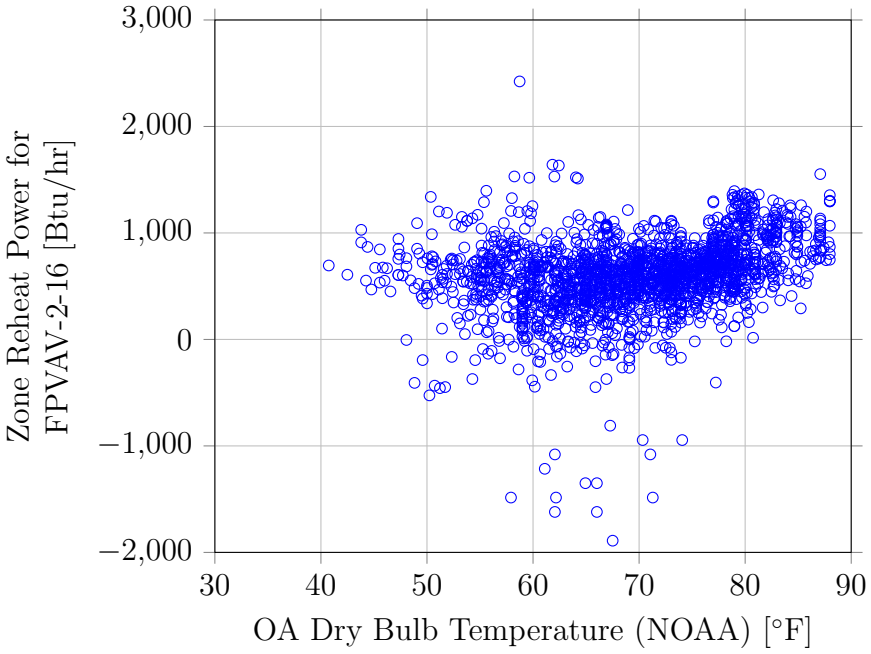

Figure 6.25: Zone reheat power for terminal unit 2-16.

plenum temperature is lower than the zone temperature that was assumed.

Figure 6.27 shows a case in which the reheat is estimated to be a negative value, which likely means that the actual plenum temperature is greater than the assumed plenum temperature equal to the zone temperature.

Another way to view the accuracy and importance of the plenum temperature on the amount of reheat necessary is to look at the difference between the discharge temperature and the predicted mixed air temperature in the terminal unit under conditions when the reheat valve is closed. During these times the values should be nearly equal, and the difference should be near zero.

Under the assumption that the plenum temperature is equal to the corresponding zone temperature, it does not appear as if this assumption is valid for the corresponding energy calculations. Figure 6.28 shows as much as an 8°F difference for FPVAV-

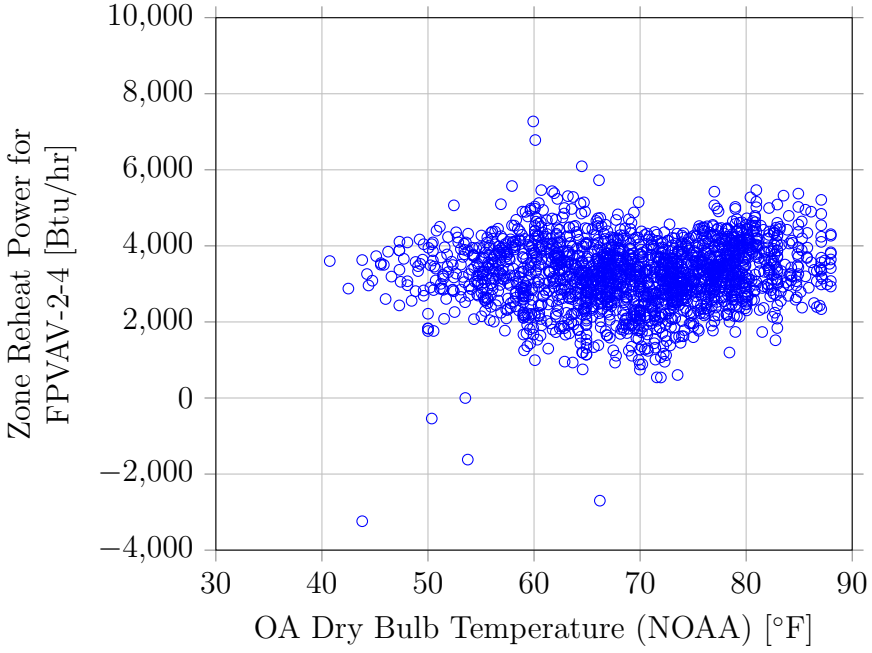

Figure 6.26: Zone reheat power for terminal unit 2-4.

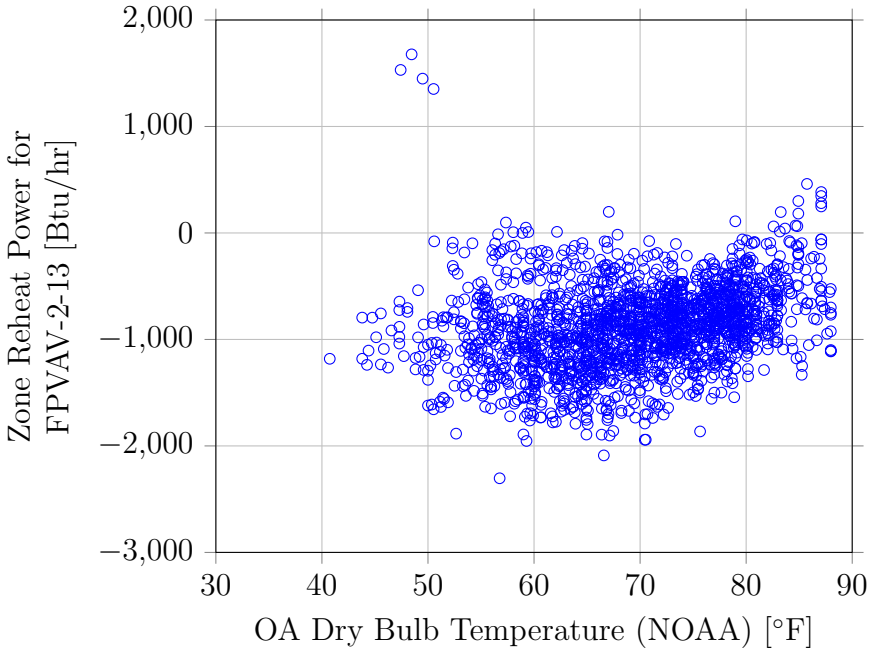

Figure 6.27: Zone reheat power for terminal unit 2-13.

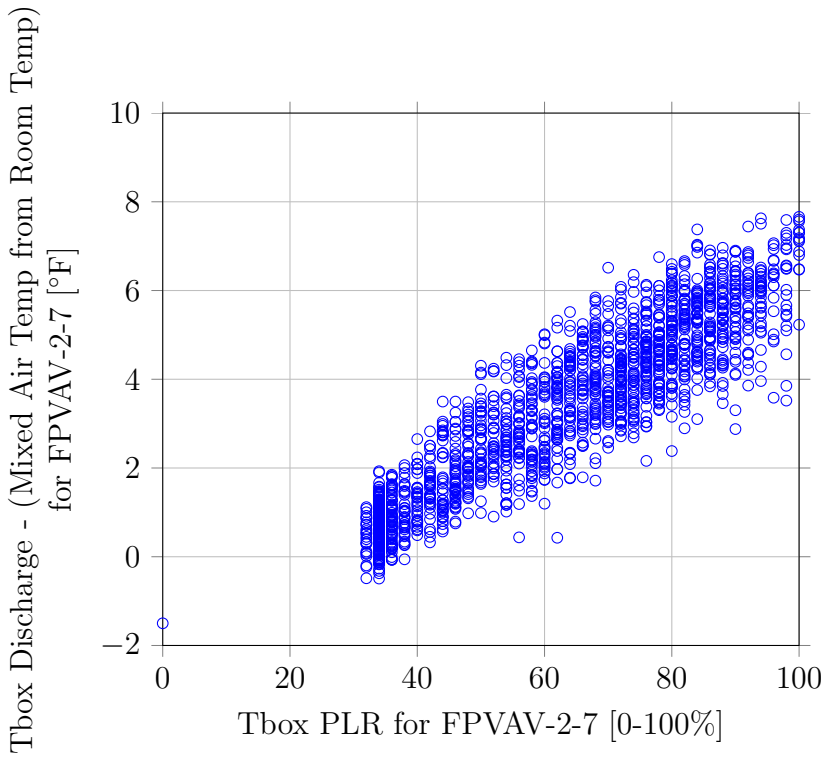

Figure 6.28: Difference between discharge temperature and predicted mixed air temperature using the zone temperature assumption for FPVAV-2-7.

2-7. Because the value is positive, this means that the plenum temperature is likely higher than the assumed zone temperature, assuming that the measured discharge temperature is more accurate that the estimation of the plenum temperature.

The opposite case can be seen with FPVAV-2-15, as shown in Figure 6.29. In this case, the values are all negative, indicating that the plenum temperature is lower than the zone temperature. The plots are from the same period and cover a broad range of outdoor air temperatures from 36°F to 96°F. Both plots do appear linear with regards to the PLR of the terminal unit. This linearity indicates that there is some relationship with the plenum temperature and the amount of conditioned air coming from the parent air handling unit.

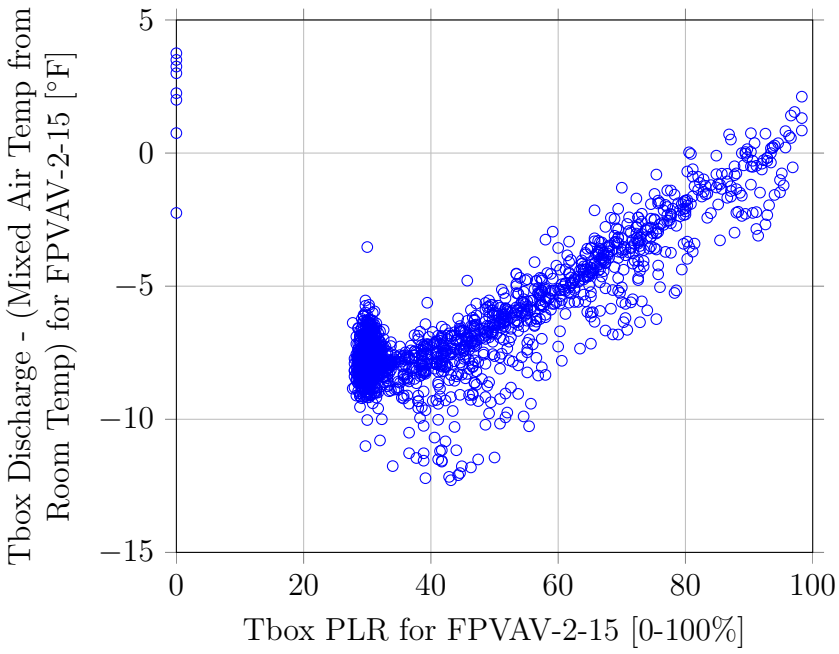

Figure 6.29: Difference between discharge temperature and predicted mixed air temperature using the zone temperature assumption for TU-2-15.

This linear dependence on the PLR does not carry to all the terminal units. As a counterexample to the previous plots, FPVAV-2-10 has a zig-zag pattern.

6.4 Analysis of Zone Load Predictions

An important factor in the optimization methodology is the prediction of the zone loads at a given time, without access to current live sensor information.

Before analyzing how well different zone loads can be predicted, it is important to gather insight into the nature of the calculated zone load variable that is proposed to be used as the surrogate for the actual zone load.

If the zone loads are being met and steady-state conditions are assumed, the sensible zone load will be

$$\dot{Q}_z = \dot{V}_z \rho_a c_{p,a} \left(T_{dis} - T_z\right) \approx 1.08 \cdot \dot{V}_z \left(T_{dis} - T_z\right) \tag{6.12}$$

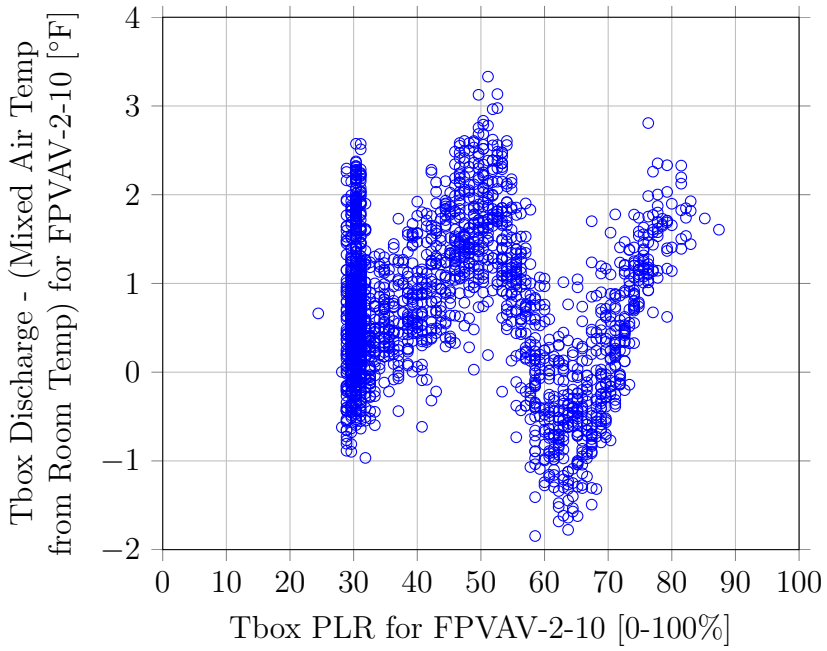

Figure 6.30: Difference between discharge temperature and predicted mixed air temperature using the zone temperature assumption for FPVAV-2-10.

where $\dot{Q}$ is in units of $\frac{\text{BTU}}{\text{h}}$, $\dot{V}_z$ is in CFM, and the temperatures are in °F.

As a result of the dynamics of how terminal units are controlled in reality, the estimated zone load can vary back and forth, while the true zone load is expected to be a smoother function over the course of a day. Figure 6.31 shows how the estimated zone load using Equation 6.12 can change directionality several times over the course of a day. The zone load for terminal unit FPVAV-1-7 typically varied from 6,000 BTU/hr to 20,000 BTU/hr over the course of the week from June 6, 2016, to June 11, 2016.

Figure 6.32 shows another example of how the estimated zone load may vary throughout a typical week. Figure 6.32 shows the zone load for FPVAV-2-2, which experiences a significant load compared to the other terminal units at NCTM. The zone load varies from near 10,000 BTU/hr to near 50,000 BTU/hr at its peak.

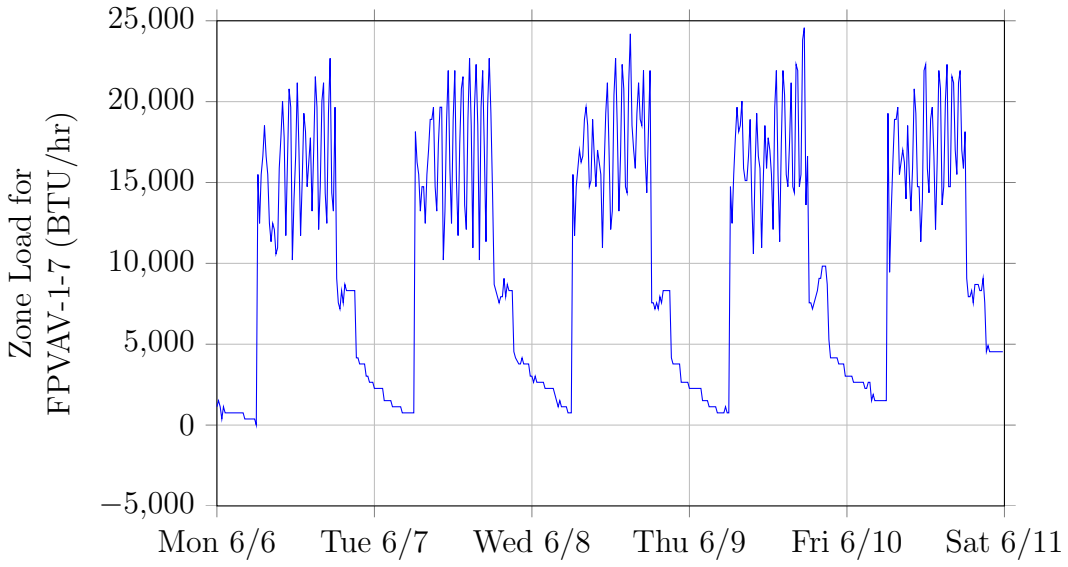

Figure 6.31: Zone load estimation for FPVAV-1-7.

With Figure 6.31 as evidence, it is clear that the "true" zone load cannot be reasonably estimated with the trend data that is available in typical BAS systems. However, the ratio of magnitudes of the load from zone to zone can still be inferred and be useful in improving the energy efficiency of the system.

Figure 6.33 shows an example of the zone load plotted against outdoor air dry-bulb temperature. Notice that the load is not a well-defined function of T_{oa}. This turns out to be the case for many of the internal zones, which have a higher dependence on the time of day parameters.

Figure 6.34 shows the zone load for FPVAV-2-9 versus T_{oa}. FPVAV-2-9 serves only internal zones, and the load only ranges from approximately 0 $\frac{\text{BTU}}{\text{h}}$ to 10,000 $\frac{\text{BTU}}{\text{h}}$.

Statistics related to the predictions of the zone loads for data ranging from October 6, 2015, to June 1, 2016, are given in Table 6.11.

The highest errors in the prediction were for FPVAV-1-4, the zone that has the highest overall zone load in the building, by a significant margin. It has estimated

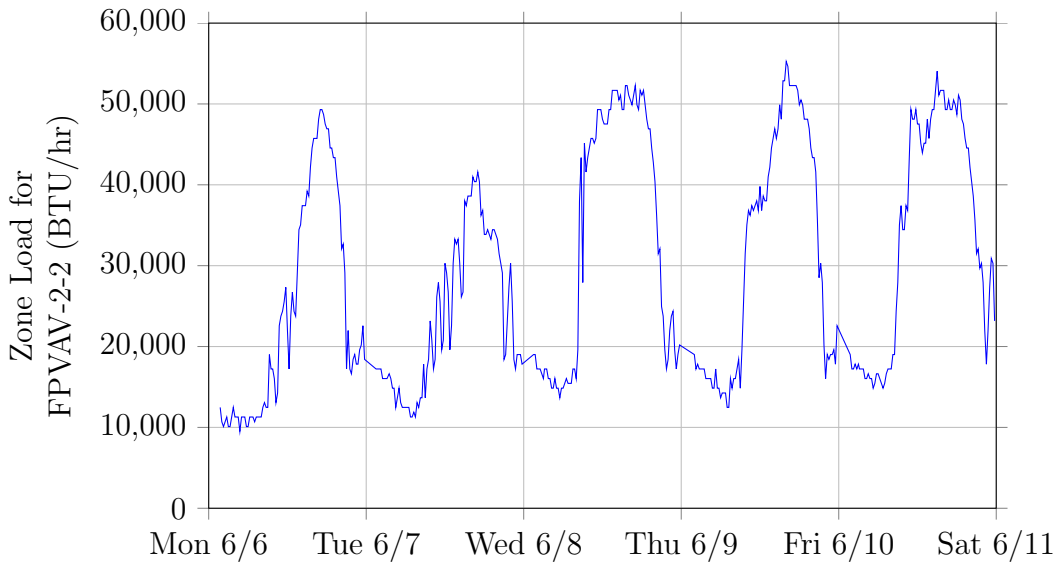

Figure 6.32: Zone load estimation for FPVAV-2-2.

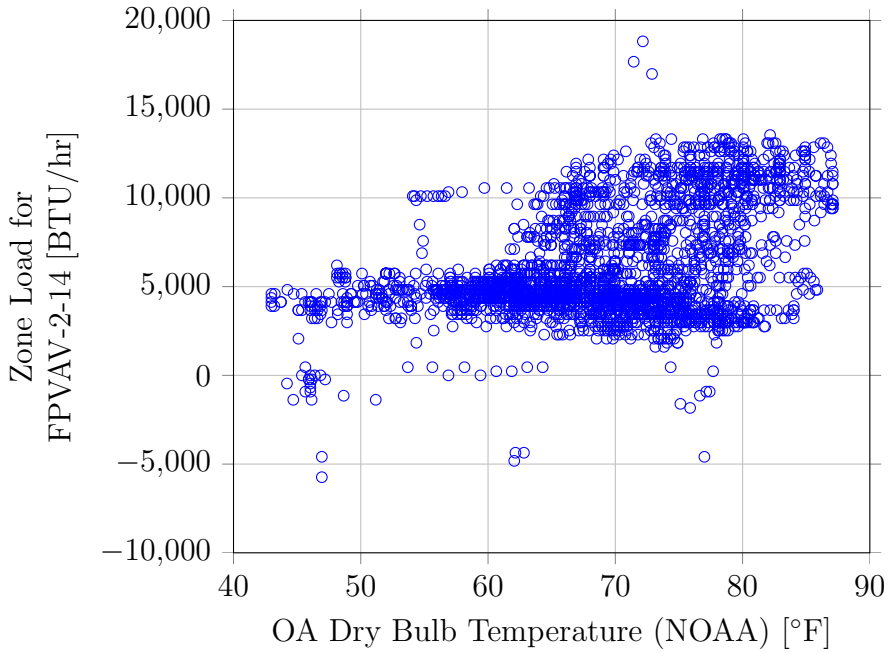

Figure 6.33: Calculated zone load for FPVAV-2-14 during the month of April 2016.

Table 6.11: Statistics related to the prediction of the zone loads at NCTM.

Terminal Unit	Med. Abs. Error (BTU/hr)	Mean Abs. Error (BTU/hr)	RMSE (BTU/hr)	MBE (BTU/hr)
FPVAV-2-7	108	171	298	-41
FPVAV-2-16	135	385	704	59
FPVAV-2-5	162	221	328	-22
FPVAV-2-12	203	1,058	1,885	-896
FPVAV-2-6	216	488	836	24
FPVAV-2-13	270	784	1,841	68
FPVAV-2-10	292	631	1,000	-87
FPVAV-2-11	302	708	1,062	-68
FPVAV-2-18	324	914	1,614	77
FPVAV-1-11	324	703	1,585	115
FPVAV-2-14	459	1,004	1,780	-9
FPVAV-2-4	540	1,036	2,012	84
FPVAV-1-2	626	1,201	2,056	-385
FPVAV-2-8	648	991	1,519	-43
FPVAV-2-9	648	1,236	1,763	635
FPVAV-2-17	691	1,386	2,327	122
FPVAV-2-15	756	3,852	12,353	552
FPVAV-1-8	945	1,371	1,978	336
FPVAV-2-3	972	1,789	3,587	-171
FPVAV-2-1	1,080	1,609	2,871	-559
FPVAV-1-9	1,296	1,850	2,805	209
FPVAV-1-5	1,404	2,463	4,105	-17
FPVAV-1-10	1,512	2,819	4,634	1,054
FPVAV-1-1	1,598	3,783	6,267	-1,359
FPVAV-1-3	1,755	3,164	4,868	-237
FPVAV-1-6	1,814	3,186	4,861	261
FPVAV-1-7	2,268	2,827	3,942	-326
FPVAV-2-2	2,376	4,422	7,184	1,773
FPVAV-1-4	3,024	5,569	8,502	19

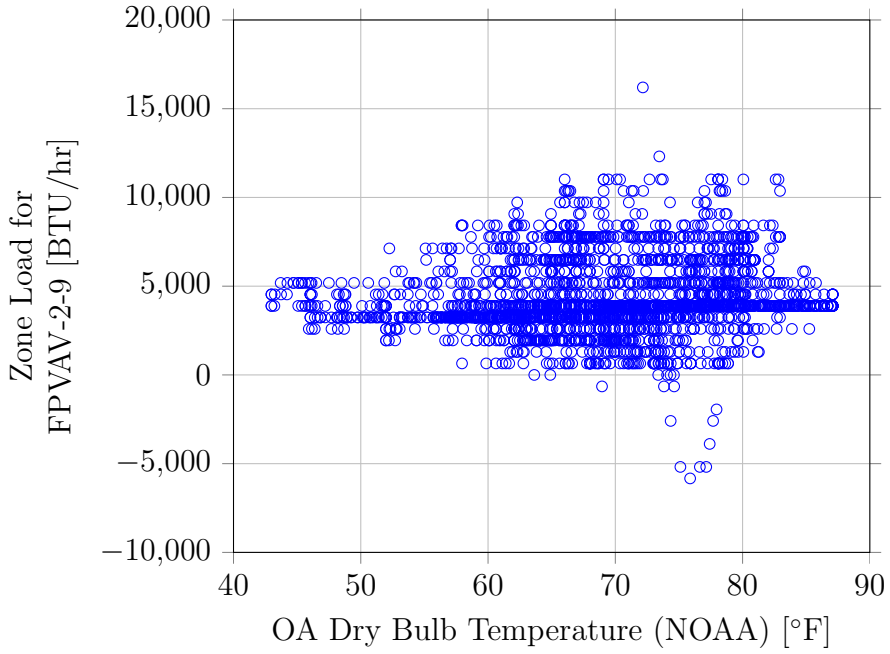

Figure 6.34: Calculated zone load for FPVAV-2-9, which serves only internal space, during the month of April 2016.

loads near 50,000 BTU/hr.

An interesting pattern was that the nearest neighbor prediction function overpredicted the zone load (as calculated by Equation 6.12) when the zone cooling load was small or was a heating load and underpredicted the zone load during times of high cooling load.

The residual is defined as the predicted value minus the estimated value, so a positive value indicates overprediction, while a negative value indicates underprediction.

This bias was seen in every terminal unit in the building, and this bias occurred with both the largest and smallest terminal units. Figures 6.35 through 6.37 show examples of this phenomenon. The explanation for this is that the median of data under similar conditions was used for the prediction. The function therefore cannot

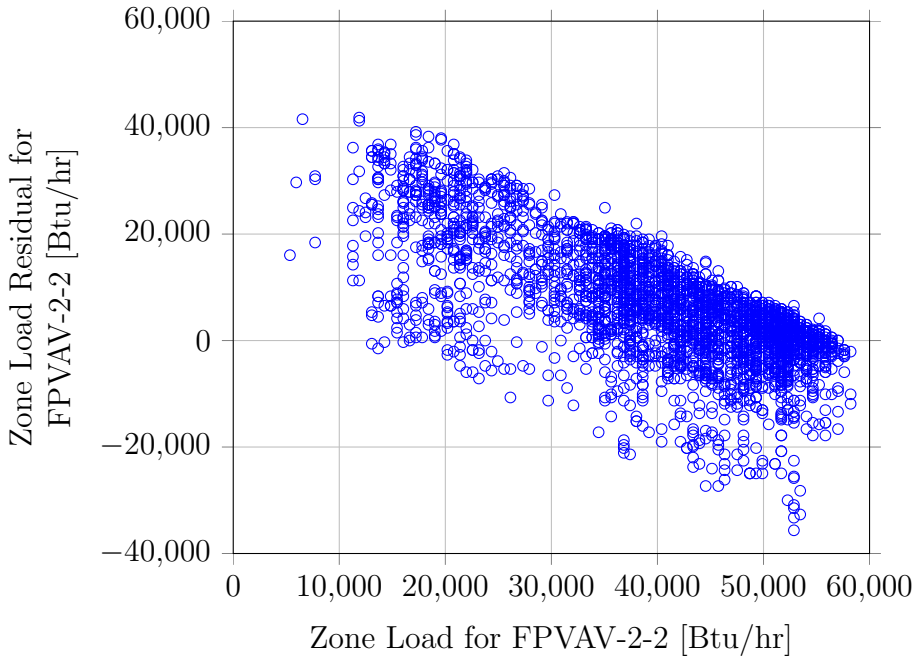

Figure 6.35: Bias in zone load prediction for FPVAV-2-2.

overpredict the highest value or underpredict the lowest value. The date period analyzed was from March 1, 2016, to August 1, 2016, ignoring when the AHUs were off, federal holidays and weekends, and hours from 5 PM to 9 AM.

An analysis was also completed regarding the optimal parameters for the nearest neighbor approach. The three parameters for the function are the time of day threshold, the outdoor air temperature threshold, and the number of data points to use.

Three different tests cases for each variable were used. The time of day threshold was adjusted from 1 timestamp away, 2 timestamps away, and 4 timestamps away. For 15 minute interval data, this means that the threshold was 15 minutes, 30 minutes, and 1 hour.

The outdoor air temperature threshold was tested at 1°F, 3°F, and 5°F. The

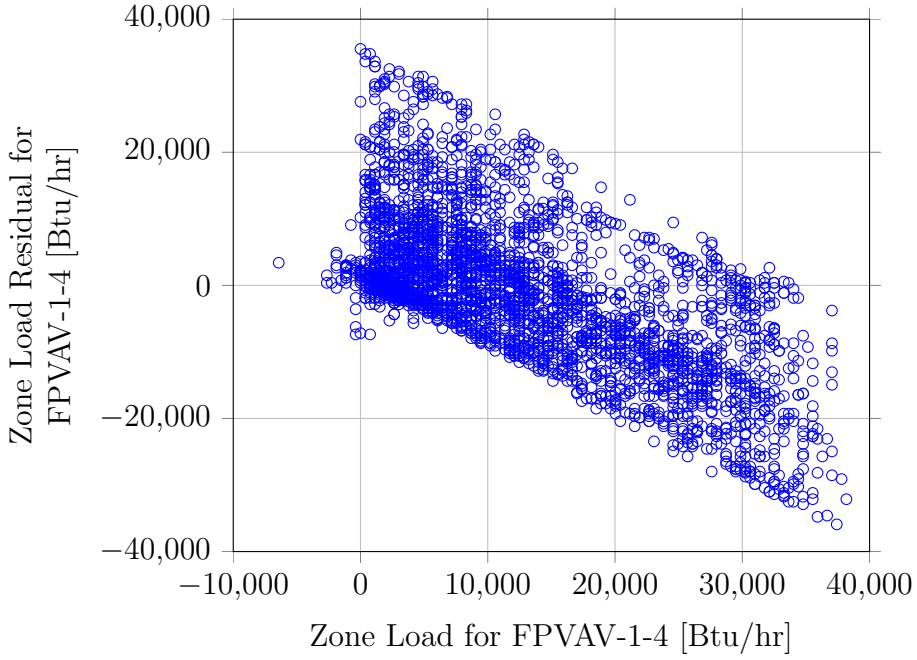

Figure 6.36: Bias in zone load prediction for FPVAV-1-4.

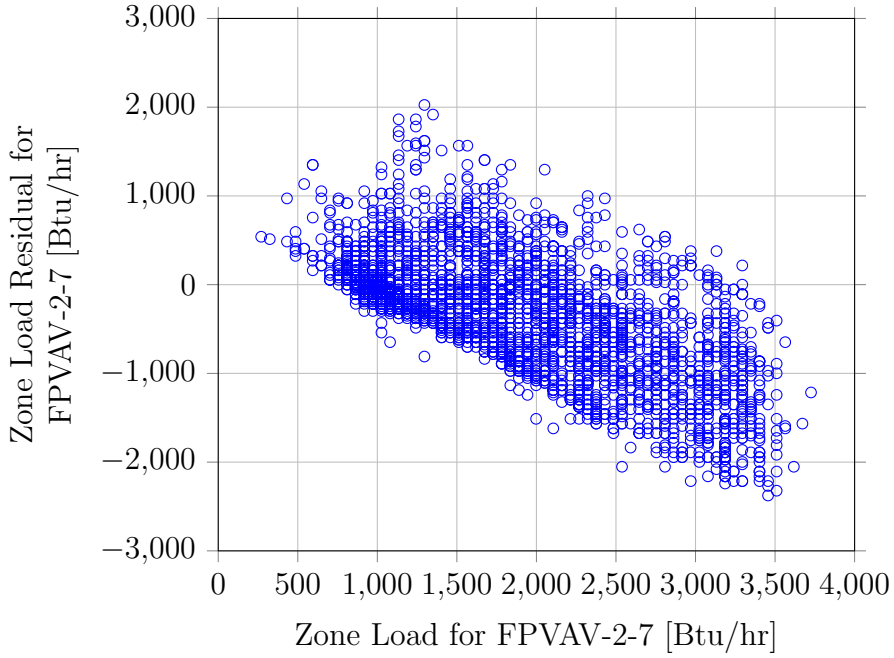

Figure 6.37: Bias in zone load prediction for FPVAV-2-7.

number of data points used in the median was 15, 30, and 45.

The objective function for these tests was the average root mean squared error (RMSE) divided by the range of the calculated zone loads for all the terminal units in NCTM, which is defined as CV-RMSE*.

$$\text{CV-RMSE*} = \frac{\text{RMSE}}{y_{max} - y_{min}} \tag{6.13}$$

Note that for data sets such as zone load which can be both above and below zero, that the coefficient of variation using the mean as the normalization factor, a commonly used metric in evaluating model fits, can be arbitrarily high because the mean can be close to zero (implying that the zone load is both positive and negative).

The tests were done for data from January 1st, 2016 through January 1st, 2017. Times when the air handling units were off and the first and last hour of operation, weekends, and federal holidays were all ignored.

The results show that the goodness-of-fit metrics were insensitive to the various parameters. In addition, the results indicate that looser thresholds, which results in more recent data being used, gave the best model fits. The best average CV-RMSE* was 11.6% was under the conditions of thresholds of plus or minus one hour, 5°F, and using 45 data points. The worst models had an average CV-RMSE* of 13.5%, for the thresholds of plus or minus 15 minutes, 1°F, and 45 data points. The rest of the tests are also shown in Table 6.12.

A main takeaway of the tests, however, was that the results were insensitive to the parameters. This means that the parameters may be adjusted for benefits in other areas such as performance. By having large thresholds and requiring less data points, less historical data needs to be searched, and the time to complete the calculations is reduced.

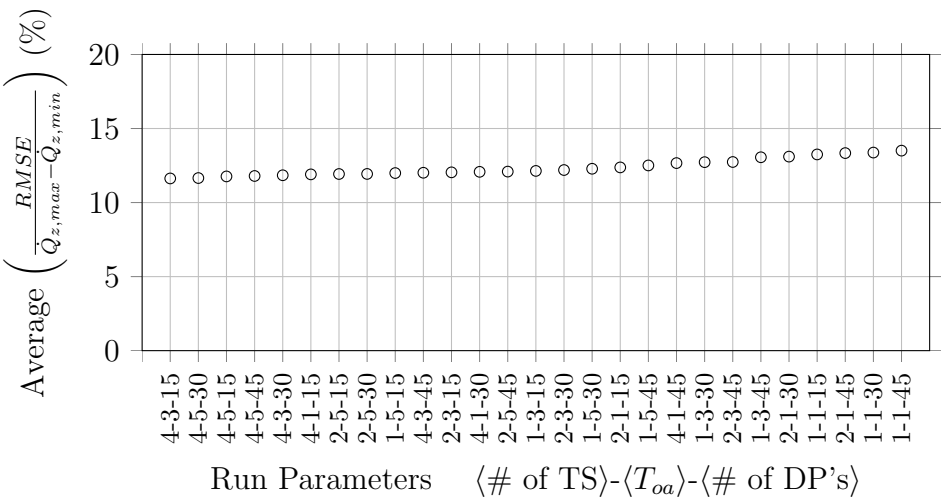

Figure 6.38: Zone load prediction results using the Nearest Neighbor approach.

A plot of these results in order of predictive ability is shown in Figure 6.38.

6.5 Analysis of the Critical Zones

The critical zone/damper could be used to determine the static pressure setpoint that can be used to supply the desired flows found from the optimization. An important consideration in the methodology is checking how well this assumption holds. Data from NCTM was used to test the validity of the approach.

The following figures show the maximum damper position of the terminal units for each of the air handlers during the month of April 2016. During this time, for AHU-2-1 and AHU-2-2, there was no time in which a terminal unit damper was fully open, which indicates that there is potential for the supply air static pressure setpoints of these AHUs to be reduced.

An investigation into the critical zones based on historical data was completed. 15 minute interval data from January 1, 2016, through June 1, 2016, was used to check which damper positions were most open at a given timestamp. Table 6.13

Table 6.12: Testing results for zone load prediction.

Run	TS	T_{oa}	# of Data Points	Average $\left(\frac{\text{RMSE}}{\dot{Q}_{z,max}-\dot{Q}_{z,min}}\right)$ (%)
1	1	1	15	10.12
2	2	1	15	9.68
3	4	1	15	9.80
4	1	3	15	9.61
5	2	3	15	9.41
6	4	3	15	8.97
7	1	5	15	9.28
8	2	5	15	9.18
9	4	5	15	8.98
10	1	1	30	10.58
11	2	1	30	10.07
12	4	1	30	9.39
13	1	3	30	9.95
14	2	3	30	9.63
15	4	3	30	9.16
16	1	5	30	9.61
17	2	5	30	9.25
18	4	5	30	9.00
19	1	1	45	10.75
20	2	1	45	10.47
21	4	1	45	9.80
22	1	3	45	10.08
23	2	3	45	9.58
24	4	3	45	9.32
25	1	5	45	9.74
26	2	5	45	9.52
27	4	5	45	9.08

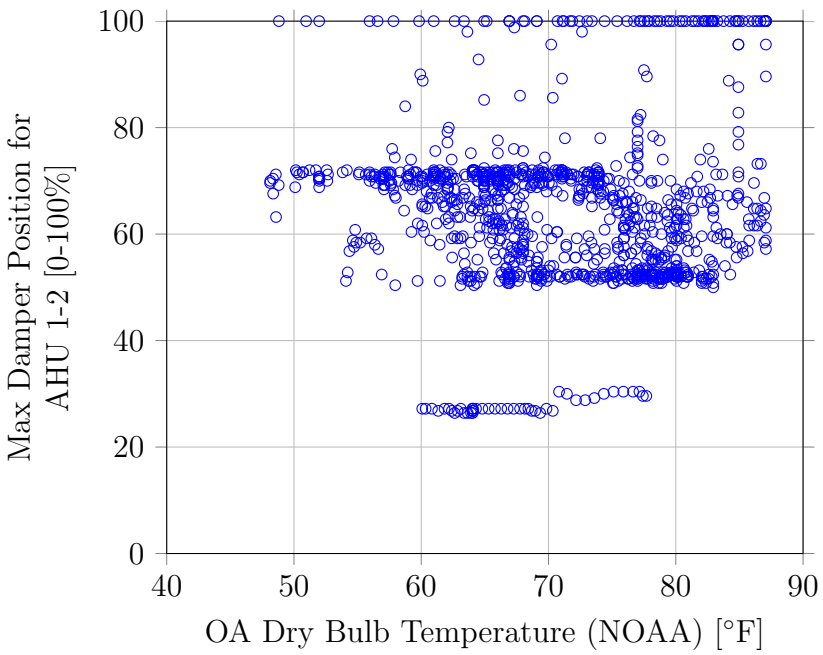

Figure 6.39: Maximum damper position of all terminal units versus T_{oa} for AHU-1-2 during the month of April 2016.

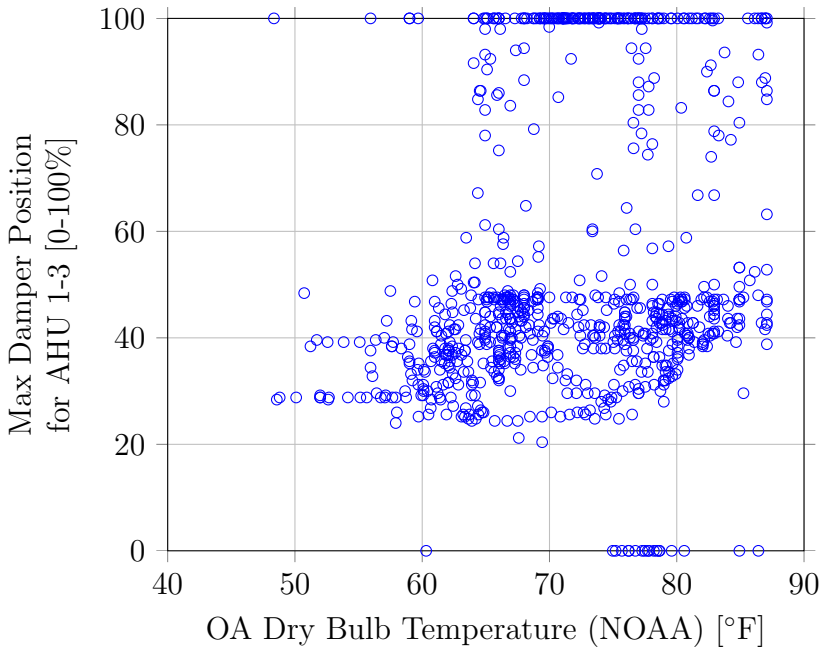

Figure 6.40: Maximum damper position of all terminal units versus T_{oa} for AHU-1-3 during the month of April 2016.

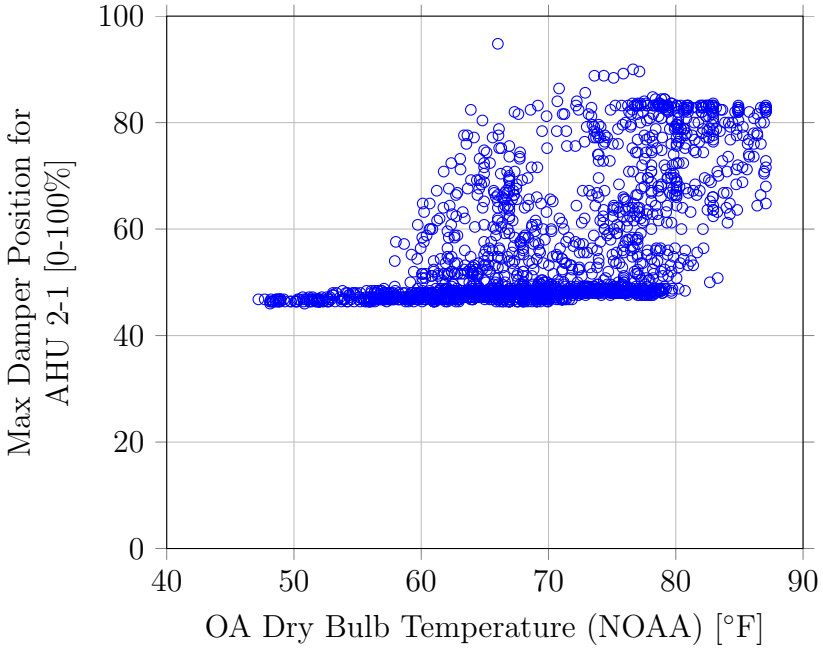

Figure 6.41: Maximum damper position of all terminal units versus T_{oa} for AHU-2-1 during the month of April 2016.

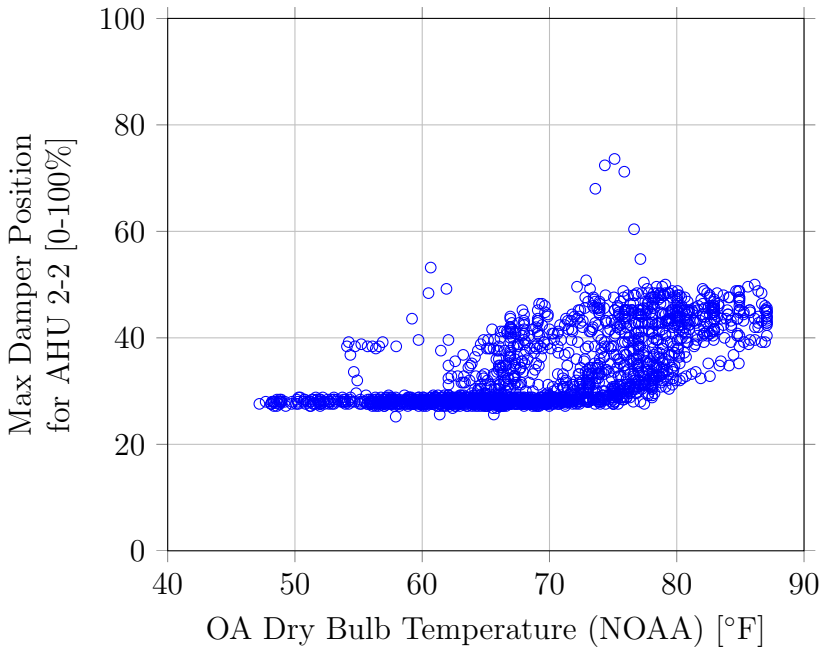

Figure 6.42: Maximum damper position of all terminal units versus T_{oa} for AHU-2-2 during the month of April 2016.

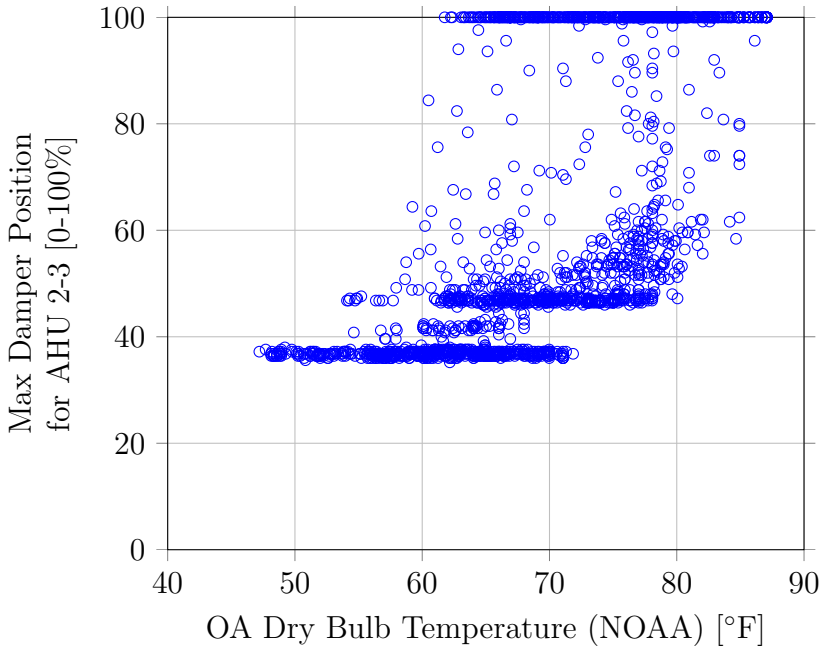

Figure 6.43: Maximum damper position of all terminal units versus T_{oa} for AHU-2-3 during the month of April 2016.

shows the results of this analysis. In all five of the applicable air handling units, there is a damper that is critical at least 59% of the time.

This analysis was not actively used to optimize the air handling unit system at NCTM. However, if more information were available regarding the fan and duct system, it could be used to also optimize the supply air static pressure setpoint in combination with the supply air temperature. It is useful to see, however, that potential exists to reduce fan power and the pressure drop throughout the system, which would aid in the goal of energy efficient operation.

6.6 Accuracy of Mechanical Specifications

In the simplified analysis and modeling being proposed, it would be ideal if the specifications in the mechanical drawings can be used directly. One important parameter is the design flow rate for the terminal unit. Table 6.4 shows the design

Table 6.13: Percentage of time that different terminal units for various AHUs were the most open during the period of January 1, 2016 - June 1, 2016.

AHU (# of term. units)	Unit	Count of Max	Percent as Critical (%)
AHU-1-2 (4)	FPVAV-1-8	3,518	68
	FPVAV-1-9	1,281	25
	2 others	354	7
AHU-1-3 (6)	FPVAV-1-5	2,331	59
	FPVAV-1-4	1,006	25
	4 others	622	15
AHU-2-1 (3)	FPVAV-2-1	10,965	79
	FPVAV-2-2	2,648	19
	FPVAV-2-3	258	2
AHU-2-2 (8)	FPVAV-2-18	10,003	72
	FPVAV-2-14	3,171	23
	6 others	648	5
AHU-2-3 (7)	FPVAV-2-6	9,883	72
	FPVAV-2-11	3,743	27
	FPVAV-2-10	184	1

flow rates for all the series fan powered terminal units in the NCTM building. The results show that the design specifications were sufficiently accurate. All data that were available at the time (October 6, 2015, through June 7, 2016) were analyzed to capture a large number of timestamps (over 22,000 timestamps). Over half the absolute differences between the measured maximum flow and the specified design flow are less than 100 CFM. There are several reasons for potential differences between the maximum measured flow and the design flow rates in the mechanical drawings. It may be the case that the terminal unit was oversized and the design flow rate was never necessary. There may be bias in the flow rate measurements.

The largest percent difference and absolute difference between the measured maximum flow rate and design value was for FPVAV-1-9. The difference was due to less than 15 outliers in the data (out of over 20,000 data points in total), and if they were to be removed, the maximum is in line with the design value of 1,200 CFM for the vast majority of the data, as seen in Figure 6.44.

6.7 Optimal Supply Air Temperature Results

The methods described in the previous sections were used to determine the optimal supply air temperature for various air handling units at the NCTM building. Figure 6.45 shows the results for AHU-2-3 during the work week from Monday, November 7, 2016, through Friday, November 11, 2016. During that week, the actual T_{sa} hovered between 58°F and 60°F. The optimal T_{sa} was predicted using different parameters for the simple fan curve exponent and plenum temperature. The optimization was completed using a fan exponent of 2 and 3, and the plenum temperature was assumed to be the room temperature or assumed to be the static median values shown in Table 6.10. Notice that even with the fan curve exponent varying from 2 to 3, the optimal T_{sa} is approximately 66°F, 7°F higher than the current operation.

Table 6.14: Comparison of design flow specifications to actual data.

AHU	Terminal Unit	Flow (CFM)	Maximum Meas. Flow (CFM)	Difference (CFM)
AHU-1-2	FPVAV-1-7	1,400	1,496	96
(5 hp)	FPVAV-1-8	700	840	140
	FPVAV-1-9	1,200	1,688	488
	FPVAV-1-10	1,600	1,712	112
AHU-1-3	FPVAV-1-1	1,480	1,676	196
(7.5 hp)	FPVAV-1-2	1,160	1,240	80
	FPVAV-1-3	1,300	1,364	64
	FPVAV-1-4	1,400	1,760	360
	FPVAV-1-5	1,040	612	−428
	FPVAV-1-6	1,120	1,288	168
AHU-2-1	FPVAV-2-1	2,000	2,016	16
(7.5 hp)	FPVAV-2-2	2,200	2,060	−140
	FPVAV-2-3	1,800	1,824	24
AHU-2-2	FPVAV-2-9	2,400	2,448	48
(10 hp)	FPVAV-2-12	500	452	−48
	FPVAV-2-13	1,000	1,032	32
	FPVAV-2-14	850	892	42
	FPVAV-2-15	1,400	1,332	−68
	FPVAV-2-16	500	484	−16
	FPVAV-2-17	1,280	1,304	24
	FPVAV-2-18	600	604	4
AHU-2-3	FPVAV-2-4	2,000	1,944	−56
(7.5 hp)	FPVAV-2-5	600	504	−96
	FPVAV-2-6	400	228	−172
	FPVAV-2-7	200	252	52
	FPVAV-2-8	1,200	1,184	−16
	FPVAV-2-10	540	588	48
	FPVAV-2-11	560	656	96

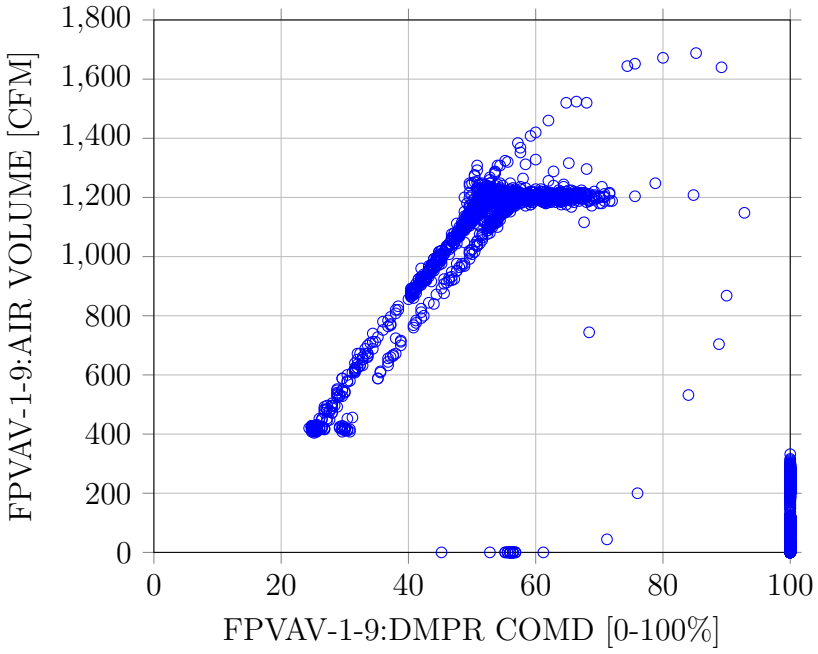

Figure 6.44: Damper position versus primary air flow for FPVAV-1-9.

It is also apparent that for this case study that the optimal supply air temperature is near the maximum of the search range. The maximum possible T_{sa} searched is the minimum between the T_{ma} and the minimum calculated discharge temperature. The T_{sa} cannot be above the T_{ma} because that would require heating in the air handling unit, and cannot be above the minimum calculated discharge temperature because then that particular zone would be starved for cooling capacity. For the second floor air handling units, the minimum discharge temperature is always less than the mixed air temperature indicating that cooling will always be required.

Figure 6.46 shows the results for the same computations as Figure 6.45, but for AHU-2-1. AHU-2-1 has 3 terminal units supporting a computer lab with higher measured loads than the rest of the second floor. The T_{ma} is also shown in Figure 6.46 for reference. The optimal T_{sa} appears to be higher than the current operation,

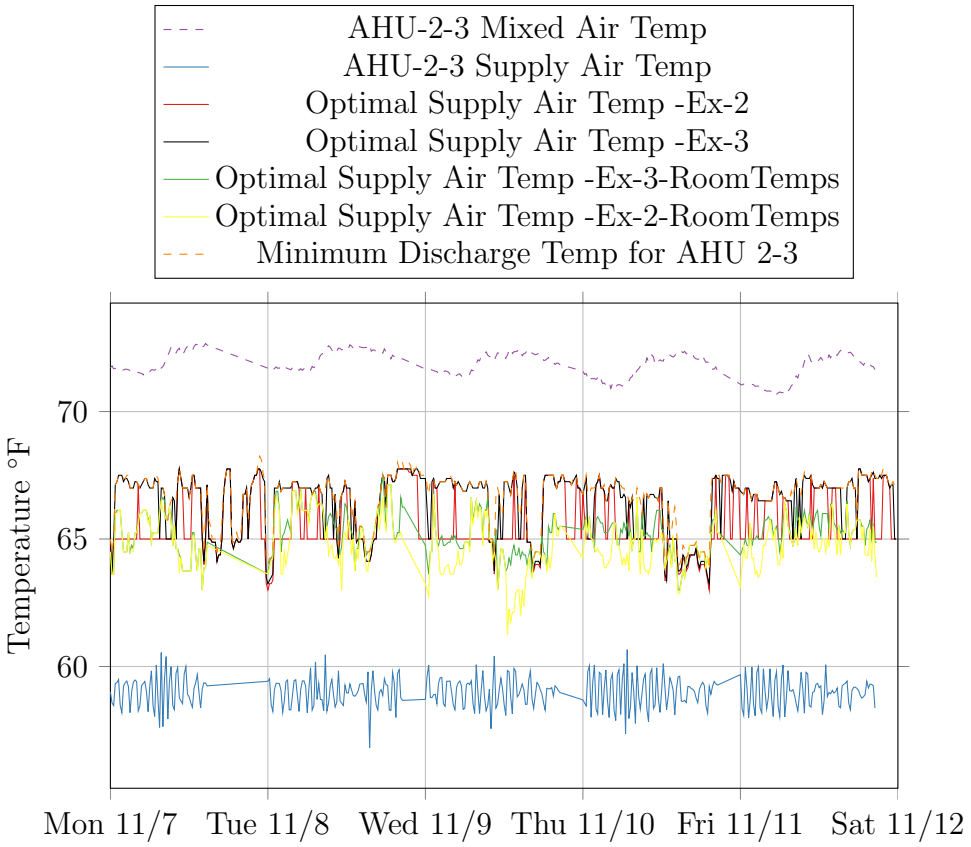

Figure 6.45: Optimal supply air temperature for AHU-2-3.

although a smaller difference compared to AHU-2-3 shown in Figure 6.45.

Figure 6.47 shows the results for AHU-2-2. In this case, the actual operation is near the estimated optimal T_{sa}.

6.8 Savings Potential

The potential for energy savings at the NCTM building was investigated for the second floor AHUs.

Energy savings were estimated for a period from June 1st, 2016 to January 1st, 2017. Weekends, times when the AHUs were off, federal holidays, and times from 5:00 PM to 9:00 AM were all ignored.

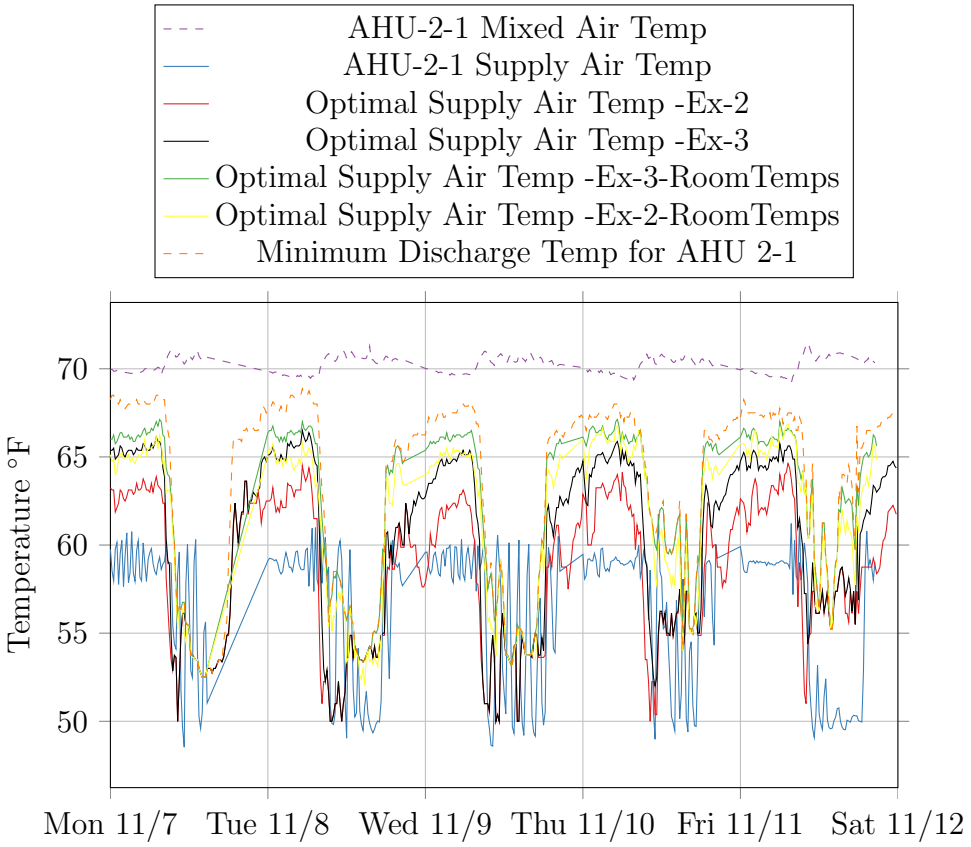

Figure 6.46: Optimal supply air temperature for AHU-2-1.

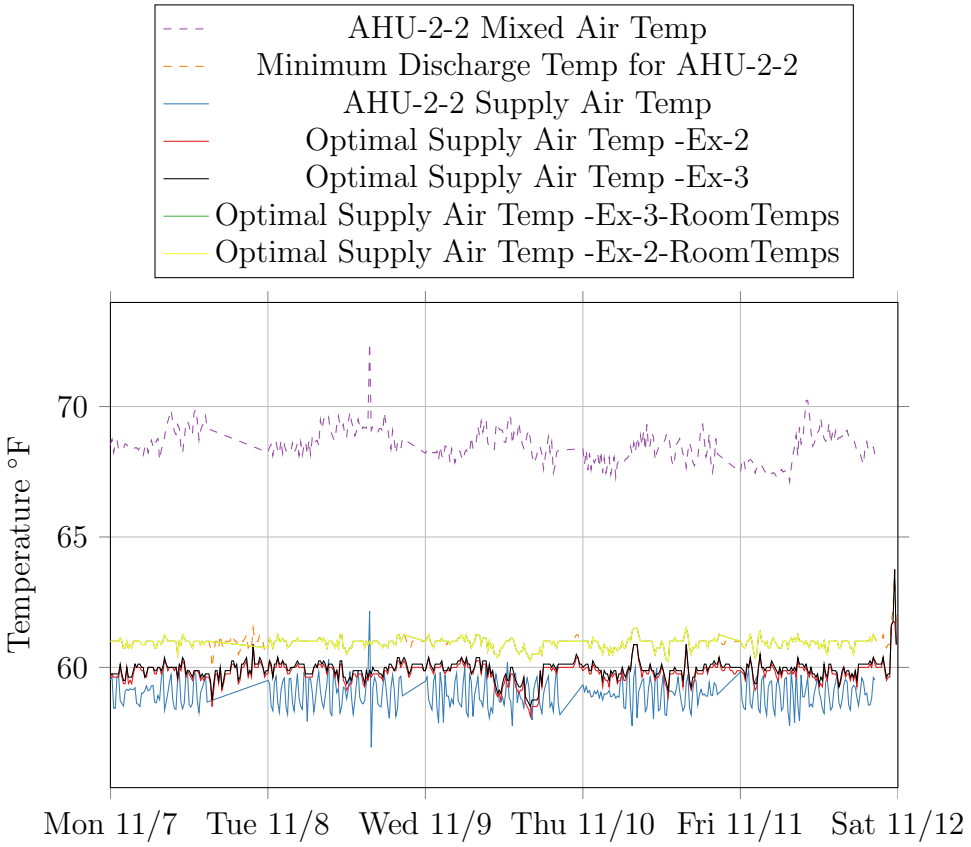

Figure 6.47: Optimal supply air temperature for AHU-2-2.

Also, since the calculation of reheat power in the terminal units had a high uncertainty level, it was decided to ignore times in which at least one of the reheat valves in the terminal units was open. Because most of the necessary reheat can be accomplished by mixing plenum air in the series fan powered terminal units, this only removed a small portion of the data. In this sense, the only components to the AHU energy were the cooling energy at the cooling coil and the fan energy.

To provide a sense of the sensitivity to the assumed parameters in the optimization, savings were determined using different exponents ranging from 2 to 3 for the PLR curve, along with the plenum temperature assumed to be the corresponding room temperature and the estimated constant plenum temperatures shown in Table 6.10.

Based on the optimal supply air temperatures shown in Section 6.7, the potential savings in AHU-2-1 and AHU-2-2 was small since the systems are already operating near optimal. However, the savings potential in AHU-2-3 appeared promising since there was approximately a 5°F difference between the operating supply air temperature and the predicted optimal supply air temperature. The savings results for AHU-2-3 under various different assumptions is shown in Table 6.15.

Figure 6.48 shows the difference in the combined energy of the fan and cooling from actual to optimal. Periods in which reheat was occurring were ignored in the analysis. As expected, the energy use has a dependence on T_{oa} and the optimal is less than the actual at all times. Regardless of the different parameters tested, over 20% savings were found for AHU-2-3.

The energy savings were primarily caused by increasing the supply air temperature, as seen in Figure 6.49. There already was a supply air temperature reset programmed for AHU-2-3, but the optimal reset would, in general, have a higher T_{sa}.

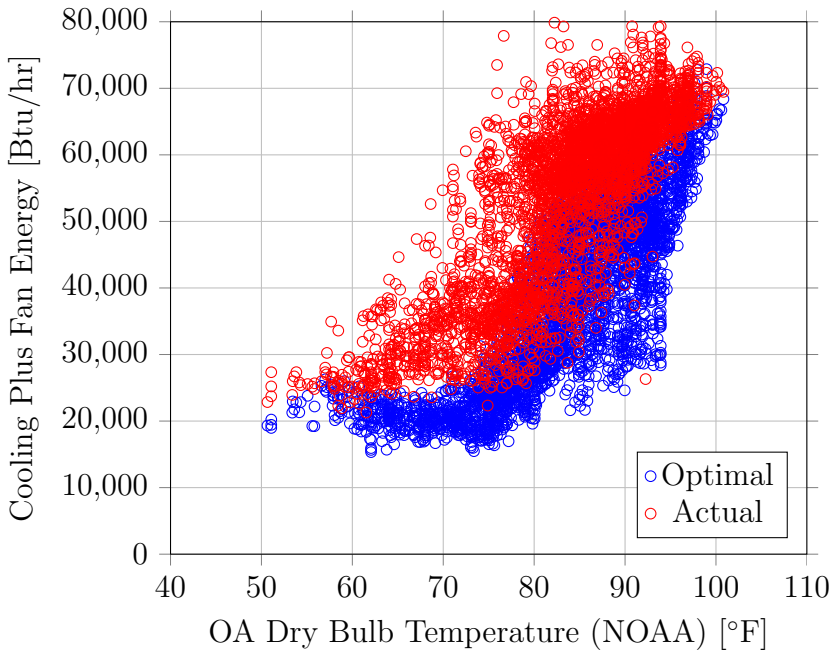

Figure 6.48: Energy savings for AHU-2-3 assuming a fan PLR exponent of 2 and plenum temperatures equal to the corresponding room temperature. There is a 13.98 MMBTU difference, or 26%.

Table 6.15: Savings results for AHU-2-3, depending on model assumptions.

Fan Exponent	Plenum Temperature Assumption	Actual (MMBTU)	Savings (MMBTU)	% Savings
2	Room Temperatures	53.43	13.98	26%
3	Room Temperatures	51.46	12.01	23%
2	Static Temperature	53.71	15.51	29%
3	Static Temperature	51.73	13.53	26%

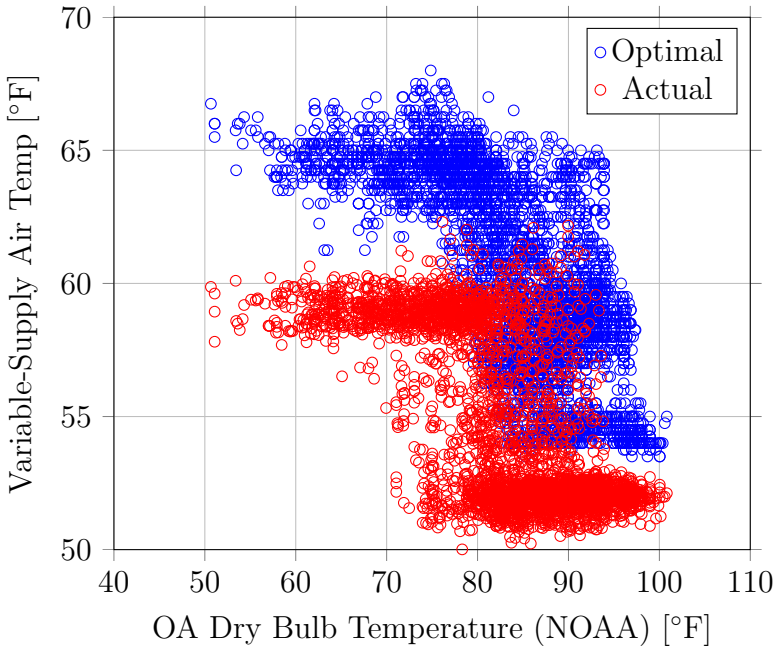

Figure 6.49: Supply air temperature difference between actual and optimal for AHU-2-3.

6.9 Discussion

A first comment is that it appears plausible that the "zone load" can be reasonably estimated to provide useful information with regards to optimization. In fact, the general relationship in the size of the thermal loads of the different zones is more important than the precise value, which is difficult to estimate.

The second is that the design specifications from mechanical drawings can be used as the first approximation for flows and power. There was general agreement between the terminal unit design flows and the actual maximum realized flows at NCTM, as seen in Table 6.14.

A third conclusion is that the uncertainty in the optimal T_{sa} was small enough that in most cases the current operation at NCTM does not fall within the bounds.

In the cases shown in Figure 6.45 through Figure 6.47, the optimal T_{sa} was higher than the current operation.

7. PRESTON ROYAL CASE STUDY

Preston Royal Branch Library is a one-story building with 12,400 ft^2 of gross floor area in Dallas, TX. The library opened in 1954. The facility consists of an open-space reading room and circulation, staff area, and an auditorium.

The library is served by a single air handling unit. A BAS graphic of the AHU is shown in Figure 7.1.

The AHU has 14 terminal units that serve the various areas of the library and are shown in Figure 7.2.

The terminal units are parallel fan powered boxes. A BAS graphic of one of the terminal units is shown in Figure 7.3. The graphics were provided through the Energy Systems Laboratory.

7.1 Preston Royal Zone Load Analysis

The zone load profiles for Preston Royal showed similarities to the NCTM building. During operation, the estimated zone load fluctuated up and down throughout the day. Figure 7.4 shows an example of how the zone load cycles up and down many times per hour. Again, the hypothesized explanation for this is not that the actual heat gain in the space is fluctuating, but that the HVAC controls are oscillating.

Figure 7.5 shows the zone load for all the terminal units at Preston Royal Library for 3 days from October 19th, 2016 through October 21st, 2016. Of interest to note is that within the same space, one terminal unit can be experiencing a relatively large cooling load (FPB-11) while another terminal unit is calling for heating (FPB-08).

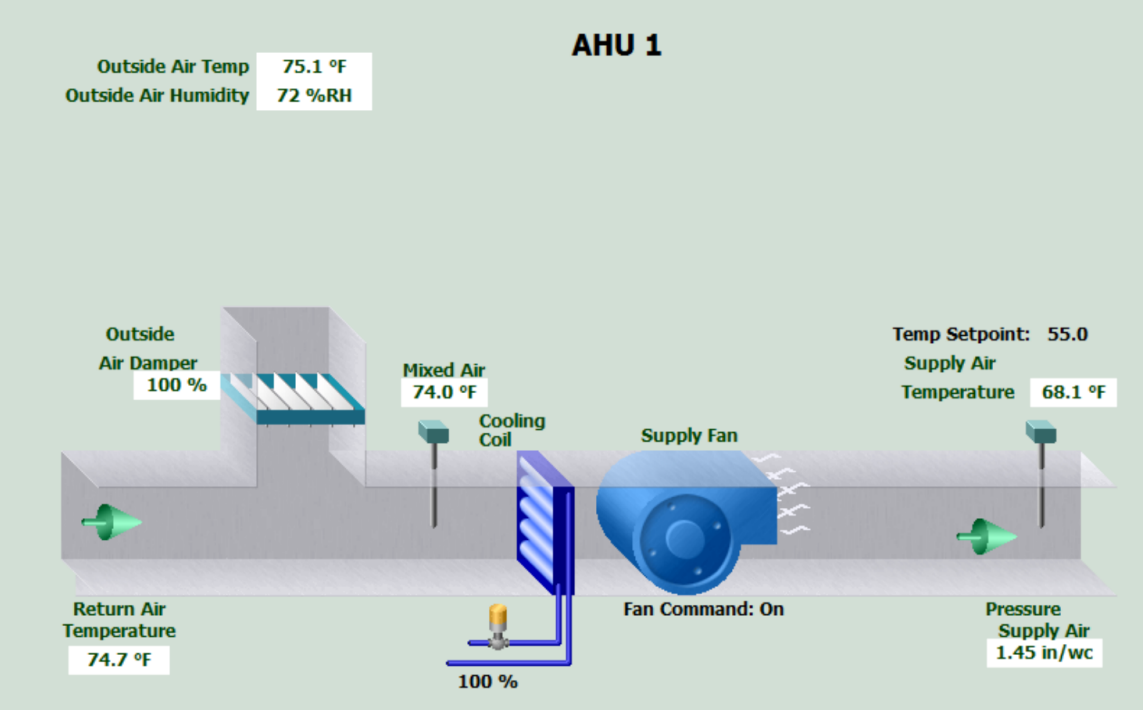

Figure 7.1: Preston Royal AHU BAS Graphic.

7.2 Estimated Savings

Only 7 of the 14 terminal units at Preston Royal Library had usable data. The estimated savings from this pseudo-synthetic data set was examined. A portion of the library was able to be optimized, utilizing several assumptions to make the analysis possible.

- There was no mixed air temperature sensor available, so the mixed air temperature was assumed to be between the outdoor air temperature and the return air temperature with the following relationship:

$$T_{ma} = 0.3\, T_{oa} + 0.7\, T_{ra} \tag{7.1}$$

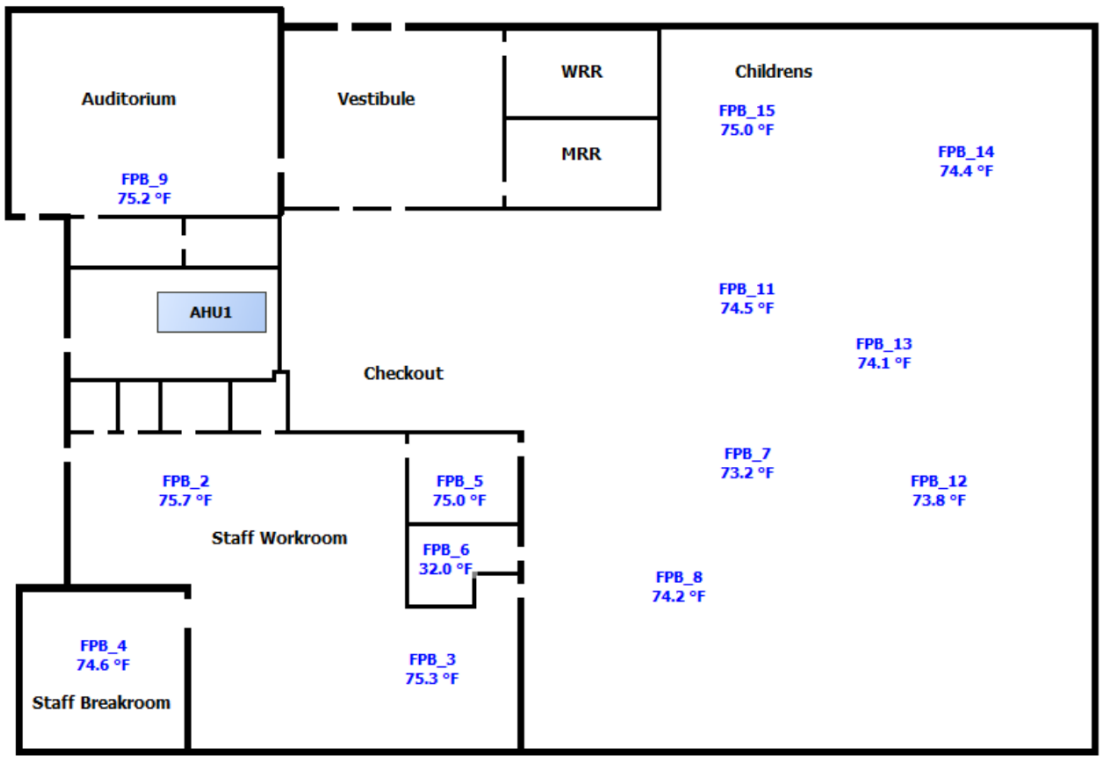

Figure 7.2: Preston Royal terminal unit layout.

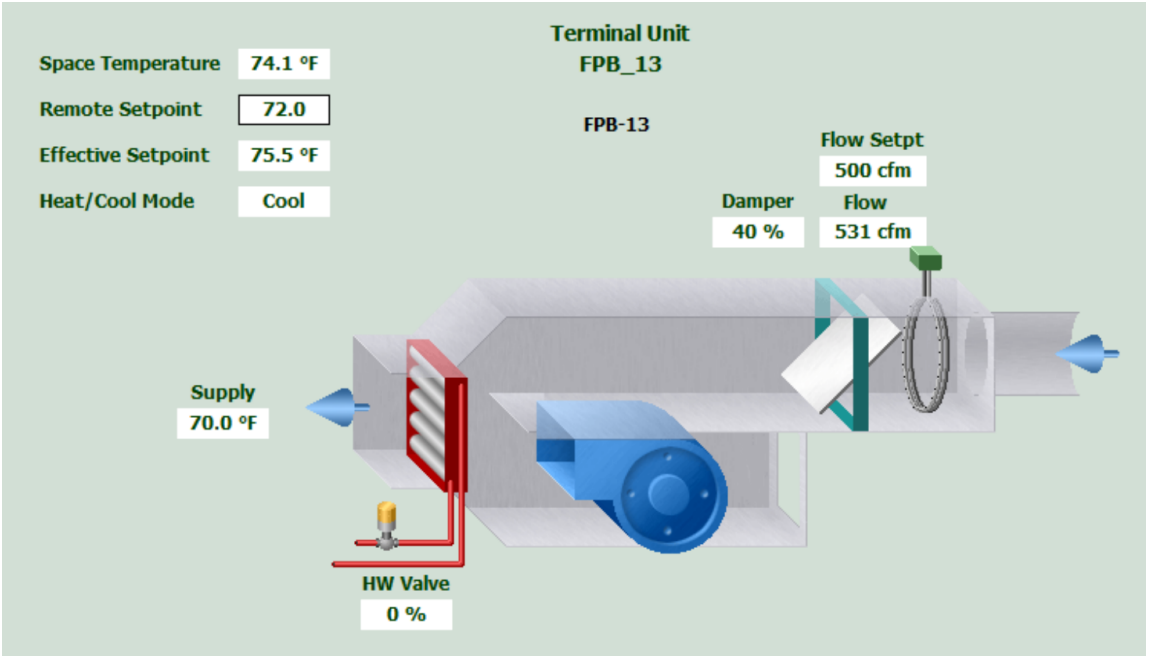

Figure 7.3: Preston Royal terminal unit graphic.

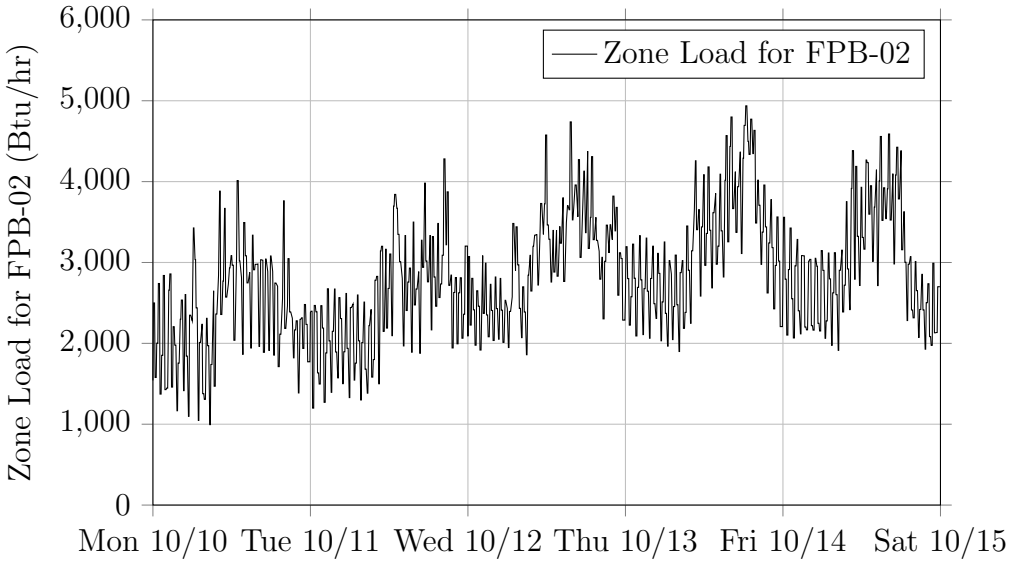

Figure 7.4: Zone load for FPB02 at Preston Royal Library.

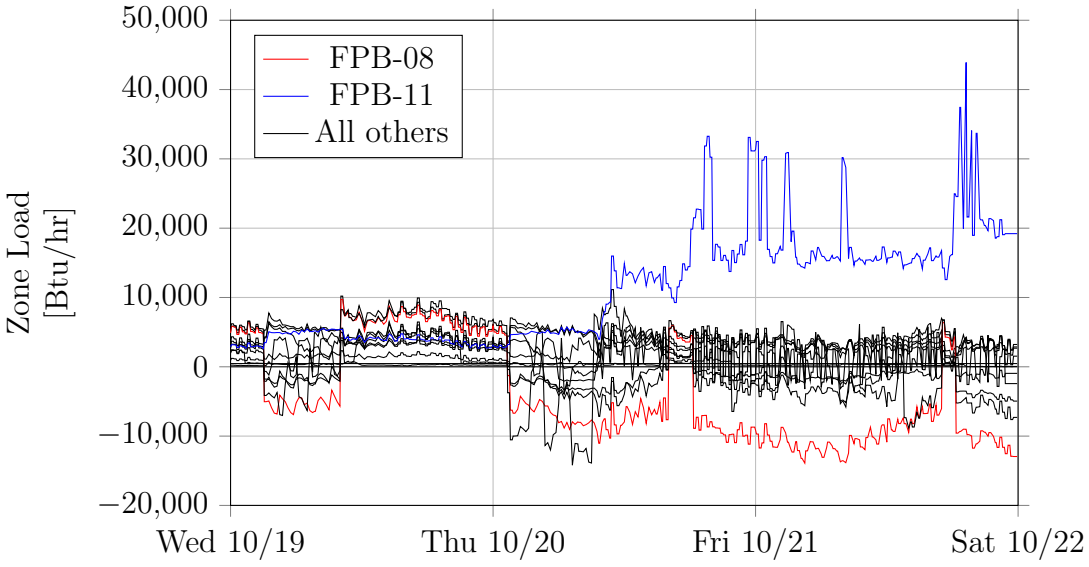

Figure 7.5: Zone load for all terminal units at Preston Royal Library.

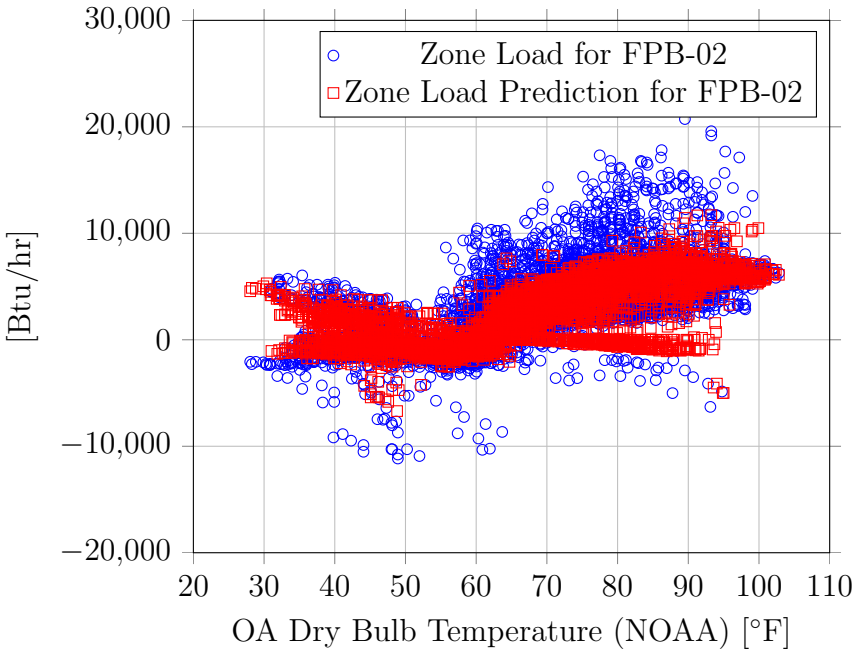

Figure 7.6: Zone load and prediction for FPB-02.

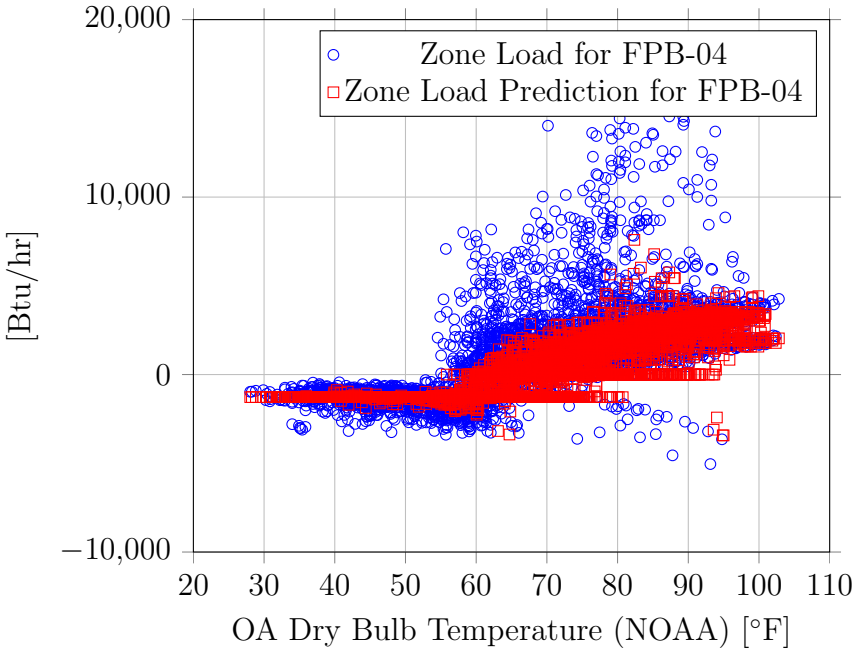

Figure 7.7: Zone load and prediction for FPB-04.

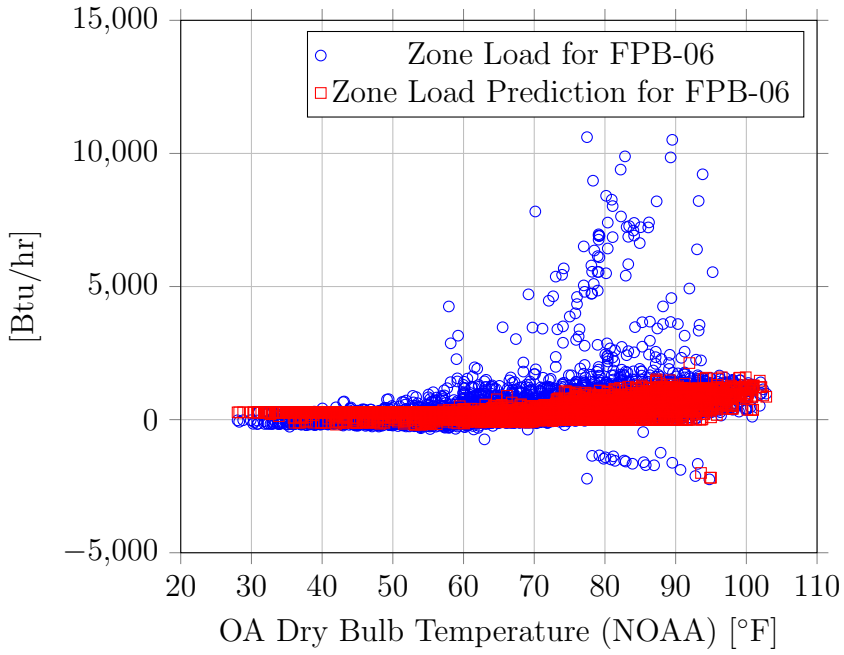

Figure 7.8: Zone load and prediction for FPB-06.

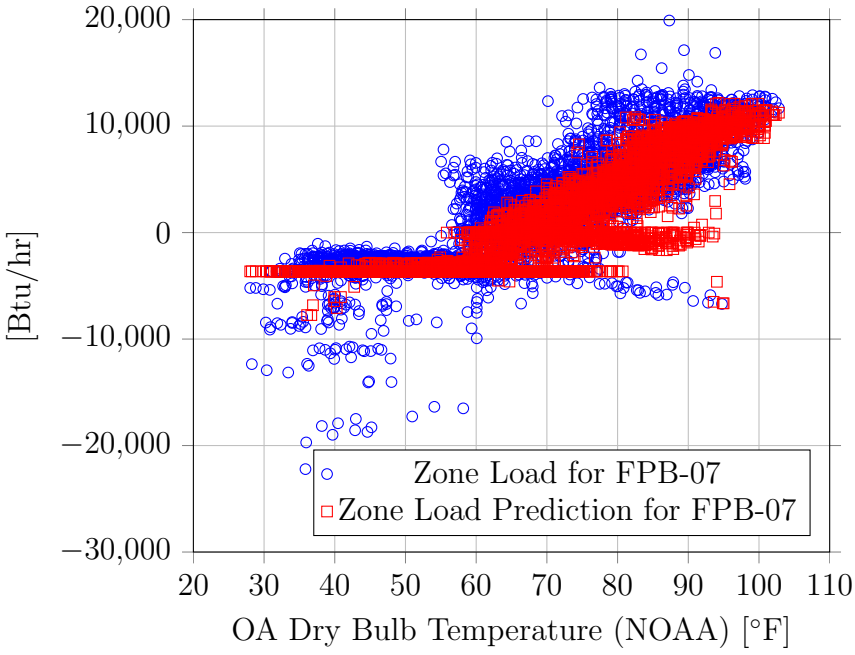

Figure 7.9: Zone load and prediction for FPB-07.

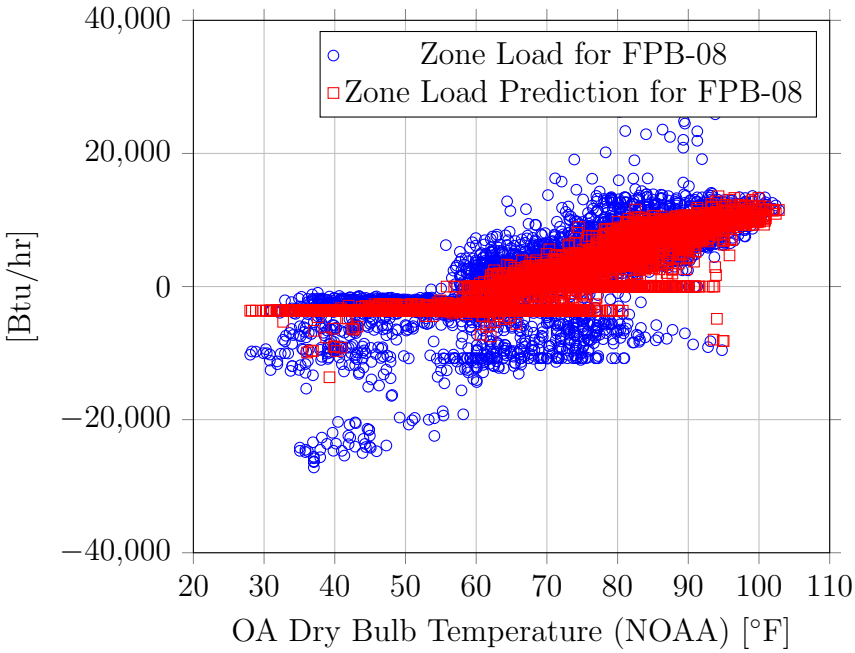

Figure 7.10: Zone load and prediction for FPB-08.

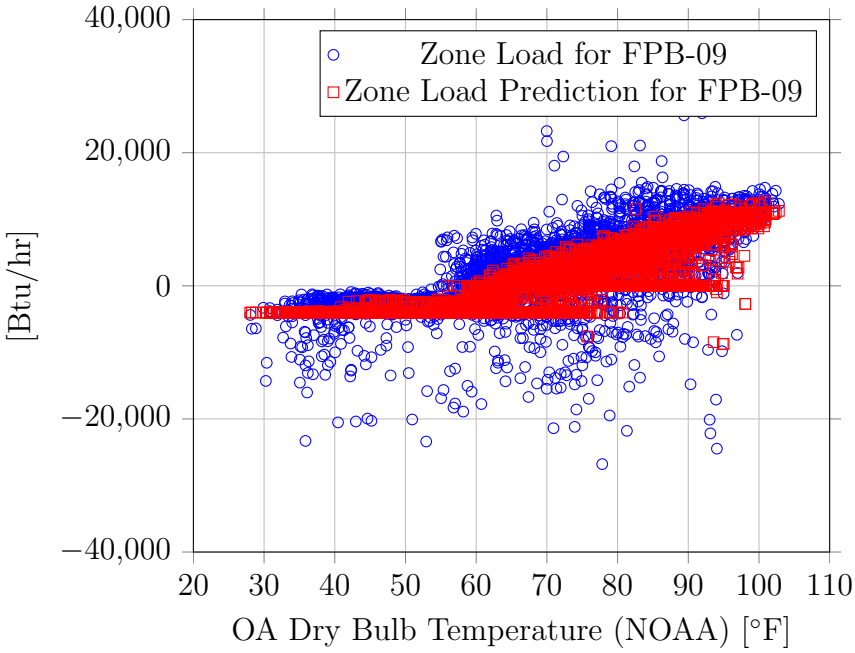

Figure 7.11: Zone load and prediction for FPB-09.

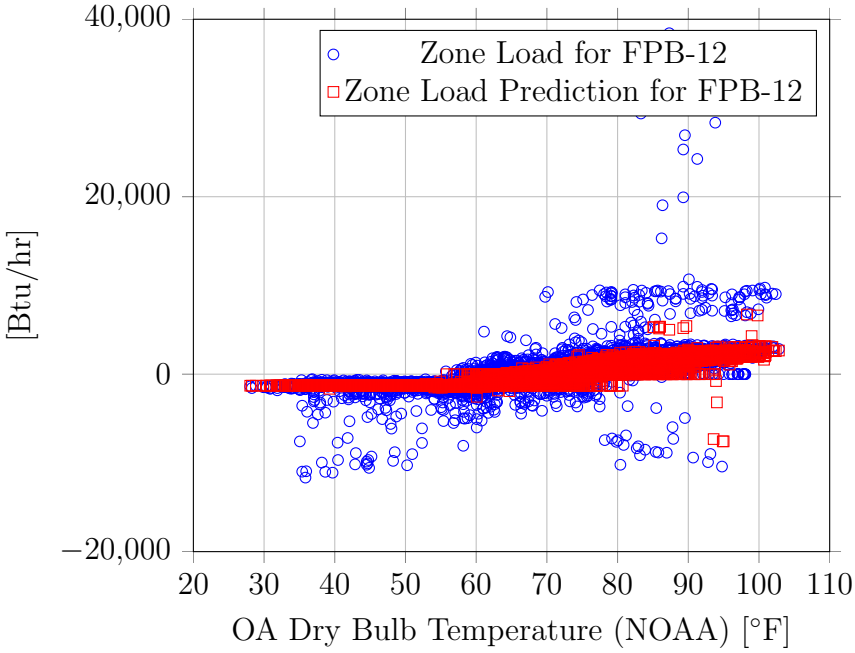

Figure 7.12: Zone load and prediction for FPB-12.

- The mixed air humidity ratio was also not known. It was assumed to have a similar relationship as the mixed air temperature, however, during times of low humidity, the mixed air humidity ratio will just be the outdoor air humidity ratio.

$$\omega_{ma} = \text{MIN}\left(\omega_{oa}, 0.3\omega_{oa} + 0.7\omega_{sa}\left(T_{sa}\right)\right) \tag{7.2}$$

- The minimum flow rate percentage for the terminal units was assumed to be 30%.

Data existed from December 1$^{\text{st}}$, 2015 to October 22$^{\text{nd}}$, 2016. Timestamps when the air handling unit was off were ignored.

Times when the actual supply air temperature was out of a reasonable range was also ignored.

Table 7.1: Estimated savings from the partial data set originating from Preston Royal library.

Component	Estimated Actual ($)	Optimal ($)	Savings ($)
Fan Energy	431 (11%)	563 (17%)	−132
Sensible Cooling Energy	2,220 (55%)	1,990 (59%)	236
Latent Cooling Energy	643 (16%)	462 (14%)	181
Reheat Energy	717 (18%)	377 (11%)	340
Total	4,010	3,390	623

Over the course of the 323 day period, the potential percent dollar savings was 15%. In general, the savings were due to raising the supply air temperature, which while increasing the total fan energy, decreased the required cooling and reheat energy.

The cost of sensible cooling was the largest component, over 50% for both the actual and optimal operations.

8. CONCLUSIONS AND FUTURE WORK

The following conclusions can be derived from this work.

1. Savings are highly dependent on the current operation. For two of the second floor air handlers in the NCTM building, no savings were to be found. However, in AHU-2-3, over 20% energy savings were possible, and over 15% savings were possible in the air handling unit at the Preston Royal Library.

2. Setup in the prototype approach is fast and extensible to future buildings and system types and has been implemented into the software tool *Implementer*.

3. The nearest neighbor method for predicting zone loads and the mixed air temperature was insensitive to variations in the threshold parameters. The models tended to have better results with looser thresholds, meaning more recent data was a better predictor than data under closer conditions.

4. There are significant differences in the percentage of time certain sensors are available from trend data. Certain sensors should be prioritized for trending over others. Quantifications of this and suggestions for commissioning agents are given in Section 2.5.

5. The mixed air temperature was able to be predicted within 2°F for 5 of the 6 AHUs at NCTM (See Table 6.8). This provides evidence that the nearest neighbor approach is viable for predicting the mixed air temperature.

6. With no plenum temperature sensor, for terminal units that bring in plenum air, it was difficult to predict the plenum temperature in a useful manner. Assuming a constant value for the temperature of the corresponding space

was not acceptable for this work with regards to estimating the reheat at the terminal units.

7. The estimated zone load based on terminal unit flow and discharge temperature will depend on the sensitivity of the controls at the terminal unit. Hunting is present, which makes it difficult to gauge what the true zone load in the space is.

8. The difference between the maximum measured flow and the design flow from the terminal units was under 200 CFM for all but one terminal unit at NCTM. This provided confidence in the possibility of using manufacturers' specifications in setting up the system.

9. At the current time, missing sensors and sensor uncertainty reduces the potential effectiveness of the approach described. Additional sensors, especially those related to duct air flow, would improve the capabilities of the methodology.

There are also areas for future work on this topic.

1. With additional sensors related to the fans and air flow, in particular, fan power and pressure rise across the fan, modification of the supply air static pressure setpoint can be included in the optimization.

2. Development of a prototype script to implement the logic on an existing BAS.

3. Application to more potential case study buildings. There are numerous different styles of terminal units (single duct with and without reheat, parallel fan powered, dual-duct, bypass, induction, and underfloor) which all need further investigation.

4. Development of the Application Programming Interface (API) that would be used to interact with the different BAS systems, allowing these methods to scale effectively to thousands of buildings.

REFERENCES

[1] Jean-Pascal Bourdouxhe, Marc Grodent, and Jean Lebrun. *Reference Guide for Dynamic Models of HVAC Equipment*. American Society of Heating, Refrigerating, and Air-Conditioning Engineers, 1998.

[2] Yu-Pei Ke and Stanley A. Mumma. Optimized supply-air temperature (SAT) in variable-air-volume (VAV) systems. *Energy*, 22(6):601–614, 1997.

[3] Gang Wang and Li Song. Air handling unit supply air temperature optimal control during economizer cycles. *Energy and Buildings*, 49:310–316, 2012.

[4] Xiao Qin. *A Data-Driven Approach for System Approximation and Set Point Optimization, With a Focus in HVAC Systems*. PhD thesis, University of Arizona, 2014.

[5] Jung-Ho Huh and Michael J. Brandemuehl. Optimization of air-conditioning system operating strategies for hot and humid climates. *Energy and Buildings*, 40(7):1202–1213, 2008.

[6] Fredrik Engdahl and Dennis Johansson. Optimal supply air temperature with respect to energy use in a variable air volume system. *Energy and Buildings*, 36(3):205–218, 2004.

[7] B.C. Ahn and J.W. Mitchell. Optimal control development for chilled water plants using a quadratic representation. *Energy and Buildings*, 33(4):371–378, 2001.

[8] F.W. Yu and K.T. Chan. Optimizing condenser fan control for air-cooled centrifugal chillers. *International Journal of Thermal Sciences*, 47(7):942–953, 2008.

[9] James E. Braun. Reducing energy costs and peak electrical demand through optimal control of building thermal storage. *ASHRAE transactions*, 96(2):876–888, 1990.

[10] James E. Braun. A near-optimal control strategy for cool storage systems with dynamic electric rates (RP-1252). *HVAC&R Research*, 13(4):557–580, 2007.

[11] James E. Braun. Near-optimal control strategies for hybrid cooling plants. *HVAC&R Research*, 13(4):599–622, 2007.

[12] James E. Braun. A general control algorithm for cooling towers in cooling plants with electric and/or gas-driven chillers. *HVAC&R Research*, 13(4):581–598, 2007.

[13] James E. Braun and Zhipeng Zhong. Development and evaluation of a night ventilation precooling algorithm. *HVAC&R Research*, 11(3):433–458, 2005.

[14] Hugh Crowther and James Furlong. Optimizing chillers and towers. *ASHRAE Journal*, 46(7):34–44, 2004.

[15] Gregor P. Henze, Doreen E. Kalz, Simeng Liu, and Clemens Felsmann. Experimental analysis of model-based predictive optimal control for active and passive building thermal storage inventory. *HVAC&R Research*, 11(2):189–213, 2005.

[16] M. Kintner-Meyer and A.F. Emery. Optimal control of an HVAC system using cold storage and building thermal capacitance. *Energy and Buildings*, 23(1):19–31, 1995.

[17] Lu Lu, Wenjian Cai, Yeng Chai Soh, Lihua Xie, and Shujiang Li. HVAC system optimization—condenser water loop. *Energy Conversion and Management*, 45(4):613–630, 2004.

[18] Lu Lu, Wenjian Cai, Yeng Soh Chai, and Lihua Xie. Global optimization for overall HVAC systems–Part I problem formulation and analysis. *Energy Conversion and Management*, 46(7-8):999–1014, 2005.

[19] Lu Lu, Wenjian Cai, Yeng Chai Soh, and Lihua Xie. Global optimization for overall HVAC systems–Part II problem solution and simulations. *Energy Conversion and Management*, 46(7-8):1015–1028, 2005.

[20] Lu Lu, Wenjian Cai, Lihua Xie, Shujiang Li, and Yeng Chai Soh. HVAC system optimization—in-building section. *Energy and Buildings*, 37(1):11–22, 2005.

[21] M. A. Cascia. Digital controller for a cooling and heating plant having near-optimal global set point control strategy, 1999.

[22] J. E. Seem. Model based economizer control of an air handling unit, 2002.

[23] Mattias Gruber, Anders Trüschel, and Jan-Olof Dalenbäck. Alternative strategies for supply air temperature control in office buildings. *Energy and Buildings*, 82:406–415, 2014.

[24] Young-Hum Cho and Mingsheng Liu. Single-duct constant volume system optimization. *Energy and Buildings*, 41(8):856–862, 2009.

[25] Nabil Nassif, Stanislaw Kajl, and Robert Sabourin. Optimization of HVAC control system strategy using two-objective genetic algorithm. *HVAC&R Research*, 11(3):459–486, 2005.

[26] M. Zaheer-uddin and G. R. Zheng. Optimal control of time-scheduled heating, ventilating and air conditioning processes in buildings. *Energy Conversion and Management*, 41(1):49–60, 2000.

[27] Shengwei Wang and Xinqiao Jin. Model-based optimal control of VAV air-conditioning system using genetic algorithm. *Building and Environment*, 35(6):471–487, 2000.

[28] Gregor P. Henze and Jobst Schoenmann. Evaluation of reinforcement learning control for thermal energy storage systems. *HVAC&R Research*, 9(3):259–275, 2003.

[29] Simeng Liu and Gregor P. Henze. Experimental analysis of simulated reinforcement learning control for active and passive building thermal storage inventory: Part 1. Theoretical foundation. *Energy and Buildings*, 38(2):142–147, 2006.

[30] G.R. Zheng and M. Zaheer-Uddin. Optimization of thermal processes in a variable air volume HVAC system. *Energy*, 21(5):407–420, 1996.

[31] Min Ning and M. Zaheeruddin. Neuro-optimal operation of a variable air volume HVAC&R system. *Applied Thermal Engineering*, 30(5):385–399, 2010.

[32] S. Atthajariyakul and T. Leephakpreeda. Real-time determination of optimal indoor-air condition for thermal comfort, air quality and efficient energy usage. *Energy and Buildings*, 36(7):720–733, 2004.

[33] Yujie Cui, Mingsheng Liu, and Kirk Conger. Optimal airflow control of laboratory air handling unit (LAHU) systems. *Journal of Solar Energy Engineering*, 126(2):750–758, 2004.

[34] Xinhua Xu, Shengwei Wang, Zhongwei Sun, and Fu Xiao. A model-based optimal ventilation control strategy of multi-zone VAV air-conditioning systems. *Applied Thermal Engineering*, 29(1):91–104, 2009.

[35] Zhongwei Sun, Shengwei Wang, and Na Zhu. Model-based optimal control of outdoor air flow rate of an air-conditioning system with primary air-handling

unit. *Indoor and Built Environment*, 2011.

[36] S.A. Mumma and R.J. Bolin. Energy optimized-ventilation constrained variable air volume system control. *Automation in Construction*, 6(5-6):463–470, 1997.

[37] M. Mossolly, K. Ghali, and N. Ghaddar. Optimal control strategy for a multi-zone air conditioning system using a genetic algorithm. *Energy*, 34(1):58–66, 2009.

[38] Shengwei Wang and Zhenjun Ma. Supervisory and optimal control of building HVAC systems: A review. *HVAC&R Research*, 14(1):3–32, 2008.

[39] Andrew Kusiak, Guanglin Xu, and Zijun Zhang. Minimization of energy consumption in HVAC systems with data-driven models and an interior-point method. *Energy Conversion and Management*, 85:146–153, 2014.

[40] Xiaofei He, Zijun Zhang, and Andrew Kusiak. Performance optimization of HVAC systems with computational intelligence algorithms. *Energy and Buildings*, 81:371–380, 2014.

[41] Andrew Kusiak, Yaohui Zeng, and Guanglin Xu. Minimizing energy consumption of an air handling unit with a computational intelligence approach. *Energy and Buildings*, 60:355–363, 2013.

[42] Andrew Kusiak and Guanglin Xu. Modeling and optimization of HVAC systems using a dynamic neural network. *Energy*, 42(1):241–250, 2012.

[43] Andrew Kusiak, Fan Tang, and Guanglin Xu. Multi-objective optimization of HVAC system with an evolutionary computation algorithm. *Energy*, 36(5):2440–2449, 2011.

[44] Andrew Kusiak and Mingyang Li. Reheat optimization of the variable-air-volume box. *Energy*, 35(5):1997–2005, 2010.

[45] Xiupeng Wei, Andrew Kusiak, Mingyang Li, Fan Tang, and Yaohui Zeng. Multi-objective optimization of the HVAC (heating, ventilation, and air conditioning) system performance. *Energy*, 83:294–306, 2015.

[46] Xiupeng Wei, Guanglin Xu, and Andrew Kusiak. Modeling and optimization of a chiller plant. *Energy*, 73:898–907, 2014.

[47] Andrew Kusiak and Mingyang Li. Cooling output optimization of an air handling unit. *Applied Energy*, 87(3):901–909, 2010.

[48] Andrew Kusiak, Mingyang Li, and Fan Tang. Modeling and optimization of HVAC energy consumption. *Applied Energy*, 87(10):3092–3102, 2010.

[49] Andrew Kusiak, Guanglin Xu, and Fan Tang. Optimization of an HVAC system with a strength multi-objective particle-swarm algorithm. *Energy*, 36(10):5935–5943, 2011.

[50] K.F. Fong, V.I. Hanby, and T.T. Chow. HVAC system optimization for energy management by evolutionary programming. *Energy and Buildings*, 38(3):220–231, 2006.

[51] Xinqiao Jin, Haigang Ren, and Xiaokun Xiao. Prediction-based online optimal control of outdoor air of multi-zone VAV air conditioning systems. *Energy and Buildings*, 37(9):939–944, 2005.

[52] R. Parameshwaran, R. Karunakaran, C. Vinu Raja Kumar, and S. Iniyan. Energy conservative building air conditioning system controlled and optimized using fuzzy-genetic algorithm. *Energy and Buildings*, 42(5):745–762, 2010.

[53] Velimir Congradac and Filip Kulic. HVAC system optimization with CO_2 concentration control using genetic algorithms. *Energy and Buildings*, 41(5):571–577, 2009.

[54] Pengfei Li, Draguna Vrabie, Dapeng Li, Sorin C. Bengea, Stevo Mijanovic, and Zheng D. O'Neill. Simulation and experimental demonstration of model predictive control in a building HVAC system. *Science and Technology for the Built Environment*, 21(6):721–732, 2015.

[55] Abdul Afram, Farrokh Janabi-Sharifi, Alan S. Fung, and Kaamran Raahemifar. Artificial neural network (ANN) based model predictive control (MPC) and optimization of HVAC systems: A state of the art review and case study of a residential HVAC system. *Energy and Buildings*, 141:96–113, 2017.

[56] P.M. Ferreira, A.E. Ruano, S. Silva, and E.Z.E. Conceição. Neural networks based predictive control for thermal comfort and energy savings in public buildings. *Energy and Buildings*, 55:238–251, 2012.

[57] Hao Huang, Lei Chen, and Eric Hu. A new model predictive control scheme for energy and cost savings in commercial buildings: An airport terminal building case study. *Building and Environment*, 89:203–216, 2015.

[58] Antoine Garnier, Julien Eynard, Matthieu Caussanel, and Stéphane Grieu. Predictive control of multizone heating, ventilation and air-conditioning systems in non-residential buildings. *Applied Soft Computing*, 37:847–862, 2015.

[59] Wonuk Kim, Yongseok Jeon, and Yongchan Kim. Simulation-based optimization of an integrated daylighting and HVAC system using the design of experiments method. *Applied Energy*, 162:666–674, 2016.

[60] Young M. Lee, Raya Horesh, and Leo Liberti. Optimal HVAC control as demand response with on-site energy storage and generation system. *Energy Procedia*, 78:2106–2111, 2015.

[61] A. E. Ruano, S. Silva, S. Pesteh, P. M. Ferreira, H. Duarte, G. Mestre, H. Khosravani, and R. Horta. Improving a neural networks based HVAC predictive control approach. In *2015 IEEE 9th International Symposium of Intelligent Signal Processing*, 2015.

[62] Antonio E. Ruano, Shabnam Pesteh, Sergio Silva, Helder Duarte, Gonçalo Mestre, Pedro M. Ferreira, Hamid R. Khosravani, and Ricardo Horta. The IMBPC HVAC system: A complete MBPC solution for existing HVAC systems. *Energy and Buildings*, 120:145–158, 2016.

[63] Ehsan Asadi, Manuel Gameiro da Silva, Carlos Henggeler Antunes, Luís Dias, and Leon Glicksman. Multi-objective optimization for building retrofit: A model using genetic algorithm and artificial neural network and an application. *Energy and Buildings*, 81:444–456, 2014.

[64] John E. Seem, Cheol Park, and John M. House. A new sequencing control strategy for air-handling units. *HVAC&R Research*, 5(1):35–58, 1999.

[65] Min Xu, Shaoyuan Li, and Wenjian Cai. Practical receding-horizon optimization control of the air handling unit in HVAC systems. *Industrial & Engineering Chemistry Research*, 44(8):2848–2855, 2005.

[66] Shui Yuan and Ronald Perez. Multiple-zone ventilation and temperature control of a single-duct VAV system using model predictive strategy. *Energy and Buildings*, 38(10):1248–1261, 2006.

[67] Roberto Z. Freire, Gustavo H.C. Oliveira, and Nathan Mendes. Predictive controllers for thermal comfort optimization and energy savings. *Energy and Buildings*, 40(7):1353–1365, 2008.

[68] Chengyi Guo, Qing Song, and Wenjian Cai. A neural network assisted cascade control system for air handling unit. *Industrial Electronics, IEEE Transactions on*, 54(1):620–628, 2007.

[69] W. Kastner, G. Neugschwandtner, S. Soucek, and H. M. Newmann. Communication systems for building automation and control. *Proceedings of the IEEE*, 93(6):1178–1203, 2005.

APPENDIX A

APPROXIMATIONS TO THE RAMP FUNCTION

A.1 Approximation Using Fourier Series

This section shows a derivation of the Fourier Series for the ramp function, which is often used to model the output flow for a terminal unit.

In various situations related to steady state analysis of the energy use of an air handling unit, ramp functions are found. These ramp functions are usually difficult to deal with in optimization problems because they are not continuously differentiable. In this sense, it is desired to have a replacement or approximation to the function that is smooth and can be differentiated.

Fourier series are a useful tool for approximating arbitrary functions and can be used in this task. We can begin by focusing on the basic ramp function that is defined by:

$$f(x) = \begin{cases} 0 & x < 0 \\ x & x \geq 0 \end{cases} \tag{A.1}$$

If we define our Fourier series to be defined over the interval $-L \leq x \leq L$ and be equal to

$$f(x) = a_0 + \sum_{n=1}^{\infty} a_n \cos \frac{n\pi x}{L} + \sum_{n=1}^{\infty} b_n \sin \frac{n\pi x}{L} \tag{A.2}$$

The coefficients are equal to

$$a_0 = \frac{1}{2L} \int_{-L}^{L} f(x)\, dx \tag{A.3}$$

$$a_n = \frac{1}{L}\int_{-L}^{L} f(x)\cos\frac{n\pi x}{L}\,dx \tag{A.4}$$

$$b_n = \frac{1}{L}\int_{-L}^{L} f(x)\sin\frac{n\pi x}{L}\,dx \tag{A.5}$$

$f(x) = 0$ when $x \leq 0$, so that portion of the integral is equal to 0. When $x \geq 0$, $f(x) = x$ and the coefficients can be evaluated over the range $0 \leq x \leq L$.

$$a_0 = \frac{1}{2L}\int_{0}^{L} x\,dx \tag{A.6}$$

$$a_n = \frac{1}{L}\int_{0}^{L} x\cos\frac{n\pi x}{L}\,dx \tag{A.7}$$

$$b_n = \frac{1}{L}\int_{0}^{L} x\sin\frac{n\pi x}{L}\,dx \tag{A.8}$$

Solving for a_0,

$$a_0 = \frac{1}{2L}\int_{0}^{L} x\,dx = \frac{1}{2L}\left[\frac{x^2}{2}\right]_0^L = \frac{1}{2L}\left(\frac{L^2}{2}\right) = \frac{L}{4} \tag{A.9}$$

The coefficients for the cosine terms are

$$\begin{aligned} a_n &= \frac{1}{L}\int_0^L x\cos\frac{n\pi x}{L}\,dx \\ &= \frac{1}{L}\left(\cancel{x\frac{L}{n\pi}\sin\frac{n\pi x}{L}\Big|_0^L}^{0} - \int_0^L \frac{L}{n\pi}\sin\frac{n\pi}{L}x\,dx\right) \\ &= \frac{1}{L}\left(\left[\frac{L^2}{n^2\pi^2}\cos\frac{n\pi x}{L}\right]_0^L\right) \\ &= \frac{L}{n^2\pi^2}\left((-1)^n - 1\right) \end{aligned} \tag{A.10}$$

and the coefficients for the sine terms are

$$\begin{aligned} b_n &= \frac{1}{L}\int_0^L x\sin\frac{n\pi x}{L}\,dx \\ &= \frac{1}{L}\left(-x\frac{L}{n\pi}\cos\frac{n\pi x}{L}\Big|_0^L - \int_0^L -\frac{L}{n\pi}\cos\frac{n\pi}{L}x\,dx\right) \\ &= \frac{1}{L}\left(\left[\frac{-L^2}{n\pi}(-1)^n + \frac{L^2}{n^2\pi^2}\left[\sin\frac{n\pi x}{L}\right]_0^L\right]\right) \\ &= \frac{1}{L}\left(\left[\frac{-L^2}{n\pi}(-1)^n + 0\right]\right) \\ &= \frac{L}{n\pi}\left((-1)^{n+1}\right) \end{aligned} \tag{A.11}$$

A.2 Approximation Using the Logistic Function

The threshold function is the derivative of the ramp function. The threshold function can be approximated arbitrarily well using the logistic function. The logistic function has the form

$$y = \frac{1}{1 + e^{-k(x-x_0)}} \tag{A.12}$$

As $k \to \infty$, the function equals the threshold function. The integral of the threshold function is the ramp function. Integrating Equation A.12 results in the family of

solutions

$$y = x + \frac{\ln\left(1 + e^{-k(x-x_0)}\right)}{k} + C \tag{A.13}$$

When $x > x_0$, the $\ln\left(1 + e^{-k(x-x_0)}\right)$ term goes to 0, and the function is equal to $x + C$, which has a derivative of 1 with respect to x.

When $x < x_0$, the $\frac{\ln\left(1+e^{-k(x-x_0)}\right)}{k}$ term goes to $x_0 - x$, and the function is equal to

$$y = x + (x_0 - x) + C = x_0 + C \tag{A.14}$$

This function approximates the ramp function arbitrarily well as $k \to \infty$.

The function is usually applied to flow for terminal units with a minimum flow setting. In this case, the value for the constant C equals 0 so that x_0 and $x_0 + C$ are equal, and the function becomes

$$\dot{V} = \dot{V}_{req} + \frac{\ln\left(1 + e^{-k\left(\dot{V}_{req} - \dot{V}_{min}\right)}\right)}{k} \tag{A.15}$$

APPENDIX B

ZONE LOADS FOR NCTM

B.1 Estimated Zone Loads for NCTM

This portion of the appendix plots all the zone loads for the terminal units at NCTM.

B.2 Terminal Units of AHU-2-1

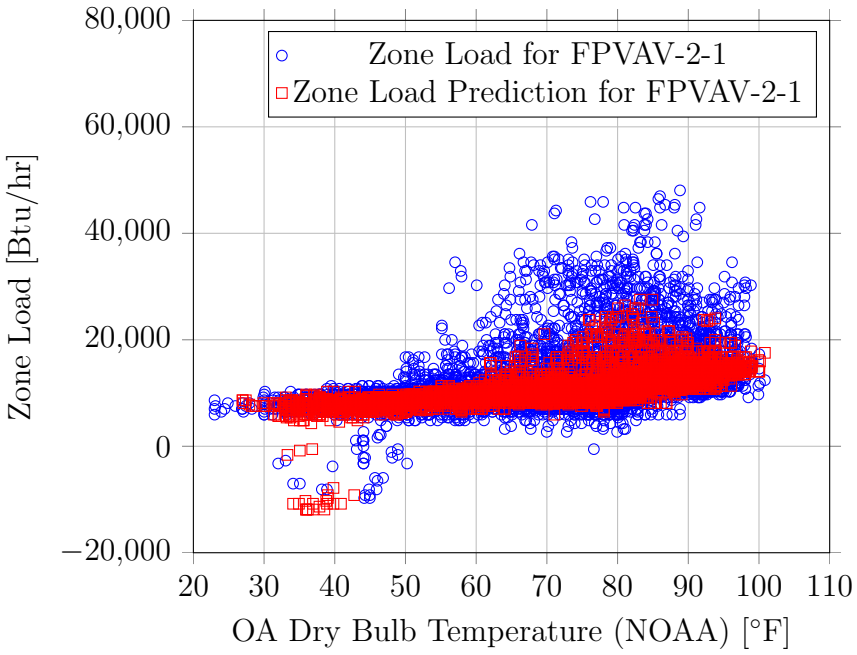

Figure B.1: Zone load for FPVAV-2-1 during the year 2016.

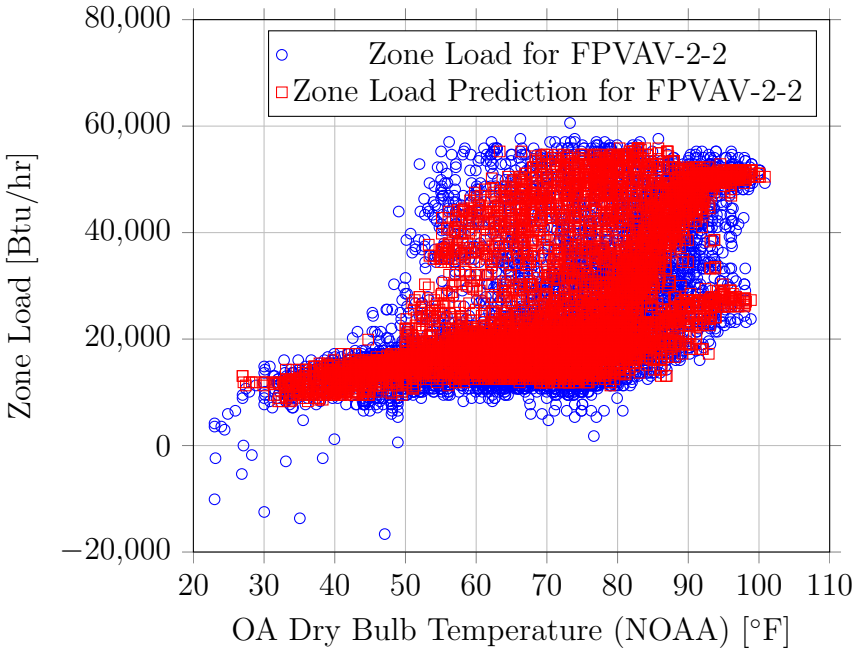

Figure B.2: Zone load for FPVAV-2-2 during the year 2016.

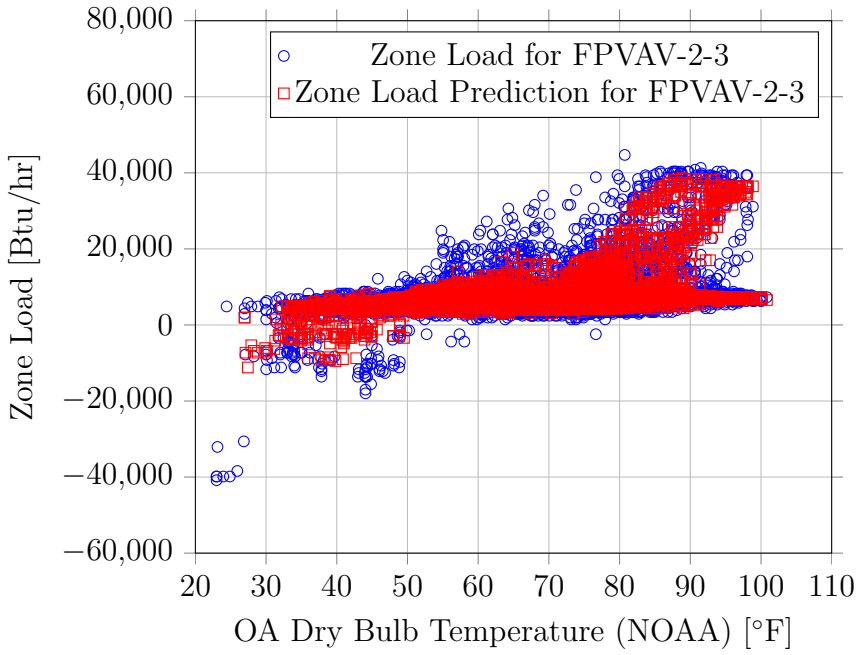

Figure B.3: Zone load for FPVAV-2-3 during the year 2016. Notice that the lower bound of the y-axis is different than the other plots.

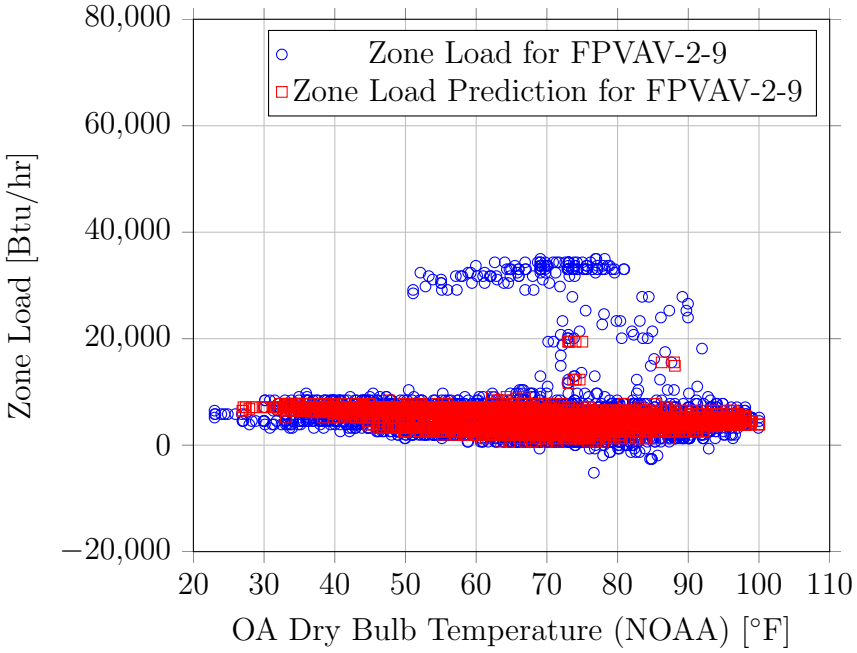

Figure B.4: Zone load for FPVAV-2-9 during the year 2016.

B.3 Terminal Units of AHU-2-2

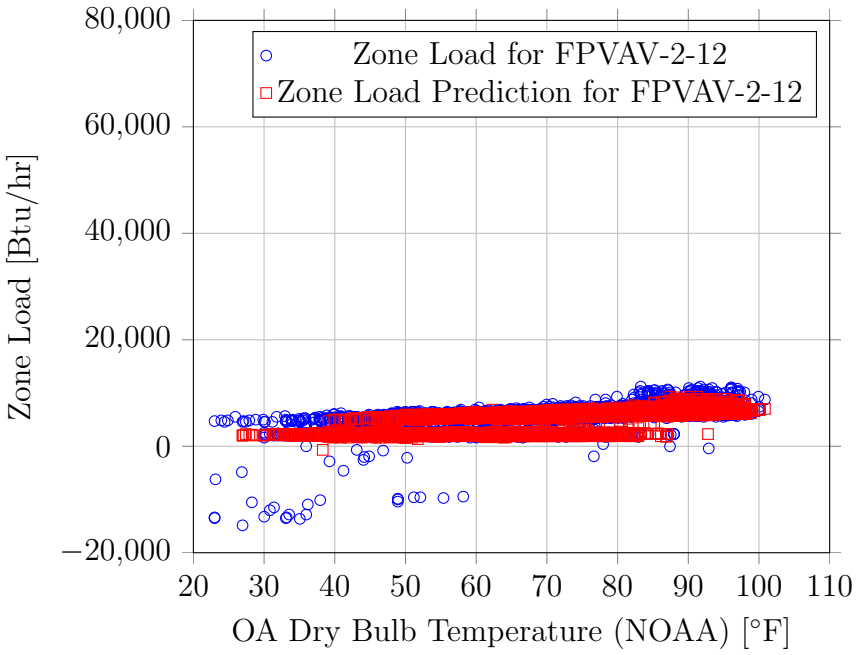

Figure B.5: Zone load for FPVAV-2-12 during the year 2016.

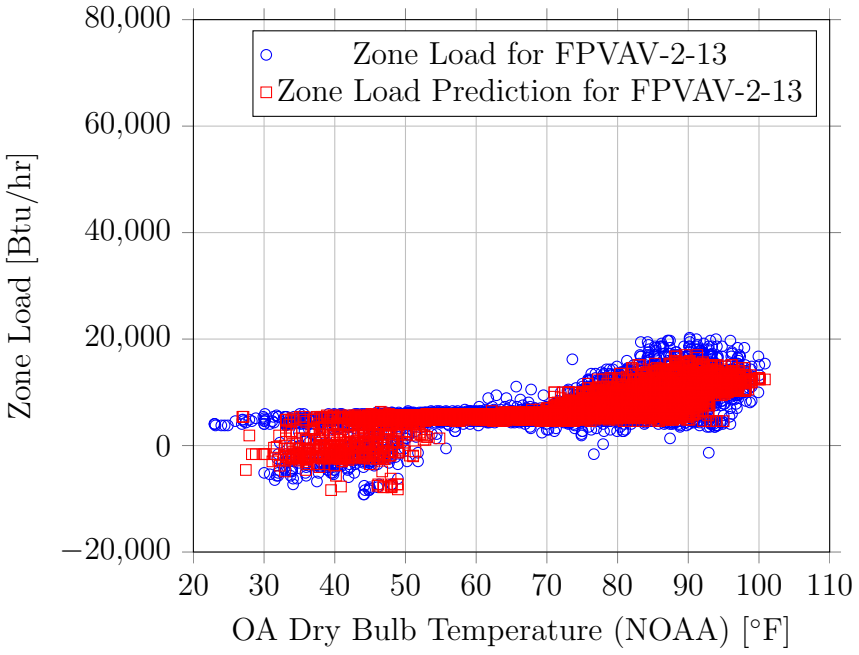

Figure B.6: Zone load for FPVAV-2-13 during the year 2016.

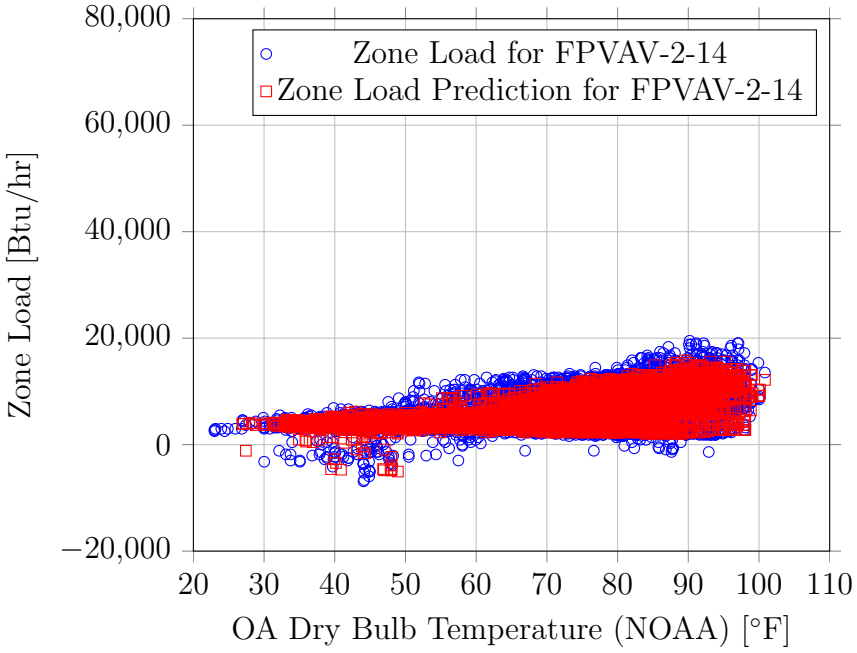

Figure B.7: Zone load for FPVAV-2-14 during the year 2016.

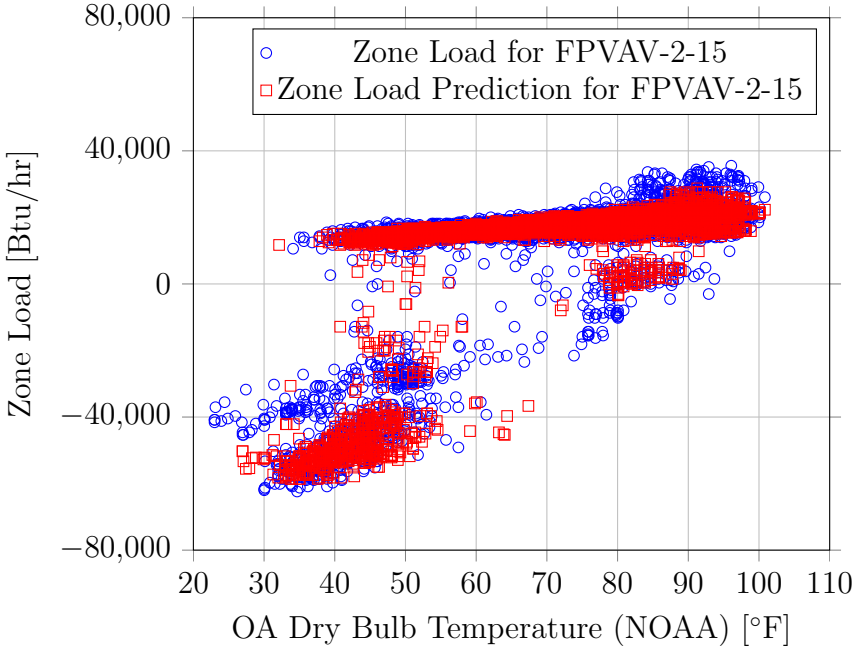

Figure B.8: Zone load for FPVAV-2-15 during the year 2016. Notice that the lower bound of the y-axis is different than the other plots.

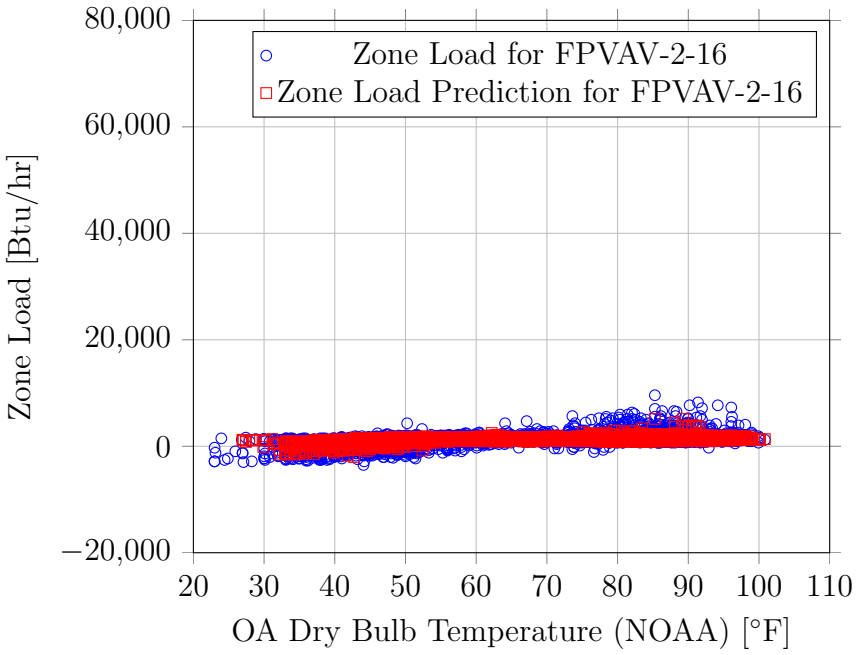

Figure B.9: Zone load for FPVAV-2-16 during the year 2016.

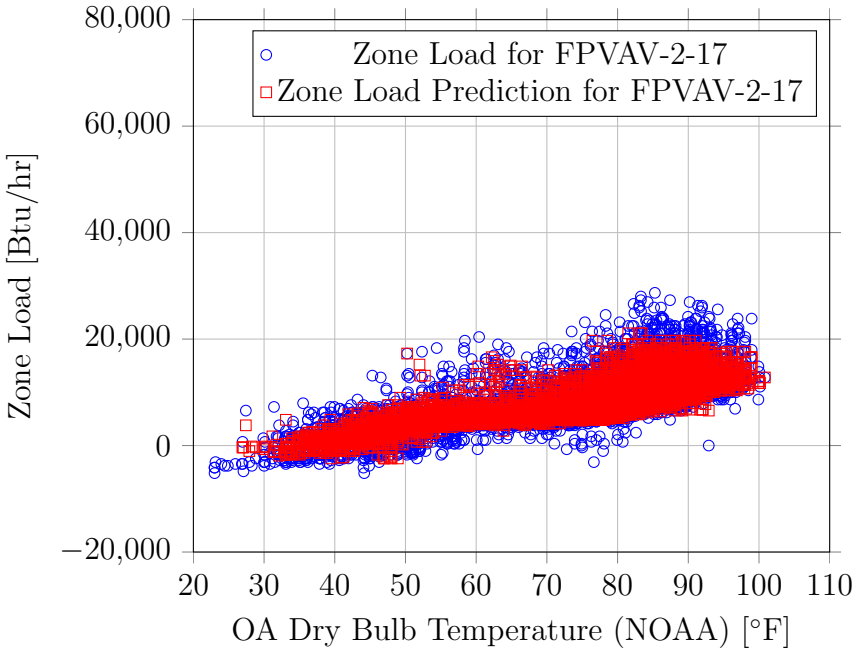

Figure B.10: Zone load for FPVAV-2-17 during the year 2016.

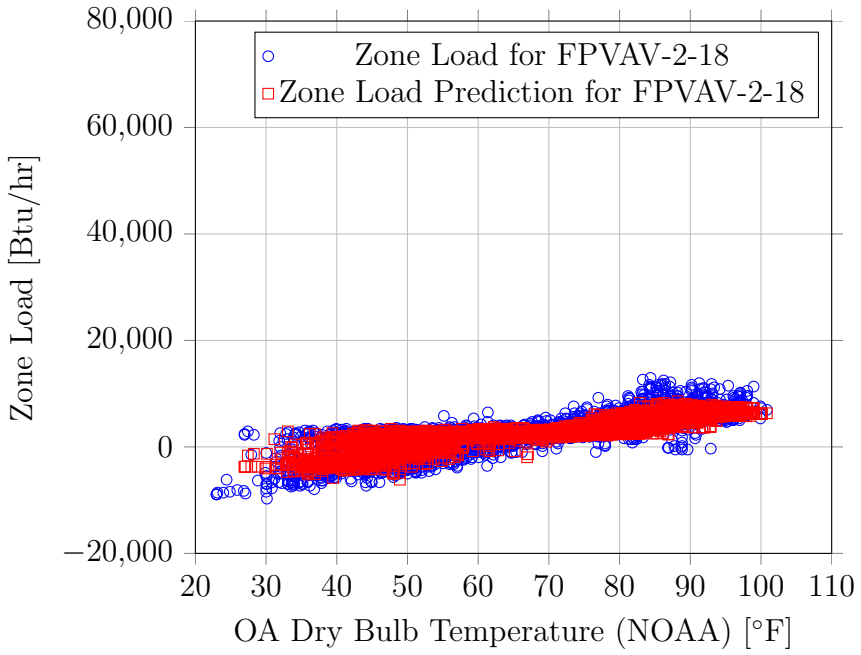

Figure B.11: Zone load for FPVAV-2-18 during the year 2016.

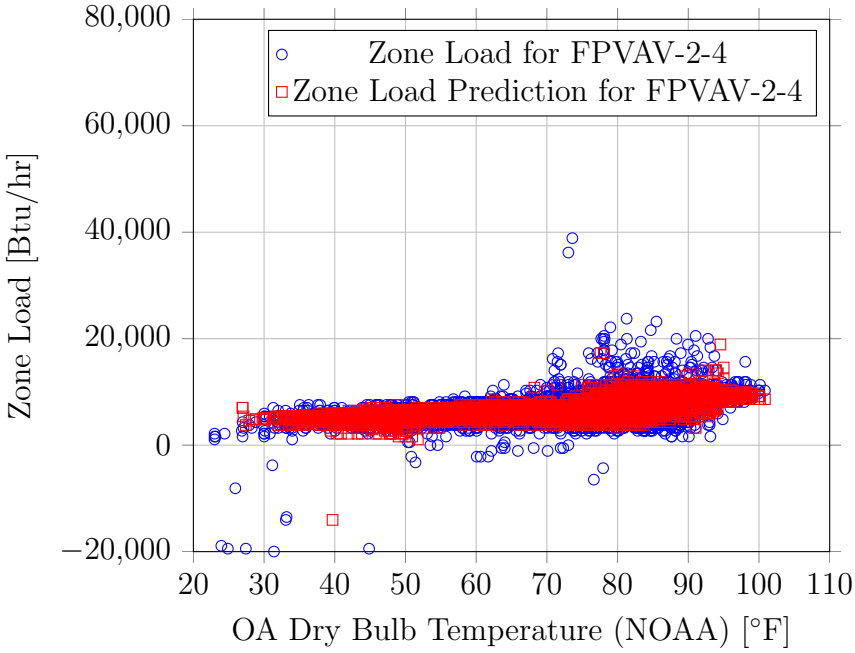

Figure B.12: Zone load for FPVAV-2-4 during the year 2016.

B.4 Terminal Units of AHU-2-3

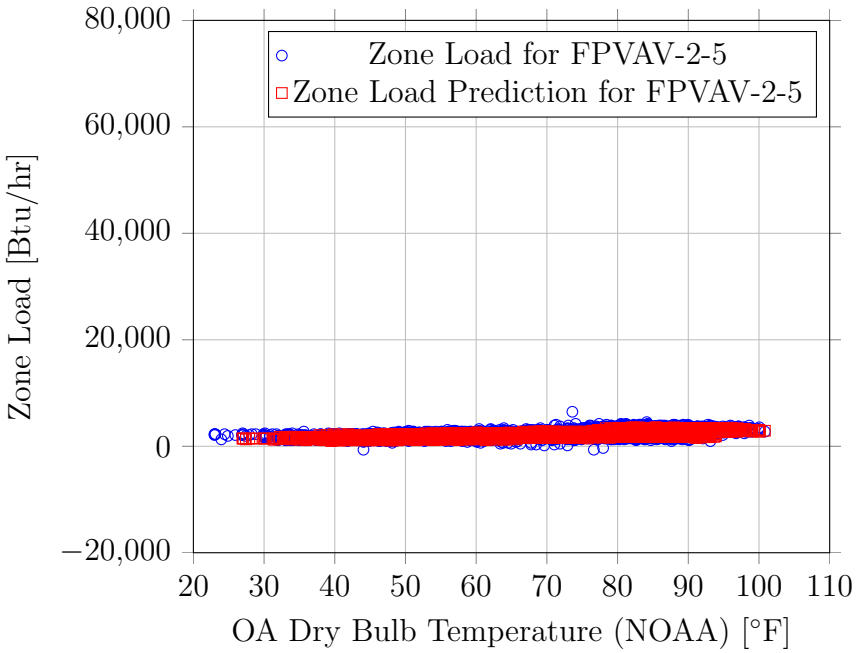

Figure B.13: Zone load for FPVAV-2-5 during the year 2016.

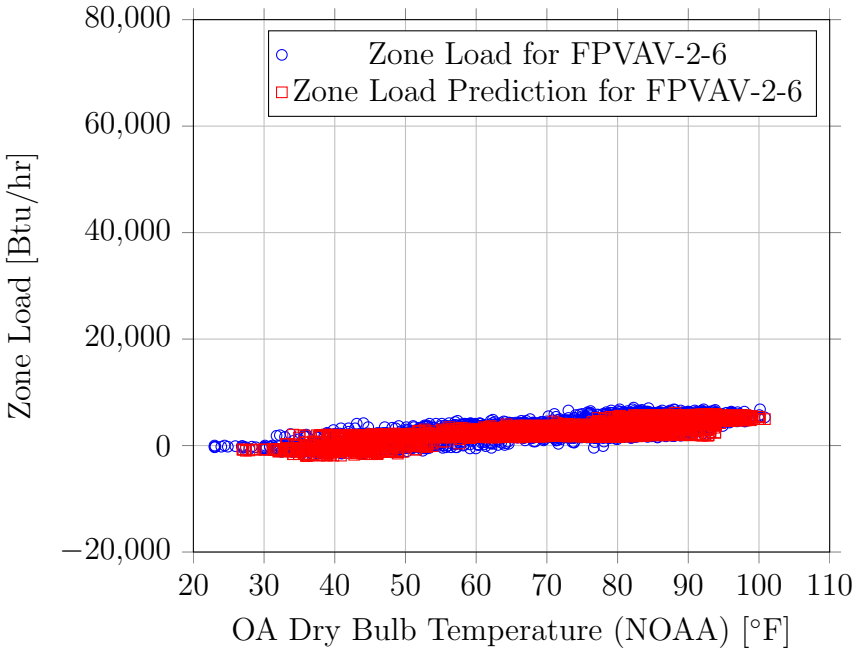

Figure B.14: Zone load for FPVAV-2-6 during the year 2016.

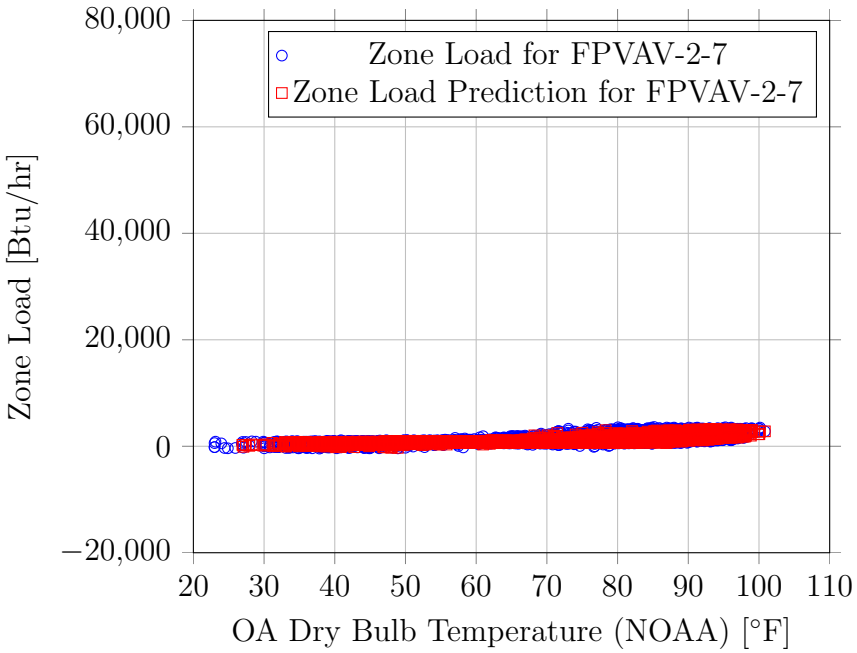

Figure B.15: Zone load for FPVAV-2-7 during the year 2016.

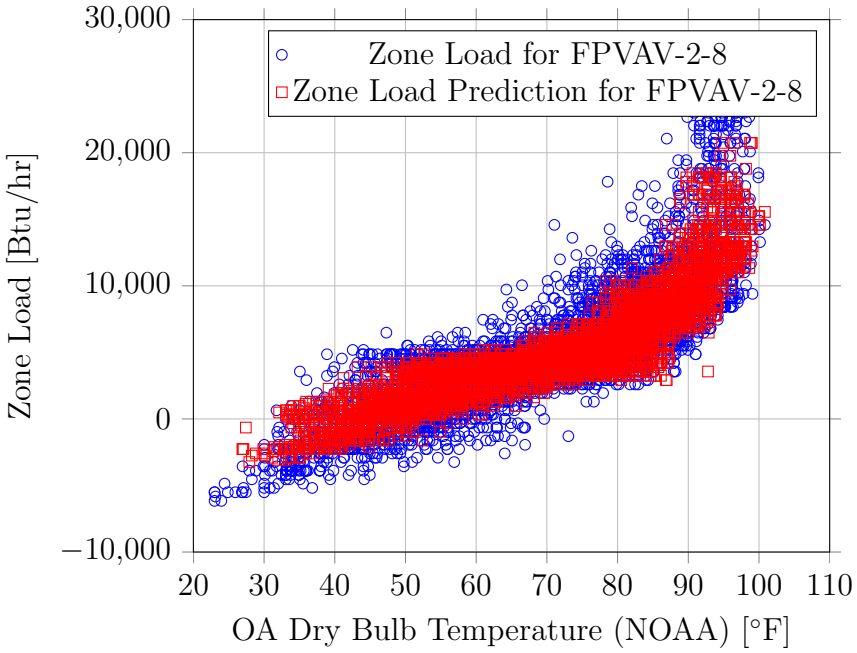

Figure B.16: Zone load for FPVAV-2-8 during the year 2016.

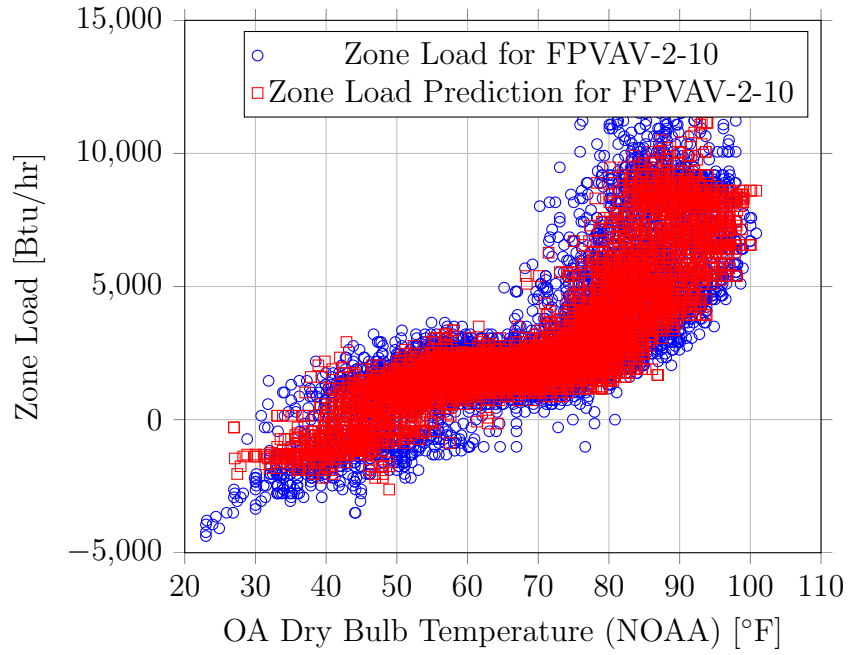

Figure B.17: Zone load for FPVAV-2-10 during the year 2016.

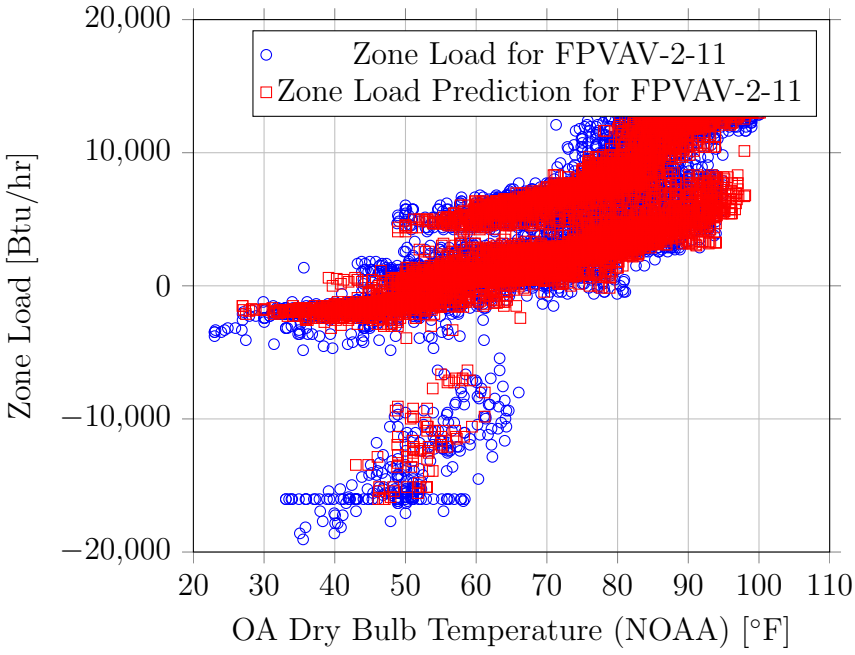

Figure B.18: Zone load for FPVAV-2-11 during the year 2016.

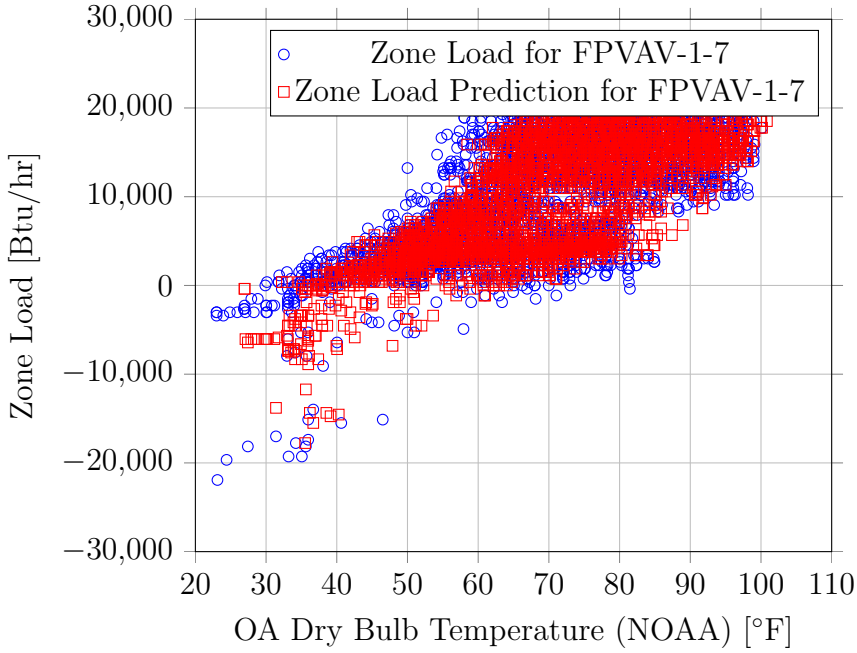

Figure B.19: Zone load for FPVAV-1-7 during the year 2016.

B.5 Terminal Units of AHU-1-2

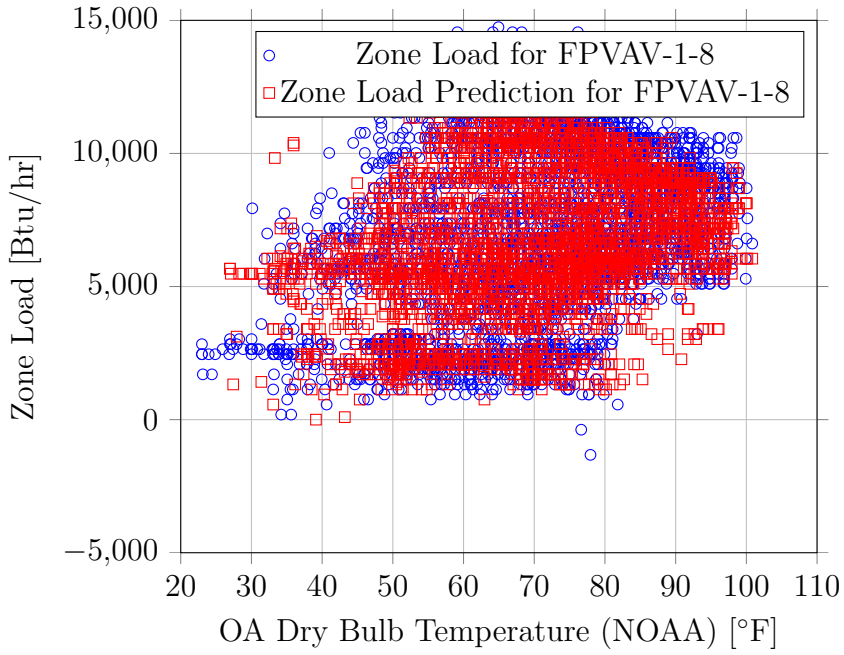

Figure B.20: Zone load for FPVAV-1-8 during the year 2016.

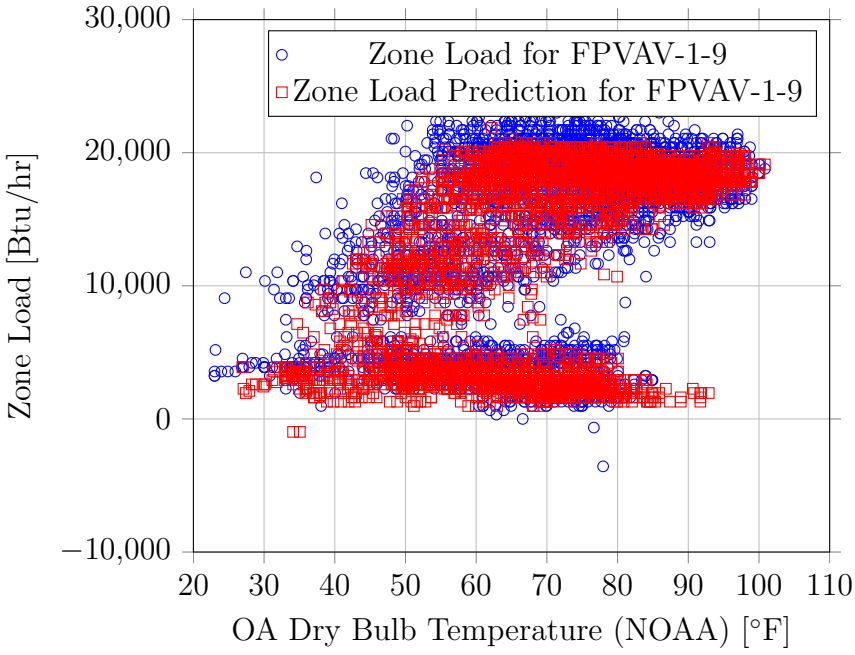

Figure B.21: Zone load for FPVAV-1-9 during the year 2016.

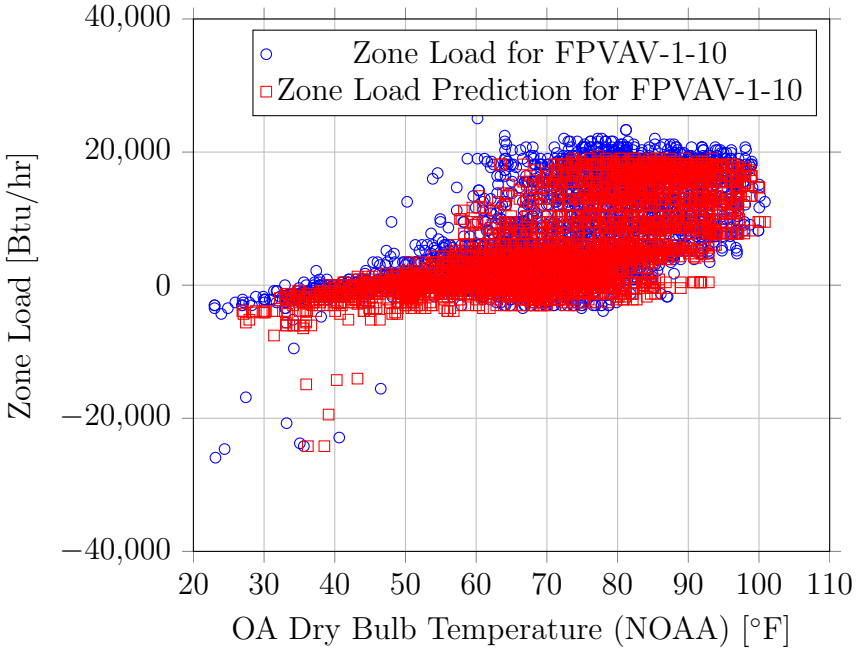

Figure B.22: Zone load for FPVAV-1-10 during the year 2016.

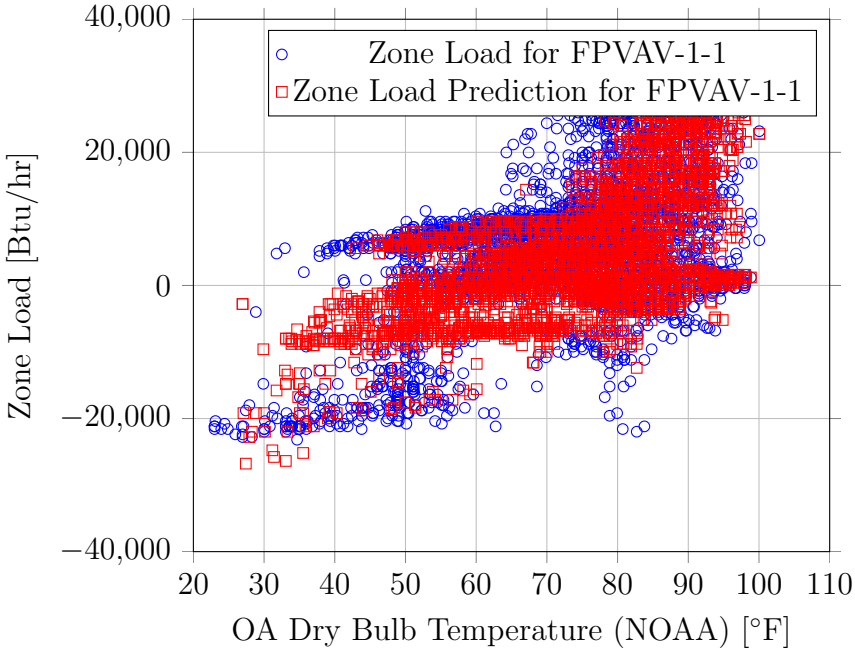

Figure B.23: Zone load for FPVAV-1-1 during the year 2016.

B.6 Terminal Units of AHU-1-3

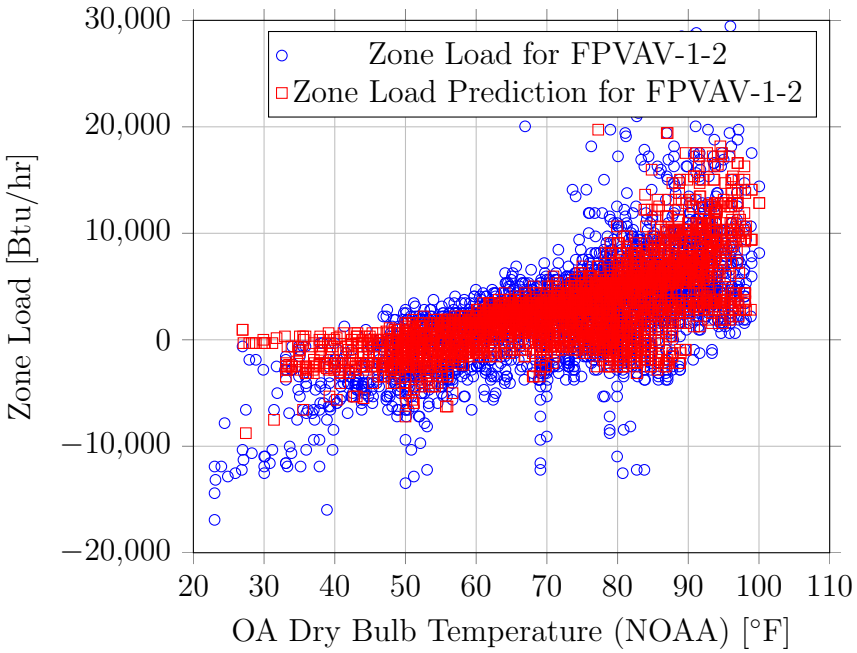

Figure B.24: Zone load for FPVAV-1-2 during the year 2016.

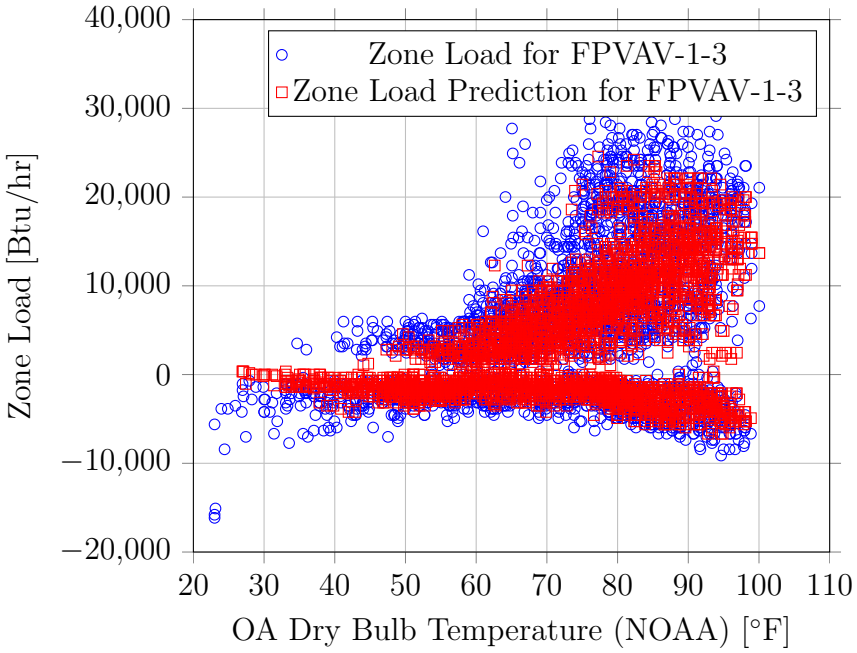

Figure B.25: Zone load for FPVAV-1-3 during the year 2016.

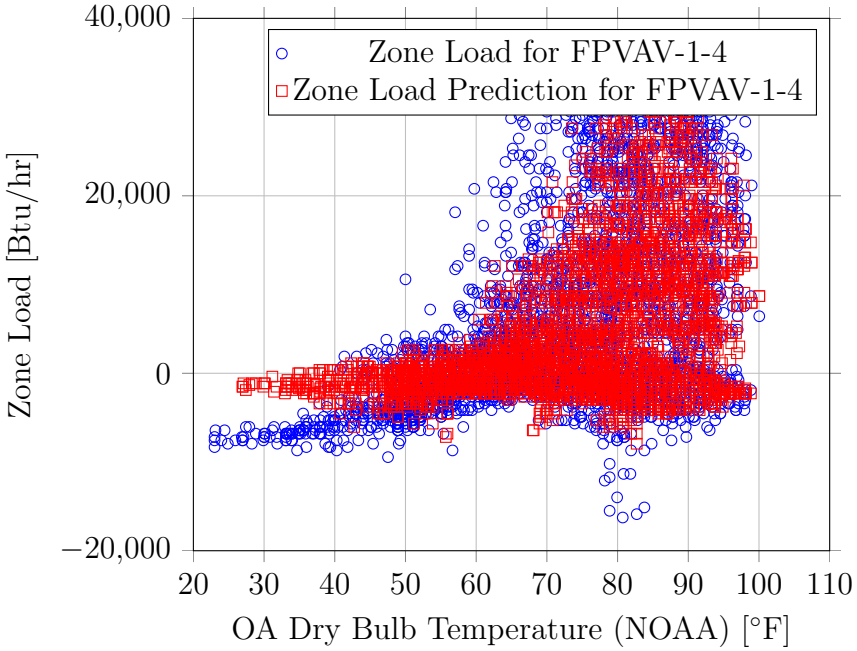

Figure B.26: Zone load for FPVAV-1-4 during the year 2016.

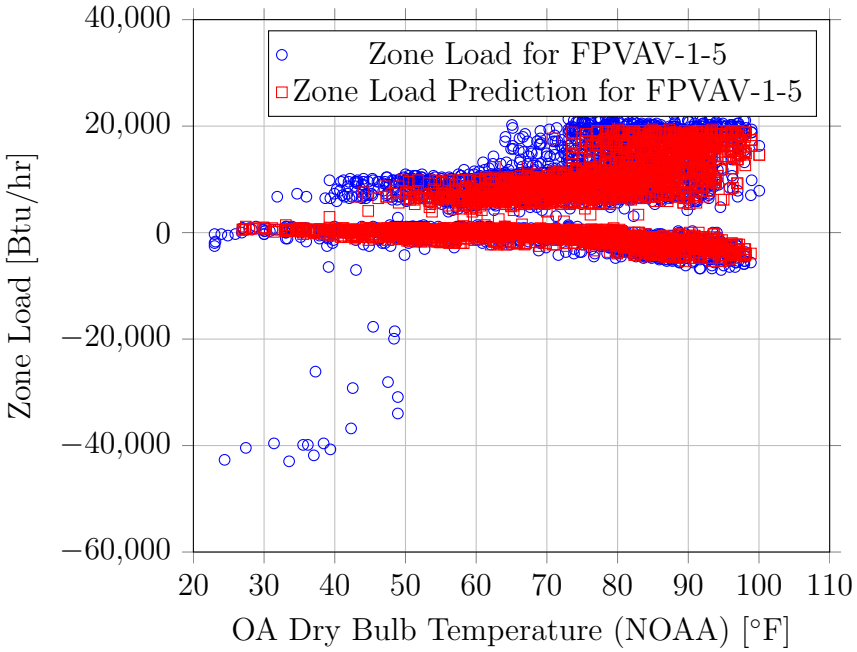

Figure B.27: Zone load for FPVAV-1-5 during the year 2016.

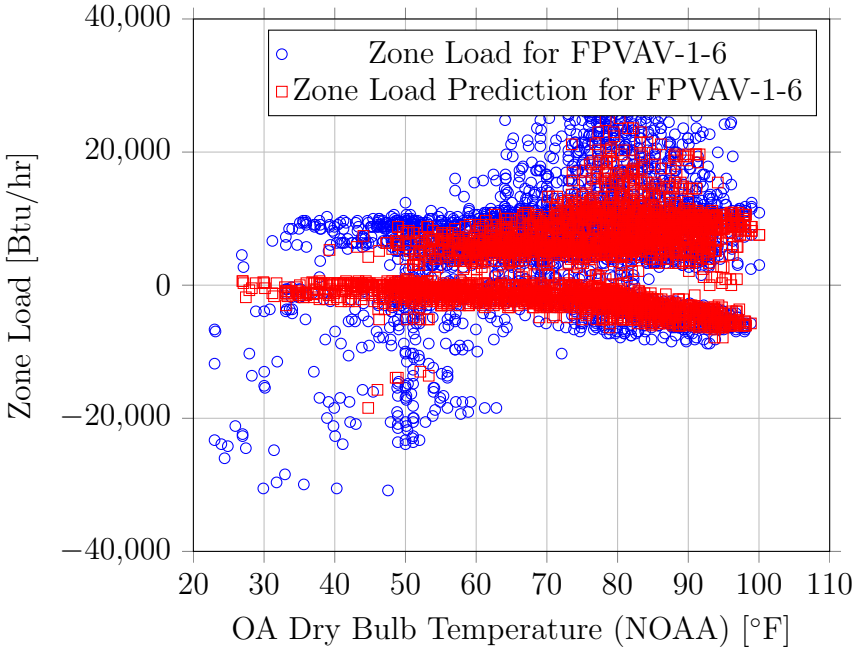

Figure B.28: Zone load for FPVAV-1-6 during the year 2016.